เดนดริติกพอลิอิเล็กโทรไลต์เพื่อเป็นแอปทาเซ็นเซอร์วาวแสงสำหรับโพแทสเซียมไอออน

นางสาววรรณนภา   ย้วนบุญหลิม

วิทยานิพนธ์นี้เป็นส่วนหนึ่งของการศึกษาตามหลักสูตรปริญญาวิทยาศาสตรมหาบัณฑิต
สาขาวิชาเคมี ภาควิชาเคมี
คณะวิทยาศาสตร์ จุฬาลงกรณ์มหาวิทยาลัย
ปีการศึกษา 2554
ลิขสิทธิ์ของจุฬาลงกรณ์มหาวิทยาลัย

DENDRITIC POLYELECTROLYTES AS FLUORESCENT APTASENSORS FOR
POTASSIUM ION

Miss Wannapa   Yuanboonlim

A Thesis Submitted in Partial Fulfillment of the Requirements

for the Degree of Master of Science Program in Chemistry

Department of Chemistry

Faculty of Science

Chulalongkorn University

Academic Year 2011

Thesis Title   DENDRITIC POLYELECTROLYTES AS FLUORESCENT
                    APTASENSORS FOR POTASSIUM ION
By   Miss Wannapa Yuanboonlim
Field of Study   Chemistry
Thesis Advisor   Associate Professor Mongkol Sukwattanasinitt, Ph.D.

Accepted by the Faculty of Science, Chulalongkorn University in Partial Fulfillment of the Requirements for the Master's Degree

………………………………………….. Dean of the Faculty of Science
        (Professor Supot Hannongbua, Dr.rer.nat.)

THESIS COMMITTEE

………………………………………….. Chairman
        (Assistant Professor Warinthorn Chavasiri, Ph.D.)

…………………………………….………. Thesis Advisor
        (Associate Professor Mongkol Sukwattanasinitt, Ph.D.)

…………………………………….………. Thesis Co-advisor
        (Assistant Professor Paitoon Rashatasakhon, Ph.D.)

………………………………………….. Examiner
        (Associate Professor Tirayut Vilaivan, Ph.D.)

………………………………………….. Examiner
        (Monpichar Srisa-Art, Ph.D.)

………………………………………….. External Examiner
        (Assistant Professor Pan Thongraung, Ph.D.)

วรรณนภา ย้วนบุญหลิม : เดนดริติกพอลิอิเล็กโทรไลต์เพื่อเป็นแอปทาเซ็นเซอร์วาวแสง สำหรับโพแทสเซียม. (DENDRITIC POLYELECTROLYTES AS FLUORESCENT APTASENSORS FOR POTASSIUM ION) อ.ที่ปรึกษาวิทยานิพนธ์หลัก : รศ.ดร.มงคล สุขวัฒนาสินิทธิ์, อ.ที่ปรึกษาวิทยานิพนธ์ร่วม : ผศ.ดร.ไพฑูรย์ รัชตะสาคร, 73 หน้า.

ฟลูออโรฟอร์ของฟีนิลลีนอีทายนิลลีนที่มีหมู่แอมโมเนียม 3 กลุ่มเป็นองค์ประกอบ สังเคราะห์ได้จากปฏิกิริยาคู่ควบโซโนกาชิรา ใช้คอปเปอร์-แพลเลเดียมเป็นตัวเร่งปฏิกิริยาระหว่าง หมู่ 4,4',4''-ไตรไอโอโดไตรฟีนิลเอมีนที่เป็นแกนกลาง กับหมู่ล้อมรอบ N,N-ไดเมทิล-4-อีทาย นิลอะนิลีน ทำการเมทิลเลชันหมู่เอมีนด้วยเมทิลไอโอไดด์ จากนั้นนำโมเลกุลที่สังเคราะห์ได้มา แลกเปลี่ยนเคาน์เตอร์ไอออนจากไอโอไดด์ไออออน เป็นคลอไรด์ไออออน เพื่อให้โมเลกุลของฟลูออโร ฟอร์ที่สังเคราะห์ได้เสถียรขึ้น และสามารถเก็บในสถานะของแข็งได้นานขึ้นโดยไม่เกิดการ เปลี่ยนแปลงสภาพการละลาย เนื่องจากลดการเกิดปฏิกิริยาดีเมทิลเลชันของหมู่ไตรเมทิลแอมโม เนียมลง เพราะคลอไรด์ไออออนมีความเป็นนิวคลีโอไฟล์น้อยกว่าไอโอไดด์ไออออน จากนั้นนำสารที่ สังเคราะห์ได้มาละลายในบัฟเฟอร์ Tris-HCl เข้มข้น 10 mM pH 7.4 พบว่าให้ค่าการดูดกลืนแสง และการคายแสงสูงสุดที่ 372 และ 386 nM ตามลำดับ และมีประสิทธิภาพในการเรืองแสงเท่ากับ 6.6% เนื่องจากสารที่สังเคราะห์มีประจุรวมเป็นไออออนบวกจึงสามารถเกิดอันตรกิริยากับโมเลกุล แอปทาเมอร์โอลิโกนิว คลีโอไทด์ได้ เนื่องจากมีประจุรวมเป็นไออออนลบ ในงานวิจัยนี้เลือกใช้สาย โอลิโกนิวคลีโอไทด์ที่มีความจำเพาะเจาะจงกับไออออนของโพแทสเซียมเรียกว่าแอปทาเมอร์ เพื่อ นำไปใช้สำหรับทำเป็นเซ็นเซอร์ตรวจวัดปริมาณโพแทสเซียมไออออนที่มีอยู่ในร่างกาย ด้วยเลือกใช้ แอปทาเมอร์ที่มี 12, 15 และ 21 เบส และใช้สายโอลิโกนิวคลีโอไทด์ที่ไม่ใช่แอปทาเมอร์อีก 1 เส้น ที่มี 15 เบส จากนั้นได้ศึกษาหาอัตราส่วนที่เหมาะสมในการจับกันระหว่างฟลูออโรฟอร์กับแอปทา เมอร์จาก Job's plot ได้เป็น 1:2, 1:1 และ 1:1 ตามลำดับ และพบว่าสัญญาณการวาวแสงเพิ่มขึ้น จากการลดขบวนการจีโอเมทริคัลรีแลกซีชัน เมื่อเติมไออออนของโพแทสเซียมลงในสารละลายของ ฟลูออโรฟอร์กับแอปทาเมอร์ จะเกิดการเปลี่ยนแปลงคอนฟอร์เมชันของแอปทาเมอร์เป็น G-quadruplex นำไปสู่การลดสัญญาณการวาวแสงจึงสามารถนำมาใช้ตรวจวัดไออออนโพแทสเซียม ได้และนำมาประยุกต์ใช้สำหรับตรวจหาปริมาณโพแทสเซียมในปัสสาวะ โดยพบว่าเป็นวิธี วิเคราะห์ที่รวดเร็ว, ง่าย, lable free และมีความจำเพาะเจาะจงในการวิเคราะห์ไออออนของ

ภาควิชา	เคมี	ลายมือชื่อนิสิต
สาขาวิชา	เคมี	ลายมือชื่อ อ.ที่ปรึกษาวิทยานิพนธ์หลัก
ปีการศึกษา	2554	ลายมือชื่อ อ.ที่ปรึกษาวิทยานิพนธ์ร่วม

5272654923: MAJOR CHEMISTRY

KEYWORDS: APTASENSORS / DENDRITIC POLYELECTROLYTES

WANNAPA YUANBOONLIM: DENDRITIC POLYELECTROLYTES AS FLUORESCENT APTASENSORS FOR POTASSIUM ION. ADVISOR: ASSOC. PROF. MONGKOL SUKWATTASINITT, Ph.D. CO-ADVISOR: ASSOC. PROF. PAITOON RASHATASA- KHON, Ph.D., 73 pp.

A tricationic phenyleneethynylene fluorophore containing three ammonium groups was synthesized from Sonogashira coupling of triiodotriphenylamine with three equivalents of *N,N*-dimethyl-4-ethynylaniline using Pd/Cu catalyst. Quaternization of the three dimethylaniline groups was accomplished by methylation with methyl iodide. The iodide salt, however, tended to demethylate upon storage in a solid form and became poorly soluble in water. The strongly nucleophilic I^- was thus exchanged to a less nuleophilic Cl^- using Amberlite IRA-410 anionic ion exchange resin. The fluorophore containing Cl^- counter ion was stable and retained its water solubility upon storage. In Tris-HCl buffer, the synthesized compound exhibited maximum absorption and emission at 372 and 386 nm, respectively, with a quantum yield of 6.6%. The polycationic periphery was designed for charge interaction with polyanionic oligonucleotide chain. Three potassium aptameric ODNs *i.e.* Apt12, Apt15 and Apt21, and one non-aptameric ODN (nApt15) were tested for K^+ aptasensing properties. A job's plot showed the binding ratios of fluorophore/aptamer of 1:2, 1:1 and 1:1 for Apt12, Apt15 and Apt21, respectively. Upon complexation with the aptamer ODNs, the fluorescent signal was enhanced probably by the reduction of geometrical relaxation and aggregation process. In the presence of K^+, the fluorescent signal decreases by the formation of the K^+-aptamer G-quaduplex structure. Monitoring the fluorescent signal provided a method for determination of K^+ concentration in urine samples.

Department : Chemistry	Student's Signature	
Field of Study : Chemistry	Advisor's Signature	
Academic Year : 2011	Co-advisor's Signature	

ACKNOWLEDGEMENTS

CONTENTS

LIST OF TABLES

LIST OF FIGURES

Figure   **Page**

LIST OF SCHEMES

LIST OF ABBREVIATIONS

A	acceptor
Ar	aromatic
calcd	calculated
^{13}C NMR	carbon-13 nuclear magnetic resonance
$CDCl_3$	deuterated chloroform
D	donor
d	doublet (NMR)
dd	doublet of doublet (NMR)
ESIMS	electrospray ionization mass spectrometry
equiv	equivalent (s)
FT-IR	fourier transform infrared spectroscopy
g	gram (s)
^{1}H NMR	proton nuclear magnetic resonance
Hz	Hertz
HRMS	high resolution mass spectrum
h	hour (s)
ICT	internal charge transfer
IR	infrared
J	coupling constant
mg	milligram (s)
mL	milliliter (s)
mmol	millimole (s)
m/z	mass per charge
m	multiplet (NMR)
mp	melting point
M.W.	molecular weight
M	molar
MHz	megahertz
rt	room temperature
s	singlet (NMR)

THF	tetrahydrofuran
UV	ultraviolet
δ	chemical shift
°C	degree Celsius
μL	microliter (s)
μM	micromolar (s)
Φ	quantum yield
% yield	percentage yield

CHAPTER I

INTRODUCTION

1.1 Supramolecular chemistry

Supramolecular chemistry is a study of new molecular systems in the field of noncovalent interactions between host and guest molecules as defined by Jean-Marie Lehn [1]. Traditionally, chemists have focused primarily on understanding the behavior of molecules and their construction from constituent atoms. At the present, researchers in the field of supramolecular chemistry are interested in the weaker and reversible noncovalent interactions, such as hydrogen bonding, dative bonding, hydrophobic forces, (London) dispersion forces, π-π stacking interactions, and electrostatic effects [2] involving in molecular self-assembly, molecular folding, molecular recognition, host-guest chemistry, mechanically-interlocked molecular architectures, and dynamic covalent chemistry [3]. In addition, the study of noncovalent interactions is crucial to understanding many biological forms and processes. The desire to understand and imitate biological systems often provides the motivation behind supramolecular chemical research [4-5].

1.2 Molecular structures of some conjugated fluorophores

Attention in chemical and bio-sensing systems relies upon rapid and high selectivity. The methods have been progressively improved using redox [6], chromogenic [7], or fluorogenic [8] changes as the detection signals. Conjugated polymers (CPs) have emerged as one of the most important classes of transducing materials. They transform a chemical signal to easily measurable electrical or optical events. Fluorescence based methodologies have attracted much interest due to their intrinsic sensitivity and selectivity [9]. Considerable efforts have been devoted to the design of fluorescent compounds to be used as transducers. CPs with delocalized π-electron systems have attracted an overpowering interest due to their versatile optical and electrical properties [10]. Figure 1.1 shows structures of a variety of CPs commonly investigated, including polythiophene (1) [11], polypyrrole (2) [12], polyfluorene (3) [13], poly(para-phenylene vinylene) (4) [14], and poly(para-phenyleneethynylene) (5) [15]. The delocalized electronic structure of CPs enables

them to exhibit efficient absorption and strong emission, and produce amplified signal changes upon interacting with various analytes.
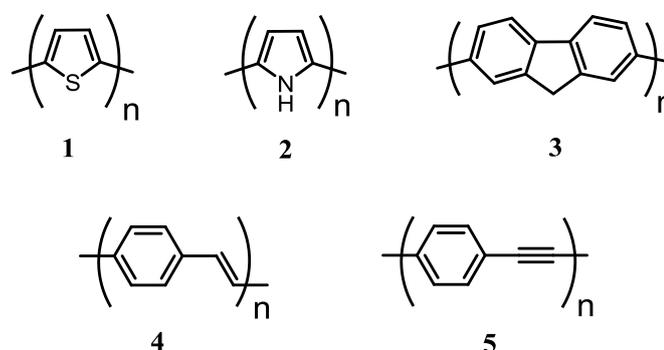
Figure 1.1 Molecular structures of some common conjugated polymers (CPs).

Phenyleneethynylene is an important class of π-conjugated molecules currently applied as fluorescent transducers in various optical sensing systems. Critical features spurring interest in and usefulness of this class of compounds include their structural rigidity allowing more predictable geometry, high fluorescence quantum efficiency and efficient syntheses. During the past decade, a number of crucial developments of both small and polymeric phenyleneethynylene conjugated systems have been witnessed, mostly containing para-phenyleneethynylene moieties, into more sensitive and selective sensors for wider applications. Palladium-catalyzed cross-coupling polymerization offers the benefits of mild reaction conditions, wide functional group, and solvent compatibility for preparation of many para-phenyleneethynylenes [16].

This thesis focuses mainly on the synthesis, photophysical investigations and sensing applications of polycationic phenyleneethynylenes by incorporation of appropriate interfacial groups as sensing probes for specific or selective biological sensors.

1.3 Water-soluble dendrimer

Conjugated polymeric polyelectrolytes (CPEs) are conjugated polymers containing multiple charges which make them water-soluble (Figure 1.2). Polyelectrolytes can either be cationic or anionic and commonly used ionic side groups including sulfonate ($-SO_3^-$), phosphonate ($-PO_3^{2-}$) carboxylate ($-CO_2^-$), and alkyl ammonium ($-NR_3^+$); zwitterionic polymers called polyampholytes [9, 16, 17].

This interesting class of polymers has been under intense research for applications in optical sensors during the past few decades [18]. The most CPE-based sensor approaches developed based on electrostatic interaction between the probes and the target ionic species, such as metal ions, anions, DNA, proteins, virus bacteria and cancer cells [9].
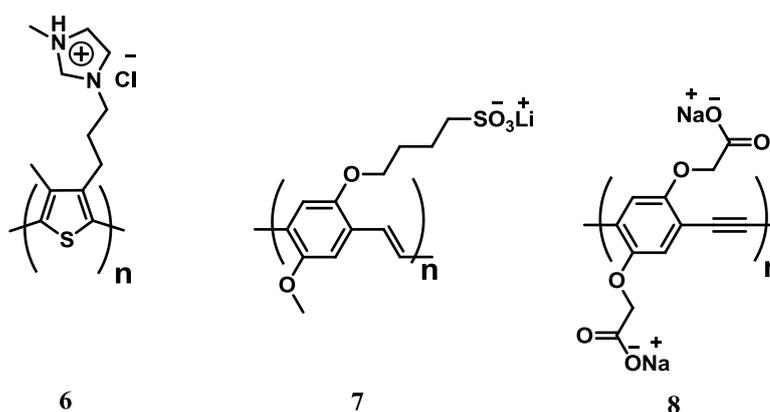
Figure 1.2 Molecular structures of some common CPEs.

Poly(para-phenyleneethynylene)s (PPEs) are representatives of poly(arylene-ethynylene) (PAE) in the CP family having benzene rings as the aromatic groups connecting via triple bonds with 180° bond angle between the phenyl carbon and sp^1 carbon [19]. Compared with its PPV analogues, the first group of CP used in fluorescence-based sensors for biological targets [20], PPEs [21] have more predictable geometry and exhibit higher quantum yield in solution. Due to their optimal photophysical characteristics, PPEs have been explored as an important class of CPs for sensing applications as potential fluorescent transducers [22, 23]. PPEs have been well studied and applied to many sensory systems, including methyl viologen salt sensor [24], TNT sensors [25], and metal ion sensors [26]. The PPEs not only feature superior photostability compared to other CPEs, such as PPVs, but they also demonstrate different electronic and optical properties from the parent molecules upon structural modifications. The main chains of PPEs have three isomers: ortho-, meta- and para-, defined by their different connectivity via the acetylenic groups. Different aromatic building blocks can also be introduced into the conjugated backbone to engineer the electronic properties (Figure 1.3) [27]. Also, variable side chains can be introduced to modify the polymer structures (**9-12**) and their

supramolecular interactions. All these strategies are meant to make the PPEs amphiphilic, water-soluble, highly fluorescent, and able to interact with targets.
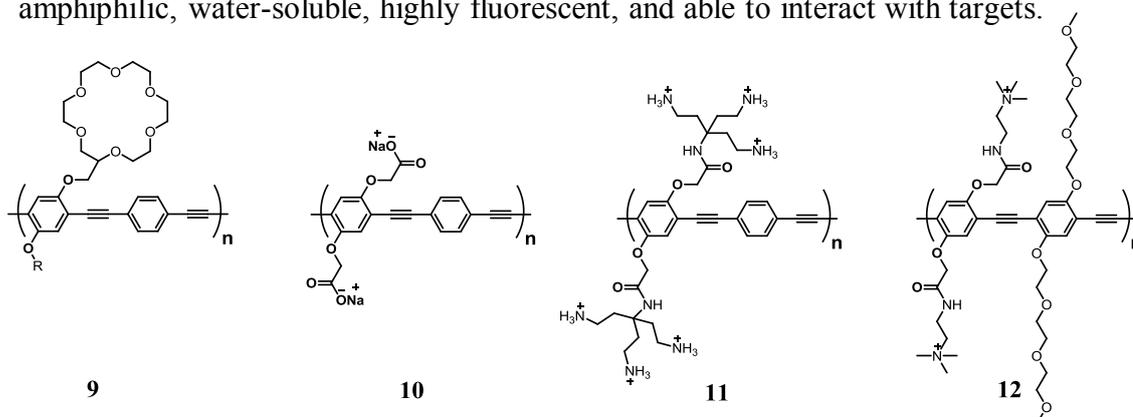
Figure 1.3 Examples of PPEs with different structural modifications.

1.4 Fluorescent sensors based on dendritic structures

Nine dendritic fluorophores structures with various electronic charges as shown in Figure 1.4 have been synthesized. The charge variation is accomplished by the combination of cationic trimethyl ammonium, anionic carboxylate and non-ionic methylester or N,N-dimethyl amino on the peripheries of the fluorophores. The series include seven zeroth generation dendrimers ($3N^+$, C^02N^+, $2C^0N^+$, $2C^-N^+$, C^-2N^0, $2C^-N^0$ and $3C^-$) with the electronic charges varied from −3 to +3 and two first generation dendritic fluorophores ($6N^+$ and $6C^-$) with −6 and +6 charges. The fluorophores have been successfully used in the development of protein sensing arrays. The array is capable of identify the types of proteins via fluorescent patterns and multivariate statistical analysis.
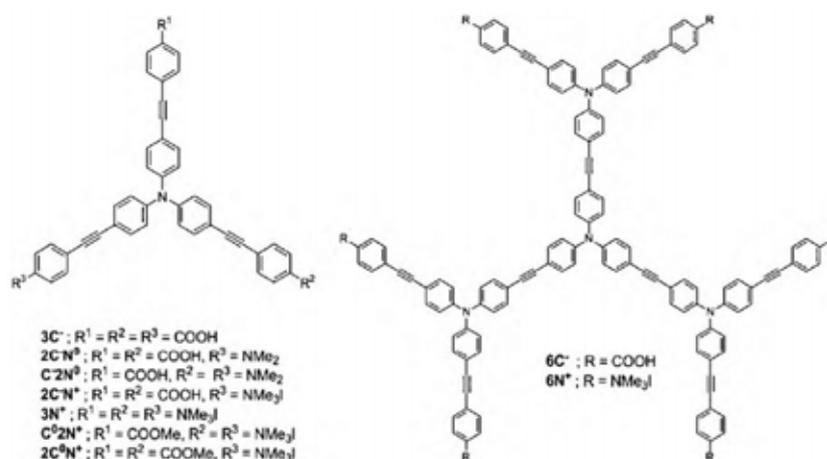
Figure 1.4 Structures of variously charged dendritic fluorophores [28].

In comparison with linear CPEs, small fluorescent molecules offer better defined structures and conformation that lead to greater understanding of the sensing mechanism. Therefore, a dendrimer obtained from controlled stepwise synthesis should provide an opportunity to study a combined amplification effect of the polymers with a well-defined structure of small molecules and will be the focus of this thesis work.

1.5 Fluorescence phenomena

The fluorescent processes that occur between the absorption and emission of light are usually described by the Jablonski diagram [29]. Jablonski diagrams are used in a variety of forms, to illustrate various molecular processes that can occur in excited states. A simplified Jablonski diagram shown in **Figure 1.5** illustrates that upon absorption of photons, a fluorophore (F) is excited to singlet excited electronic states (S1 or S2) and form an excited fluorophore (F*). The fluorescence signal is observed when F* relaxes to ground singlet electronic state (S0) via photon emission. The time required to complete this whole process takes nano-second.
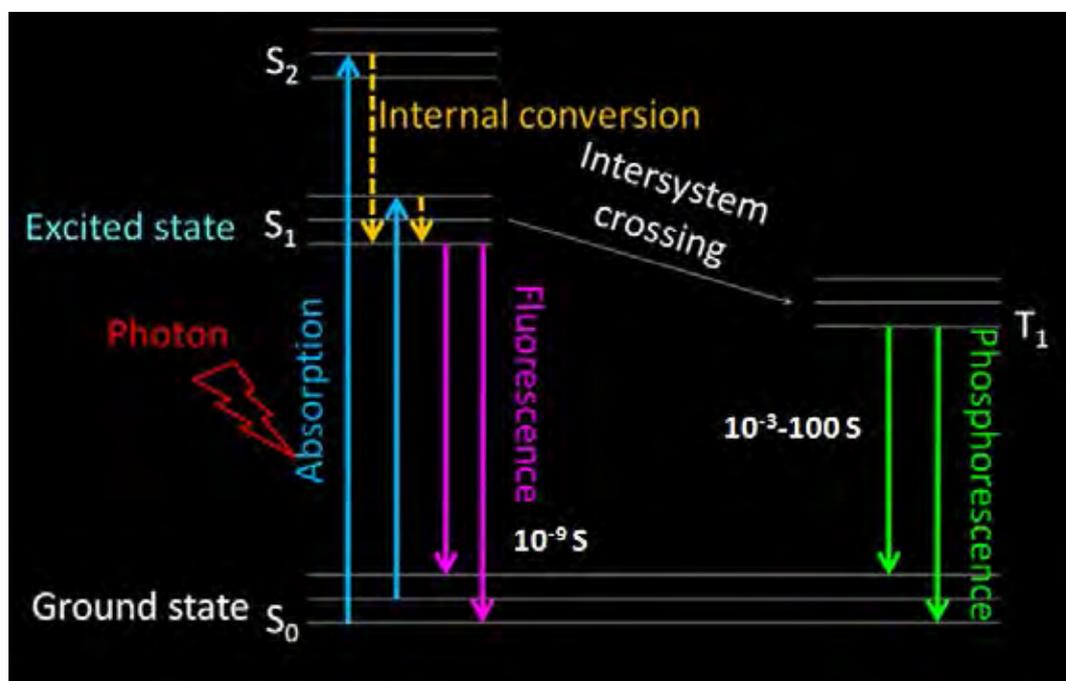
Figure 1.5 Simple Jablonski diagram illustrating fluorescent processes.

1.6 Importance of potassium ion

Potassium ions (K^+) are involved in many biological functions, such as the maintenance of extracellular osmolarity, the regulation of other ions in organisms and the production of electrical signals in nerve systems related to Na^+-K^+ pump process [30, 31], regulation of blood pressure and pH, enzyme activation of Na^+/K^+-ATPase, and the formation of collagen or elastin [32, 33, 34]. An abnormal potassium ion concentration in biological fluids can lead to several diseases such as kidney, Addison's and adrenal gland diseases [35, 36]. The normal concentration range of potassium ion in human blood plasma is 3.5-5 mM [37]. The daily reference intake (DRI) of 4000 mg potassium has been proposed [38] and a lower risk of stroke was found to be associated with a little higher intake [39]. Development of a sensing system for the reliable quantification of potassium ion is thus of importance for medical diagnosis and nutritional analysis.

1.7 Aptasensors for potassium ion

In common medical practice, potassium ion concentration is determined by a medical instrument called gas analyzer, in which the potassium ion is quantified by an ion selective electrode [40, 41]. The method is however required rather expensive operation and instrumental calibrations are generally required. An optical method is a particularly interesting alternative to the electrochemical method as its detection is fast, sensitive and requires relatively inexpensive instrument. Among all optical methods, fluorometry is one of the most attractive methods due to its operational simplicity and high sensitivity. To date, homogeneous fluorescent K^+-sensing systems are limited to a few examples. In 1999, Szmacinski et al. [40] have reported the synthesis of fluorescent marocyclic ionophores containing the crown ethers with an electron-rich cavity to bind the cation. The cavity size matches the diameter of sodium and potassium ion. The ionophores change their fluorescence intensity upon binding with either sodium or potassium cation. The probe SBFI and SBFO are selective to Na^+ while PBFI and CD222 are selective to K^+. However, these ionophores give rather high detection limit of 5 mM for potassium ion.
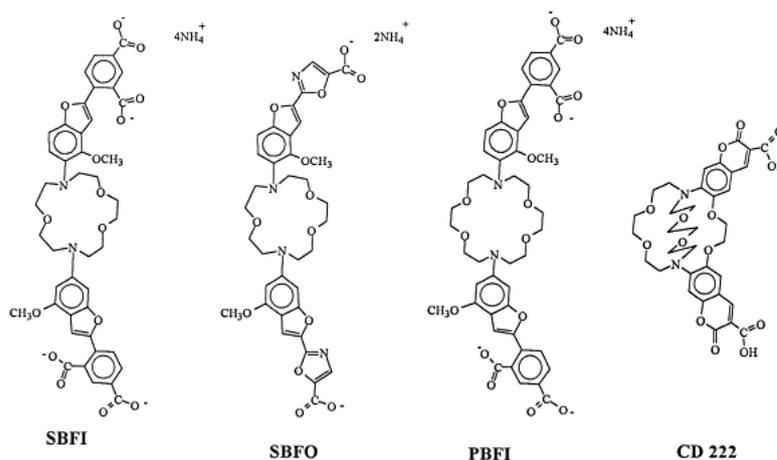
Figure 1.6 Chemical structures of sodium and potassium fluorescent probes.

For most simple fluorometric sensing systems, poor selectivity against Na^+ ion prevents them from practical uses [42, 43]. Recently, aptamer based sensing systems have gained much attention due to their high sensitivity and selectivity. A most typical aptamer is a single-stranded DNA or RNA, isolated from large a pool of random-sequence oligonucleotides, that is capable of binding a designated chemical or biological entity with high affinity and specificity [44-46]. K^+ aptamers are one of the best known classes of aptamers which have been applied in sensing systems. K^+ aptamers are a G-rich oligonucleotides which can form a four-stranded helical conformation in solution called G-quadruplex with stacked arrays of G-quartets connected by Hoogsteen-type base pairing [47-50]. The stability of this conformation is greatly enhanced by potassium ion and highly selective K^+ detection based on the formation of G-quadruplex structures of K^+ aptamers and fluorescent labeled probes have been reported.

In 2000, Marathias et al. [48] have reported that potassium can stabilize the formation of chair- or edge-type quadruplex DNA structures and appears to be the only naturally occurring cation that can do so. As quadruplex DNAs may be important in the structure of telomere, centromere, triplet repeat and other DNAs, information about the details of the K^+–quadruplex DNA interactions are of interest. The structures of 1:1 and fully saturated, 2:1, potassium–DNA complexes of d(GGTTGGTGTGGTTGG) have been determined using the combination of experimental NMR results and restrained molecular dynamic simulations. The refined

structures have been used to model the interactions at the potassium binding sites. Comparison of the 1:1 and 2:1 potassium:DNA structures indicates how potassium binding can determine the folding pattern of the DNA. In each binding site potassium interacts with the carbonyl oxygens of both the loop thymine residues and the guanine residues of the adjacent quartet.
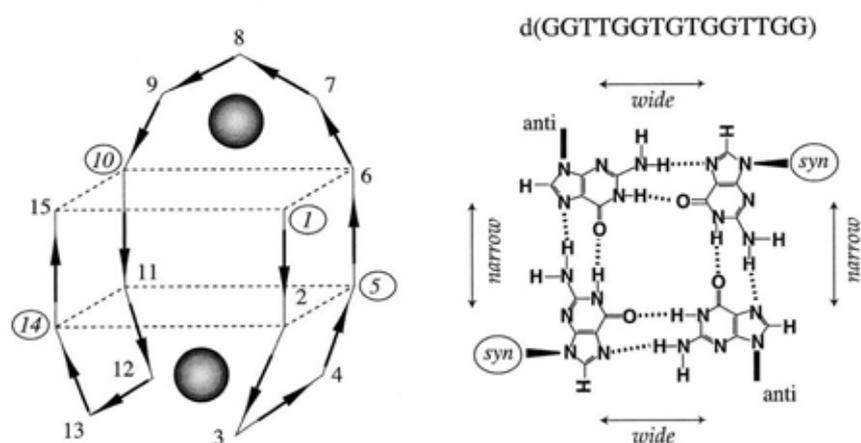
Figure 1.7 The structure of the chair-type quadruplex structure of d(GGTTGGTGT GGTTGG) is shown along with the positions of the two strong potassium binding sites. The positions of the potassium binding sites are indicated by the shaded spheres. On the right is shown the *syn-anti-syn-anti* arrangement of the dG residues in each of the two quartets of the chair-type structure.

In 2002, Ueyama et al. [51] have constructed a novel potassium sensing oligonucleotide (PSO) which can detect K^+ in water. Potassium sensing may be performed when two chromophores which can undergo Förster resonance energy transfer (FRET) are attached to the termini of the telomere oligonucleotide. PSO carries a part of the human telomere sequence, d(GGGTTAGGGTTAGGGTTA GGG), with two fluorophores, 6-carboxyfluorescein (6-FAM) and 6-carboxy tetramethylrhodamine (6-TAMRA), at the 5′- and 3′-termini of the oligonucleotide as the donor and acceptor, respectively. Conditions were set where this oligonucleotide can form a tetraplex structure in the presence of K^+ and the two chromophores come close to each other to bring about FRET, as shown in **Figure 1.8**, and therefore K^+ can be detected from the magnitude of FRET. PSO responses only to K^+ in the

concentration range from 0 to 2.5 mM. It responses to NH_4^+, Na^+, and Rb^+ at higher concentrations of 300 mM as well but not to Li^+ and Cs^+.
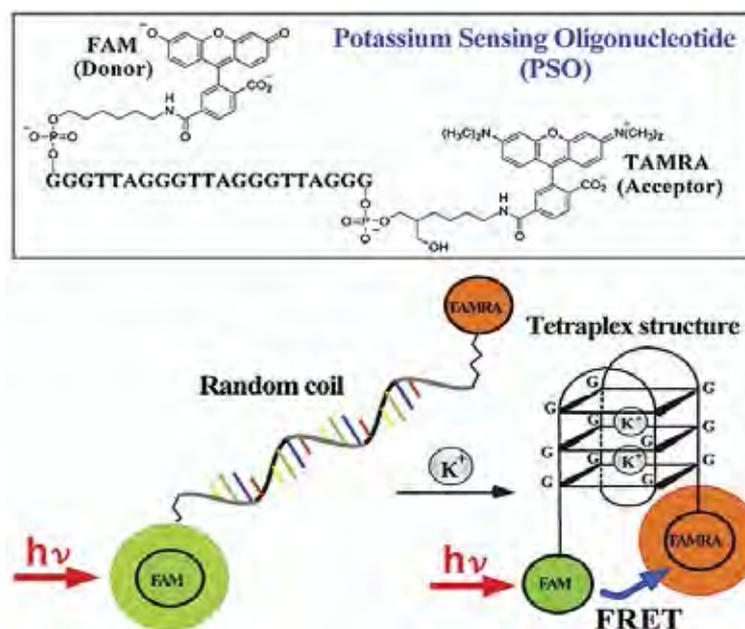
Figure 1.8 Structure of PSO and its schematic tetraplex structure induced by K^+, resulting in a FRET change.

In 2005, He et al. [52] have developed novel fluorescent biosensors based on water-soluble cationic conjugated polymers (CCPs) to detect DNA and RNA in aqueous media. This contribution shows a new FRET-based homogeneous technique to recognize the guanine quadruplex structure of the DNA that couples the conformation of a guanine-rich oligonucleotide strand with the optical amplification of CCPs. The G-quartet-DNA/CCPs assembly can also be used as a platform for sensing K^+ in water with high selectivity and sensitivity. Poly(9,9-bis(6′-*N,N,N*-trimethylammonium)hexyl)fluorenylene phenylene (PF) was used as CCP in energy-transfer experiments. The G-rich single-stranded DNA was labeled with a fluorescein at the 5′-terminus (ssDNA-Fl). The ssDNA-Fl exhibits a random coil conformation in the absence of K^+. The relatively weak electrostatic interactions of ssDNA-Fl with CCP keep the fluorescein far away from CCP, and FRET from CCP to fluorescein is inefficient (Figure 1.9). The formation of a more condensed G-quadruplex upon adding KCl increases the space charge density around the DNA macromolecule and

results in stronger G-quartet-DNA/PF electrostatic interactions, relative to ssDNA-Fl/PF, and therefore, efficient FRET from CCP (donor) to fluorescein (acceptor) is observed.
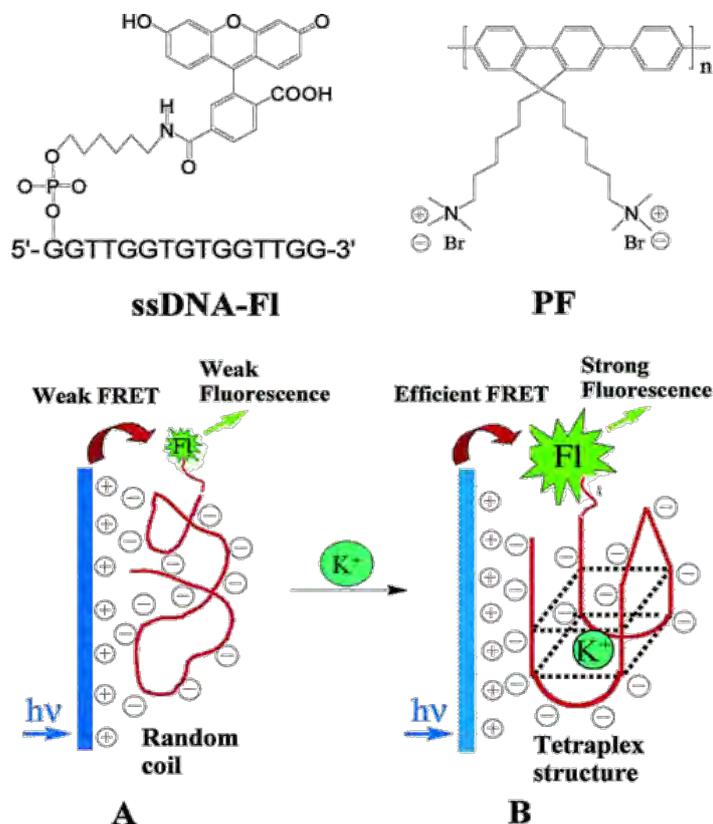
Figure 1.9 Schematic representation of the G-quadruplex structure and K^+ assays and chemical structures of ssDNA-Fl and cationic polyfluorene

In 2007, Nagatoishi et al. [53] have designed and synthesized dual-labeled oligonucleotide derivative, FAT-0, carrying 6-carboxyfluorescein (FAM) and 6-carboxy-tetramethylrhodamine (TAMRA) labeled at 5′- and 3′-termini of thrombin-binding aptamer (TBA) sequence 5′-GGTTGGTGTGGTTGG-3′ and its derivatives, FAT-n (n = 3, 5, and 7). FAT-n derivatives contained a T_mA spacer (m = 2, 4, and 6, respectively) at 5′-end of TBA sequence. The probes were developed to estimate the spacer effect on FRET efficiency and to identify the best probe for sensing of K^+. FAT-0 (no spacer) showed the lowest sensitized emission of acceptor (TAMRA) in the presence of K^+ because of the quenching of TAMRA fluorescence due to the dye–dye interactions with FAM. After DNA probes which containing spacers was added the K^+, the result show the enhancement of TAMRA fluorescence, due to the

prevention of the dye–dye interaction. Presented here results unambiguously confirmed that the addition of a spacer significantly reduced contact quenching between FRET partners and improved the performance of the FAT-*n* probes. They found that FAT-5 and FAT-7 probes were suitable for detection of K^+ under intracellular and extracellular conditions. Calibration graphs of fluorescence ratio were linear in the K^+ concentration range of 2–10 mM for extracellular conditions, showing sensitivity of 1.2% mM^{-1} K^+ and for intracellular conditions in the range of 100–200 mM with sensitivity of 0.49% mM^{-1} K^+.
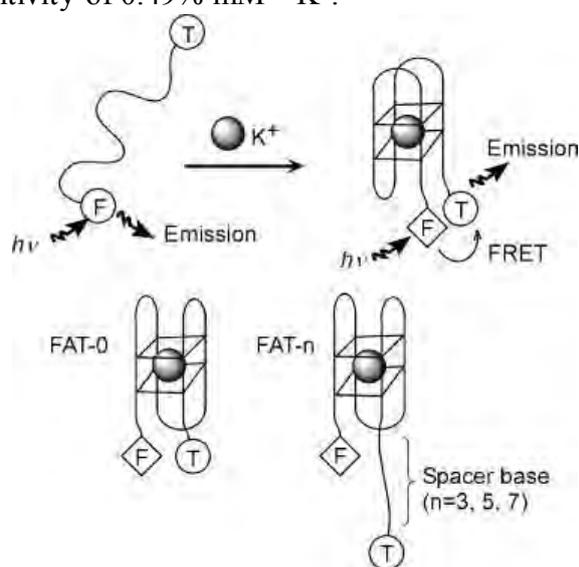
Figure 1.10 Expected structural changes of FAT-*n* exerted by the complex formation with K^+ and differences in FAT-*n* structures.

In 2008, Chen et al. [54] have reported a G-quadruplex structure and a probe for detection of K^+. Two PSOs (PSO-1 and PSO-2) were applied for potassium detection. PSO-1 and PSO-2 are oligonucleotides which have human [G3(TTAG3)3] and *Oxytricha* [G4(T4G4)3] telomere sequences carrying two fluorophores, FAM and TAMRA, at the 5′- and the 3′-end, respectively. Forunfolded structure of PSO, little FRET was expected since the average distance between the donor (FAM) and the acceptor (TAMRA) exceeds the critical radius. Under cation conditions, PSO-1 and PSO-2 were expected to form intramolecular quadruplex structures bringing the two tagging fluorophores close to each other, resulting in FRET.

a
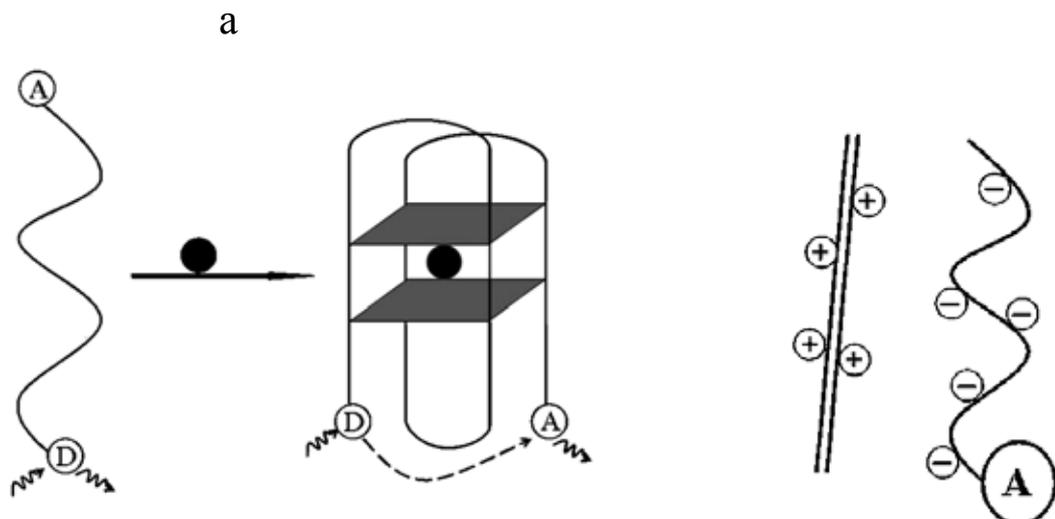
Figure 1.11 Schematic illustrations of FRET process used for K^+ detecti
donor (D) emits photons without acceptor (A) in proximity. In the presence o_ _ _ , _ _
antiparallel intramolecular quadruplex is formed bringing the two fluorophores closer.
Then the acceptor takes the energy from the donor and emits photons.

In 2010, Chao et al. [55] have developed a novel and sensitive biosensor based
on aptamer and pyrene-labeled fluorescent probes for the determination of K^+. The
aptamer was used as the ion recognition element and a partially complementary
oligonucleotide labeled by pyrene moieties at both ends as a transducer for the
binding event of K^+ with the aptamer. In the presence of K^+, the complementary
oligonucleotide was displaced from the aptamer, which was accompanied by excimer
fluorescence of pyrenes because the self-hairpin structure of the complementary
oligonucleotide brought pyrene moieties into a close proximity. However, it gave only
the monomer emission in the absence of K^+. Under an optimum condition, the relative
fluorescence intensity of pyrene was proportional to the concentration of K^+ in the
range of 6.0×10^{-4} to 2.0×10^{-2} M. A detection limit of 4.0×10^{-4} M was achieved.
Moreover, this method was able to detect K^+ with high selectivity in the presence of
Na^+, NH_4^+, Mg^{2+}, and Ca^{2+} ions in biological fluids.
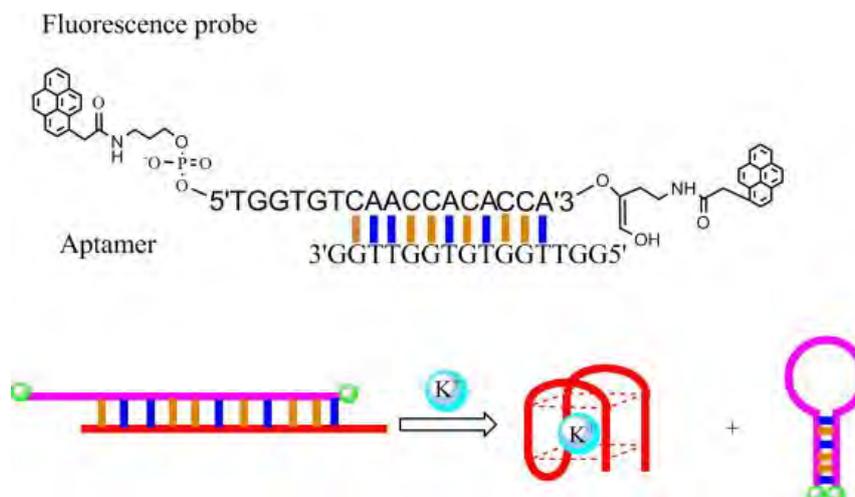
Figure 1.12 A general strategy for DNA/aptamer-based optical biosensors: a chemical structure of the pyrene-labeled molecular beacon and the expected hairpin structure formation induced by K^+ ions.

If the 5′- and 3′-ends of the oligonucleotide are labeled with a donor fluorophore and an acceptor fluorophore, respectively, the formation of G-quadruplex structures will bring the two fluorophores close to each other, thus resulting in fluorescence resonance energy transfer (FRET) [56-58]. This type of probe, frequently called molecular beacon, shows high selectivity and sensitivity for K^+ detection. However, it requires dual fluorescent-labeled oligonucleotides, which increase the cost of detection. Label-free methods for potassium ion detection using a K^+ aptamer and commercial fluorescent dyes such as Oligreen [56], crystal violet [57] and tetrakis-(diisopropylguanidino) zinc phthalocyanine (Zn-DIGP) [58] have also recently emerged as a more economical alternative.

In 2008, Huang et al. [56] reported a molecular fluorescence switching method to signal aptamer–K^+ binding using an ATP-binding aptamer dACCTGGGGGAGTA TTGCGGAGGAAGGT) and OliGreen (OG), a commercially available asymmetrical cyanine dye that is used to label oligonucleotides. OG is weakly fluorescent, but exhibits a greater-than-1000-fold enhancement in its fluorescence upon binding to ssDNA outlines the sensing mechanism shown in **Figure 1.13.** When the ATP-binding aptamer (Apt) in its random-coil (ss) structure is added to an OG solution, an OG-Apt complex is formed immediately, leading to increasing in fluorescence. After

adding K$^+$, the conformation of Apt changes from that of a random coil to two stacked G-quadruplexes and two short double-helix stems. Because OG prefers binding to ssDNA, dissociation of the OG-Apt complex occurs to some extent upon this conformational change. As a result, the fluorescence of the system decreases in the presence of K$^+$. The selectivity of this system for K$^+$ over other ions in aqueous solution is remarkably high (>10,000-fold over Na$^+$) and its LOD is 75 nM. The present approach has several advantages over other assays: it is rapid (<15 min), label-free, simple, and cost-effective.
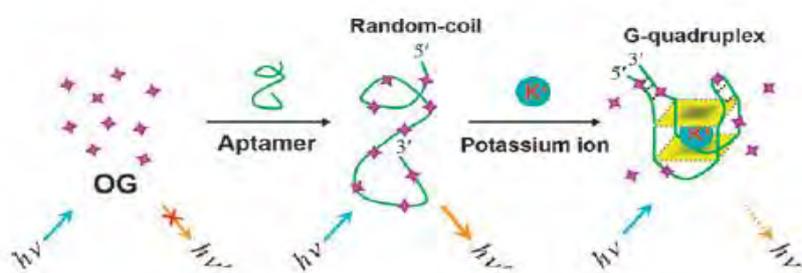
Figure 1.13 Schematic representation of a K$^+$ sensor based on modulation of the fluorescence of the complex formed between an OG dye and an ATP-binding aptamer. h: Planck's constant; *v*: frequency of light.

In 2009, Kong et al. [57] have reported a novel K$^+$ detection method using a label-free G-quadruplex-forming oligonucleotide and a triphenylmethane fluorescent dye crystal violet (CV). This method is based on the fluorescence difference of some CV/G-quadruplex complexes in the presence of K$^+$, and the fluorescence change with the variation of K$^+$ concentration. According to the nature of the fluorescence change of CV as a function of ionic conditions, two K$^+$ detection modes can be developed. One is a fluorescence-decreasing mode, in which T$_3$TT$_3$ (5'-GGGTTTGGG TGGGTTTGGG) is used, and the fluorescence of CV decreases with an increase in K$^+$ concentration. The other is a fluorescence-increasing mode, in which Hum21 (5'-GGGTTAGGGTTAGGGTTAGGG) is used, and the fluorescence of CV increases with an increase in K$^+$ concentration (Figure 1.14). This method has some important characteristics, such as its economical nature, higher concentrations of Na$^+$ that can be

tolerated, adjustable linear detection range and longer excitation and emission wavelengths.
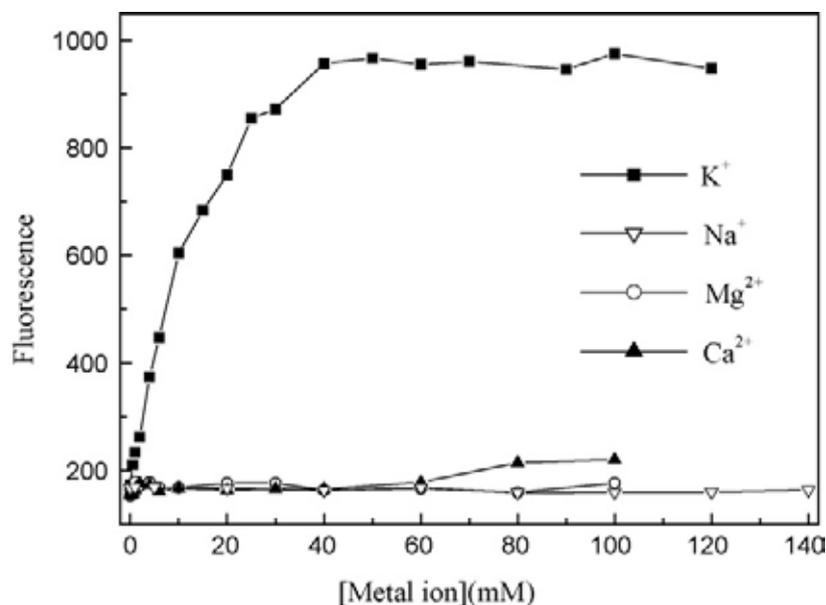
Figure 1.14 Fluorescence change of a CV/Hum21 complex as a function of K^+, Na^+, Mg^{2+} and Ca^{2+} show selectivity for potassium ion detection.

In 2010, Qin et al. [58] have reported a label-free detection of K^+ using G-quadruplex DNA (c-Myc: 5′-TGAGGGTGGGGAGGGTGGGGAA-3′) modulated fluorescence enhancement of tetrakis-(diisopropylguanidino) zinc phthalocyanine (Zn-DIGP). Upon the addition of increasing concentrations of potassium, a detection limit of 0.8 μM K^+ has been achieved. Comparative titrations using sodium, lithium, ammonium, transition metal and alkali earth salts have revealed that fluorescence enhancement was highly specific for potassium ions. This system has provided a means for detecting K^+ at a concentration of 40 μM even in the presence of a 3500-fold excess of Na^+ ions.
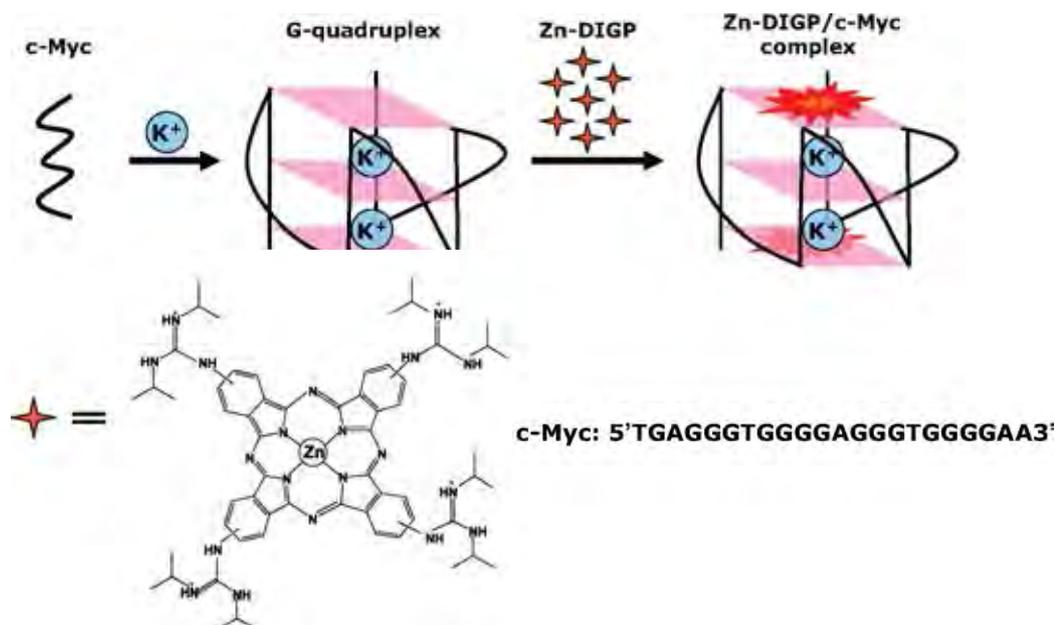
Figure 1.15 Schematic illustration of a label-free assay for K$^+$ ions.

The sensitivity and selectivity of these label-free sensing systems are likely to be interdependent on the subtle supramolecular interactions among a signal transducer, a sensing probe and ananalyst which are dye molecules, a conformationally labile oligonucleotide strand and a metal ion, respectively. It is thus of interest to investigate the effects of interactions between a aptamer with different lengths and a dye molecule on the sensitivity and selectivity of a sensing system. In this study, we chose to use three known K$^+$ aptamers (Apt12, Apt15 and Apt21 in Scheme 1.1) as K$^+$ probes and one of our recently synthesized polycationic fluorophores [59], (N^{3+} in Scheme 1.1) as the signal transducer due to its well defined structure and its multi-cationic nature which is aimed for strong coulombic interaction with the aptamers which are polyanionic oligonucleotides. The basis of this work, as illustrated in Scheme 1.1, relies on the assumption that there is a significant interaction between the cationic dendritic fluorophores N^{3+} and the aptamers. The aptamer forms complex with the fluorophore that enhances and blue shift the

fluorescence signal probably by the reduction of geometrical relaxation process, solvent and self-quenching. Upon addition of K^+, the aptamer switches to form a potassium-aptamer complex leading to the reduction of the fluorescence signal and the fluorescence change with the variation of K^+ concentration. Monitoring the fluorescent signal should provide the method for quantitative analysis of K^+.

(A)　　　(B) 12 ODNs　　Fluorescence enhancement　　(D) 21　　Fluorescence quenching

Apt 12 : s(5'-GGG GTT TTG GGG -3')

Apt 15 : s(5'-GGT TGG TGT GGT TGG-3')

Apt 21 : s(5'-GGG GTT AGG GGT TAG GGG TTA GGG G-3')

mApt 15 : s(5'-CAT TCA TGT CAT TCA A-3')
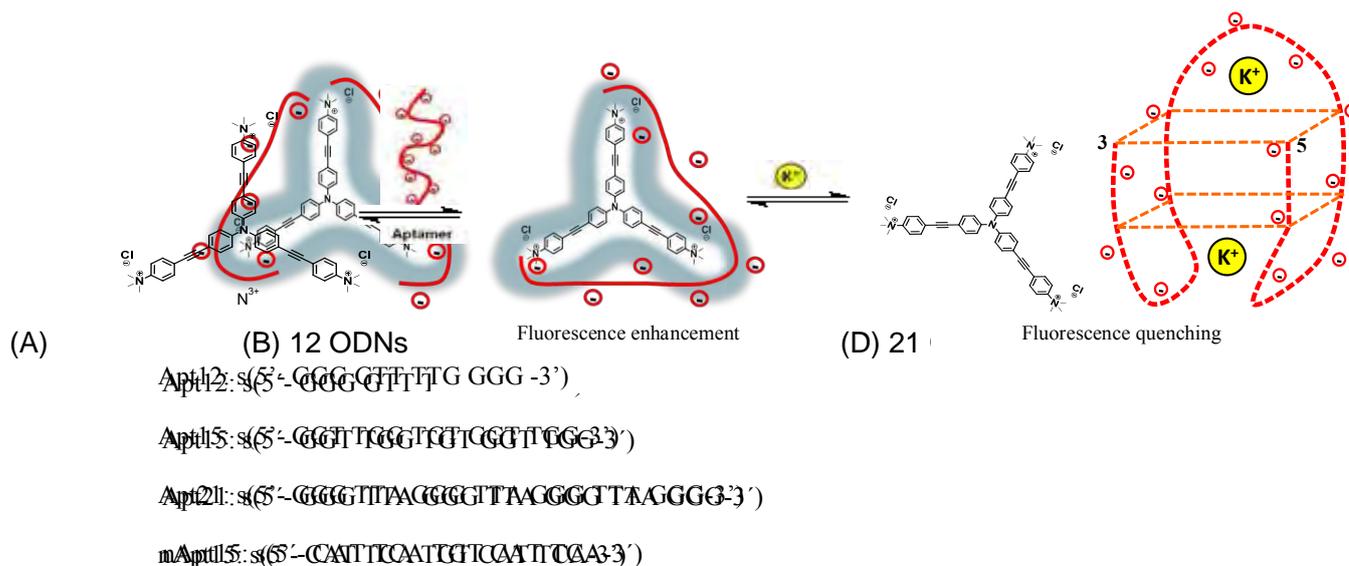
Scheme 1.1 Proposed detection of potassium ion via aptasensor and polycationic dendritic fluorophore (N^{3+}).

1.8 Objectives of this research

This research aims to synthesize a water soluble dendritic fluorophores containing positively charged peripheral groups. Its photophysical properties as well as application along with an aptamer as a selective sensor for potassium ion will be investigated. And applications for analysis of potassium ion in biological samples such as serum and urine.
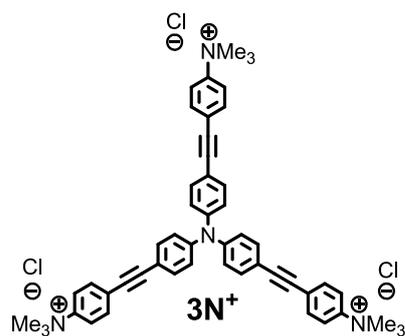
Figure 1.16 The target molecule.

Primer 1 : 5'-GGG GTT TTG GGG-3'   = Apt12

Primer 2 : 5'-GGT TGG TGT GGT TGG-3'   = Apt15

Primer 3 : 5'-GGG TTA GGG TTA GGG TTA GGG-3'   = Apt21

Primer 4 : 5'-CAT TCA TGT CAT TCA-3'   = nApt15

Figure 1.17 Primers 1-3 show aptamer oligonucleotides DNA sequences with different lengths for potassium ion and primer 4 shows the sequence of non-aptamer oligonucleotides DNA.

CHAPTER II

EXPERIMENTAL

2.1   Materials and chemicals

All oligonucleotides (Apt12: s(5'- GGG GTT TTG GGG -3'), Apt15: s(5'- GGT TGG TGT GGT TGG-3'), Apt21: s(5'- GGG TTA GGG TTA GGG TTA GGG-3') and nApt15: s(5'- CAT TCA TGT CAT TCA-3') were purchased from Biodesign. Co. Ltd. (Bangkok, Thailand) and used without further purification. N,N-dimethylaniline, trimethylsilylacetylene, $PdCl_2(PPh_3)_2$, sodium thiosulfate, benzyltrimethylammonium chloride, potassium hydroxide, potassium carbonate, calcium carbonate, lithium chloride and calcium chloride were purchased from Fluka[®] (Switzerland). Triphenylamine, iodine monochloride, copper (I) iodide, 1,8-diazabicyclo[5.4.0]undec-7-ene (DBU), sodium chloride, strontium chloride, magnesium chloride, potassium chloride, Amberlite[®] IR-410 ion-exchange resin and quinine sulfate were purchased from Aldrich. 4-Iodobenzoic acid was purchased from Merck[®] (Germany). For general reactions, solvents such as methylene chloride, methanol and acetonitrile were reagent grade and stored over molecular sieves. For anhydrous reactions, solvents such as THF and toluene were dried and distilled before use according to the standard procedures. All column chromatography were operated using silica gel 60 (70-230 mesh), Merck[®]. Solvents such as methylene chloride, hexane, ethyl acetate and methanol used for extraction and chromatography were commercial grade and distilled before use. Diethyl ether and chloroform used for extraction was reagent grade. Deionized water was used for ion exchange column and MiliQ water was used for preparation of all aqueous solution unless specified otherwise. All reactions were carried out under positive pressure of N_2 filled in rubber balloons. Dendritic polyelectrolytes fluorophore was prepared according to the literature procedures [59].

2.2   Analytical instruments

Products were characterized by a melting point apparatus (Electrothermal 9100, Fisher Scientific, USA). Elemental (C, H, N) analysis was performed on PE 2400 series II (Perkin-Elmer, USA). MS spectra were measured on an electrospray

ionization mass spectrometer (Quattro Micro 2000, Micromass) and Mass spectra were recorded on a Microflex MALDI-TOF mass spectrometer (Bruker Daltonics) using doubly recrystallized α-cyano-4-hydroxy cinnamic acid (CCA) as a matrix. ^{1}H-NMR spectra were recorded on Varian Mercury 400 MHz NMR spectrometer (Varian, USA) using the proton resonance of residual proton in the NMR solvents as the reference. ^{13}C-NMR spectra were recorded at 100 MHz on a Bruker 400 MHz NMR spectrometer. UV-Visible spectra were obtained from a Varian Cary 50 UV-Vis spectrophotometer (Varian, USA) using water as a solvent. Emission spectra were acquired on a Perkin Elmer LS 45 luminescence spectrometer (PerkinElmer, UK) for the potassium ion sensing study and a Varian Cary Eclipse spectrofluorometer (Varian, USA) for photophysical property study. The excitation wavelength was 372 nm and the emission was recorded from 390 to 700 nm. All stock solutions were prepared in 10 mM Tris-HCl buffer pH = 7.4 using a sonication bath for helping dissolution.

2.3 Synthesis of N^{3+}

2.3.1 Preparation of 4,4′,4″-triiodotriphenylamine [59]

3.3 eq. BTMAICl$_2$

CaCO$_3$, CHCl$_3$, MeOH
Reflux, 36 h

81 % yield
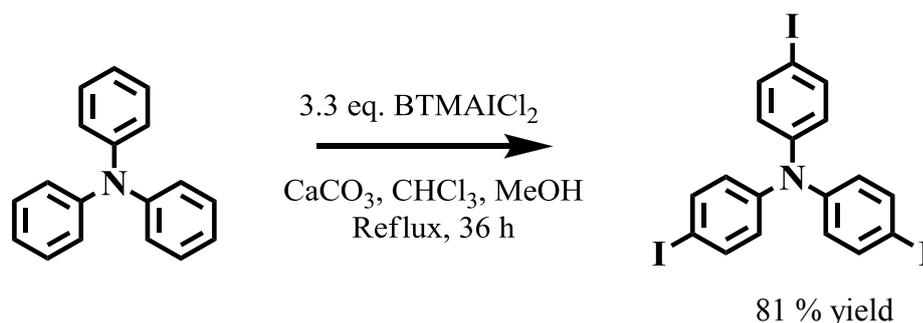
A solution of triphenylamine (7.36 g, 30 mmol) in chloroform (100 mL) and methanol (50 mL) was added with BTMAICl$_2$ (34.47 g, 99 mmol) and CaCO$_3$ (18 g, 180 mmol). The reaction mixture was allowed to reflux for 72 h and 20% Na$_2$S$_2$O$_3$ solution was then added to the mixture until the mixture became light yellow. The mixture was filtered and the filtrate was extracted with dichloromethane (3 × 50 mL). The combined organic phase was washed with water (2 × 100 mL) and dried over anhydrous MgSO$_4$. The solution was concentrated and the residue was redissolved in dichloromethane (20 mL) and dropped into stirred methanol (10 mL) for precipitation.

The desired product, 4,4′,4″-triiodotriphenylamine, was obtained as a white solid (15.15 g, 24.33 mmol, 81%). mp: 182-184°C; ^{1}H NMR (CDCl$_3$, 400 MHz): δ (ppm) 7.53 (d, J = 7.5 Hz, 6H), 6.80 (d, J = 7.5 Hz, 6H); ^{13}C NMR (CDCl$_3$, 100 MHz): δ (ppm) 146.6, 138.5, 126.1, 88.7; MALDI-TOF MS m/z Calcd. for C$_{18}$H$_{12}$I$_3$N, 622.81 Found: 622.561.

2.3.2 Preparation of 4-iodo-*N*,*N*-dimethylaniline [59]
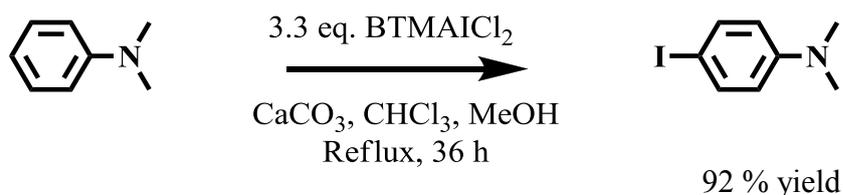
A solution of *N*,*N*-dimethylaniline (6.0 g, 50 mmol) in chloroform (100 mL) and methanol (50 mL) was added with BTMAICl$_2$(18.08 g, 52 mmol) and CaCO$_3$ (16.45 g, 0.15 mmol). After the reaction mixture was refluxed for 36 h, 20% Na$_2$S$_2$O$_3$ solution was added to the mixture until the mixture became light yellow. The mixture was then filtered and the filtrate was extracted with dichloromethane (3 × 50 mL). The combined organic phase was washed with water (2 × 100 mL) and dried over anhydrous MgSO$_4$. The solution was concentrated and the residue was redissolved in dichloromethane (20 mL) and dropped into stirred methanol (10 mL) for precipitatation. The desired product, 4-iodo-*N*,*N*-dimethylaniline, was obtained as a light white solid (11.36 g, 45.99 mmol, 92%). mp: 91-93°C; ^{1}H NMR (CDCl$_3$, 400 MHz): δ (ppm) 7.46 (d, J = 5.6 Hz, 2H), 6.49 (d, J = 5.6 Hz, 2H), 2.92 (s, 6 H); ^{13}C NMR (CDCl$_3$, 100 MHz): δ (ppm) 137.5, 114.7, 40.4.

2.3.3 Preparation of *N*,*N*-dimethyl-4-(trimethylsilylethynyl)aniline [59]
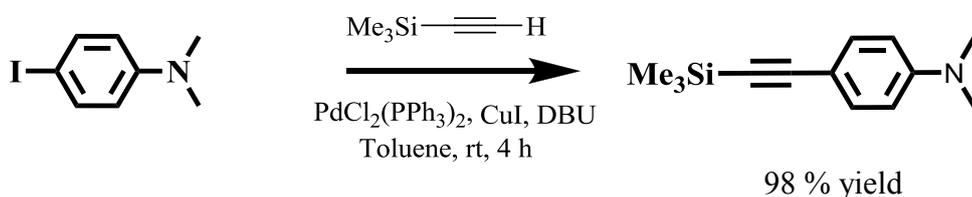
A mixture of 4-iodo-*N,N*-dimethylaniline (2.51 g, 10 mmol), PdCl$_2$(PPh$_3$)$_2$ (0.35 g, 0.5 mmol), CuI (0.08 g, 0.5 mmol) and trimethylsilylacetylene (1.08 g, 11 mmol) in toluene (10 ml) was added with DBU (1 mL) and the mixture was stirred at room temperature for 4 h. The reaction mixture was then filtered and the solid was washed with toluene (3 × 15 ml). The filtrate was evaporated and the residue was eluted through a silica gel column by gradient solvents starting from pure hexane to dichloromethane/hexane (1/3). The solvent was evaporated to afford *N,N*-dimethyl-4-(trimethylsilylethynyl)aniline as a yellow solid (2.36 g, 10.88 mmol, 98% yield). mp: 88-89°C; ^{1}H NMR (CDCl$_3$, 400 MHz): δ (ppm) 7.11(d, *J* = 7.2 Hz, 2H), 6.35 (d, *J* = 7.2 Hz, 2H), 2.72 (s, 6H), 0.01 (s, 9H); ^{13}C NMR (CDCl$_3$, 100 MHz): δ (ppm) 149.9, 132.9, 111.3, 109.6, 106.3, 90.9, 39.9, 0.01.

2.3.4 Preparation of *N,N*-dimethyl-4-ethynylaniline [59]
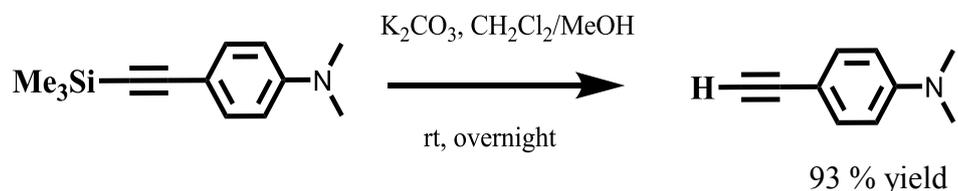
A mixture of *N,N*-dimethyl-4-(trimethylsilylethynyl)aniline (1.00 g, 4.6 mmol) and K$_2$CO$_3$ (0.059 g, 0.43 mmol) in dichloromethane (15 mL) and methanol (15 mL) was stirred at room temperature for 12 h. The reaction mixture was extracted with water (100 mL) and the organic layer was separated. The aqueous phase was extracted with dichloromethane (2 × 50 mL) and the combined organic phase was then dried over anhydrous MgSO$_4$. The filtrate was evaporated and the residue was eluted through a silica gel column by gradient solvents starting from pure hexane to dichloromethane/hexane (1/3). The solvent was evaporated to afford 4-ethynyl-*N, N*-dimethylaniline as a brown-yellow solid (0.61 g, 4.21 mmol, 93% yield). mp: 67-69°C. ^{1}H NMR (CDCl$_3$, 400 MHz): δ (ppm) 7.37 (d, *J* = 8.8 Hz, 2H), 6.62 (d, *J* = 8.8 Hz, 2H), 2.07 (s, 7H); ^{13}C NMR (CDCl$_3$, 100 MHz): δ (ppm) 150.4, 133.2, 111.7, 108.7, 84.9, 74.9, 40.0.

2.3.5 Preparation of 1, tris(*N,N*-dimethylamino-4,4′-diphenyleneethynylene) amine [59]

51 % yield
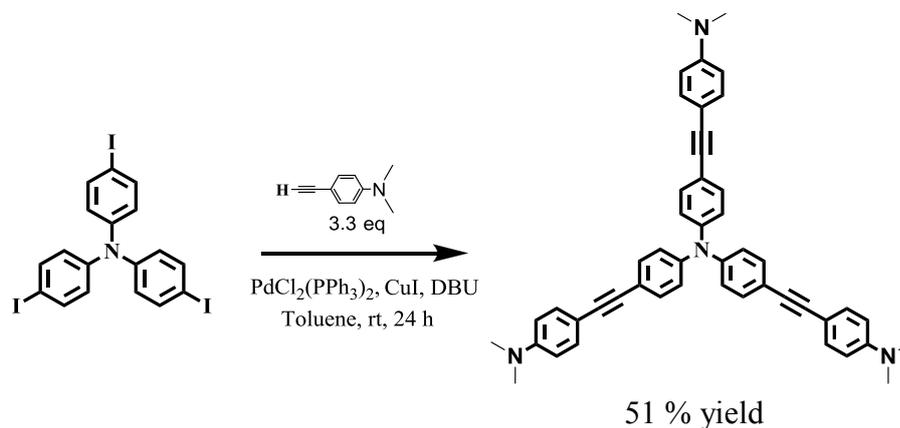
A mixture of TI$_3$ (0.30 g, 0.48 mmol), PdCl$_2$(PPh$_3$)$_2$ (55 mg, 0.080 mmol), CuI (15 mg, 0.080 mmol), 4-ethynyl-*N,N*-dimethylaniline (0.25 g, 1.6 mmol) in toluene (10 ml) was added with DBU (1 mL) and the mixture was stirred at room temperature for 24 h. The mixture was filtered and the filtrate was evaporated. The residue was eluted through a silica gel column by gradient solvents starting from pure hexane to dichloromethane/hexane (2/1) as an eluent to afford **3N^0**, **1** as a yellow solid (0.24 g, 51% yield). mp: 242-244°C; ^{1}H NMR (CDCl$_3$, 400 MHz): δ (ppm) 7.39(d, *J* = 8.8 Hz, 6H), 7.38(d, *J* = 8.8 Hz, 6H), 7.04 (d, *J* = 8.8 Hz, 6H), 6.66 (d, *J* = 8.8 Hz, 6H), 2.99 (s, 18 Hz); ^{13}C NMR (CDCl$_3$, 100 MHz): δ (ppm) 150.0, 146.2, 132.6, 132.3, 123.9, 118.6, 111.8, 110.2, 90.3, 87.2, 40.3; MALDI-TOF m/z Calcd for C$_{48}$H$_{33}$NO$_6$, 719.030 Found: 719.802.

2.3.6 Preparation of N^{3+} (3I$^-$), (2) [59]

84 %yield
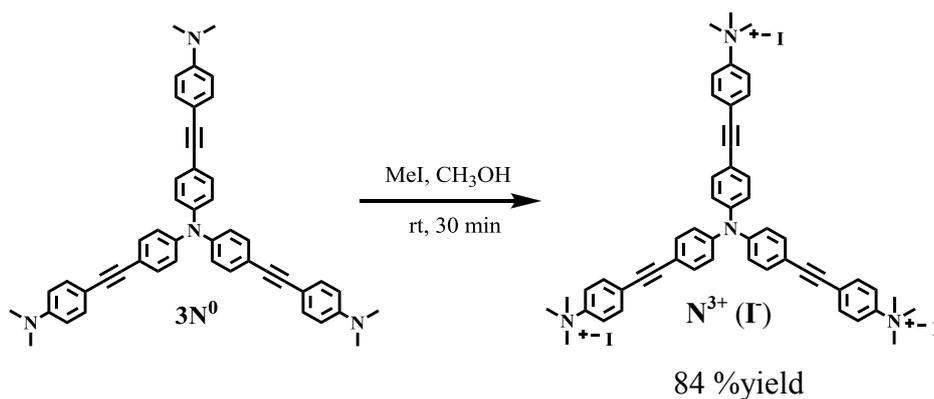
A mixture of **3N⁰**, **1** (0.20 g, 0.69 mmol) in CH_3OH (15 mL) was added CH_3I (0.5 mL) and the mixture was stirred at room temperature in a seal tube. After 30 min the solution was evaporated to afford **2** as a yellow solid (0.34 g, 72% yield). mp: > 250 °C decompose ; ^1H NMR (CD_3OD, 400 MHz) δ (ppm) 7.88 (d, J = 8.0 Hz, 6H), 7.76 (d, J = 8.4 Hz, 6H), 7.53 (d, J = 8.4 Hz, 6H), 7.15 (d, J = 8.0 Hz, 6H), 3.69 (s); ^{13}C NMR (CD_3OD, 100 MHz) δ (ppm) 147.5, 146.3, 133.3, 133.1, 125.8, 124.5, 121.0, 91.9, 87.0, 57.3; MS-ES⁺ m/z Calcd for $C_{51}H_{51}I_3N_4$, 719.691 Found: 239.177 $[M]^{3+}$. Anal. Calcd for $C_{51}H_{51}I_3N_4$: C, 55.65; H, 4.67; N, 5.09 Found: C, 54.49; H, 4.95; N, 4.97.

2.3.7 Preparation of N^{3+} (3Cl⁻), (3)
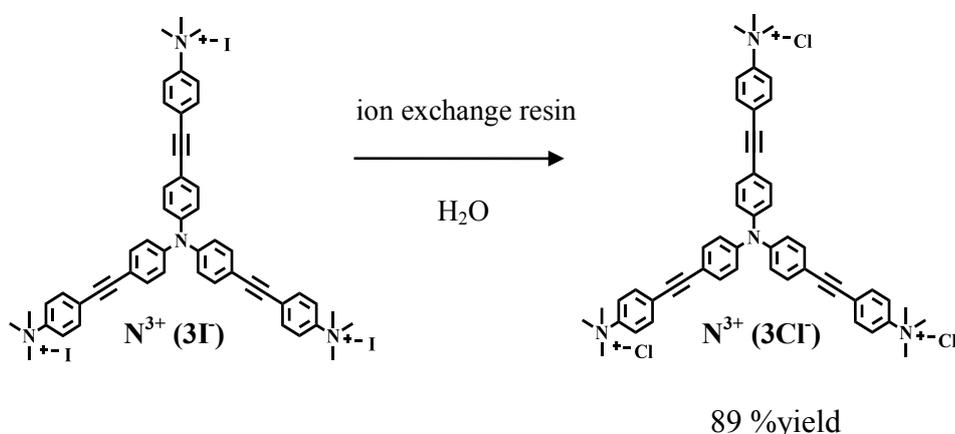
89 %yield

Compound **2** (0.1000 g, 0.14 mmol) was eluted through an Amberlite IRA-410 anionic ion exchange resin column with DI-water used as a mobile phase. The fluorophore **3** was obtained as a yellow solid after vacuum dry (89 %yield). mp:> 275 °C decompose ^1H NMR (CD_3OD, 400 MHz) δ 7.96(d, J = 9.2 Hz, 6H), 7.76(d, J = 9.2 Hz, 6H), 7.52 (d, J = 8.7 Hz, 6H), 7.13 (d, J = 8.7 Hz, 6H), 3.69 (s); ^{13}C NMR (CD_3OD, 100 MHz) δ;148.7, 147.7, 134.3, 134.2, 129.2, 127.4, 125.4, 121.7, 118.6, 93.0, 87.8, 57.8; MS-ES⁺ m/z Calcd: 719.98 Found: 239.213 $[M]^{3+}$. Anal. Calcd for $C_{51}H_{51}Cl_3N_4$: C, 74.13; H, 6.22; N, 6.78 Found: C, 70.82; H, 6.34; N, 6.40.

2.4 Photophysical property study

Stock solutions of 1-10 mM fluorophores diluted to 2 μM in phosphate buffer saline (PBS, 10 mM) pH 7.4 and Tris-HCl buffer 10 mM pH 7.4 were prepared.

2.4.1 UV-Visible spectroscopy

The UV-Visible absorption spectra of the stock solutions of fluorophores were recorded from 250 nm to 700 nm at ambient temperature.

2.4.2 Fluorescence spectroscopy

The stock solutions of fluorophores were diluted to ~0.2 and 1 μM, respectively, with their respective solvents. The emission spectra of **2** and **3** were recorded from 390 nm to 700 nm at ambient temperature using an excitation wavelength at 374 and 372 nm, respectively.

2.4.3 Fluorescence quantum yields

The fluorescence quantum yield of fluorophores were performed in phosphate buffer saline (PBS, 10 mM) pH 7.4 and Tris-HCl buffer 10 mM pH 7.4 using quinine sulphate ($\Phi_F = 0.54$) in 0.1 M H_2SO_4 as a reference [60]. The UV-Visible absorption spectra of five analytical samples and five reference samples at varied concentrations were recorded. The maximum absorbance of all samples should never exceed 0.1. The fluorescence emission spectra of the same solutions using appropriate excitation wavelengths selected were recorded based on the absorption maximum wavelength (λ_{max}) of each compound. Graphs of integrated fluorescence intensities were plotted against the absorbance at the respective excitation wavelengths. Each plot should be a straight line with 1 interception and gradient *m* [61].

In addition, the fluorescence quantum yield (Φ_F) was obtained from plotting of integrated fluorescence intensity *vs* absorbance represented into the following equation:

$$\Phi_X = \Phi_{ST} \left(\frac{Grad_X}{Grad_{ST}} \right) \left(\frac{\eta_X^2}{\eta_{ST}^2} \right)$$

The subscript Φ_{ST} denote the fluorescence quantum yield of a standard reference which was quinine sulphate in 0.1 M H_2SO_4 ($\Phi = 0.54$) and Φ_X is the fluorescence quantum yield of sample and η is the refractive index of the solvent.

2.5 Fluorescent sensor study

The experiments involving concentration variation, the mixtures were prepared by mixing of stock solutions and the total volumes were adjusted using 10 mM Tris–HCl buffer (pH 7.4) solution. G-quadruplex solutions, polycationic fluorophore and salt solutions were prepared in the same buffer solution. The samples were mixed thoroughly and incubated for 5 min at room temperature prior to the measurement. Each sample was prepared in triplicate solution and three measurements were performed for each solution to provide the reported average value of nine measurements along with their standard deviation.

2.5.1 Selectivity and sensitivity test

By fixing concentration of polycationic fluorophore, **3** at 0.2 μM and oligonucleotide solution at 0.02 μM, the final volume of the mixture was adjusted to 1500 μL using10 mM Tris–HCl buffer pH 7.4. Following, different types of metal chloride (LiCl, NaCl, KCl, NH$_4$Cl, MgCl$_2$ CaCl$_2$, and SrCl$_2$) were added at the same concentration (10 mM) and the mixtures were incubated for 5 min at room temperature prior to the measurement. Selectivity and sensitivity were shown by plotting quenching efficiency (1–(F/F$_0$)) quenching efficiency and the various lengths of aptamer chain (Apt12, Apt15, Apt21 and nApt15).

2.5.2 Fluorescence detection of potassium ion

G-quadruplex, (Apt15) solutions were diluted from the 100 μM stock solution to 0.02 μM. Polycationic fluorophore, **3** was added to the final concentration of 0.2 μM. Following the addition of different concentrations of K$^+$ (0.004, 0.02, 0.2, 1, 2, 3, 4, 5, 10, 50, 100, 140 and 196 mM), the solutions were adjusted a final volume to 1500 μL with Tris–HCl buffer and were incubated for 5 min at room temperature prior to the measurement for competitive binding of K$^+$ ions with the aptamer.

2.5.3 Interference test of potassium ion detection

The final concentrations of polycationic fluorophore, **3** and Apt15 were fixed at 0.2 μM and 0.02 μM. Following, the addition of different concentrations of K$^+$ ions at 0.2 mM and 6 mM. Then adding each of the othermetal chloride (LiCl, NaCl, NH$_4$Cl,

MgCl$_2$ CaCl$_2$, and SrCl$_2$) had quantity more than concentrations of K$^+$ ions 10 times (2 mM and 60 mM). The solution were adjusted a final volume to 1500 μL with Tris–HCl buffer and were incubated for 5 min at room temperature prior to the measurement.

2.5.4 Detection of potassium ion under biological conditions

Fixing final concentration of polycationic fluorophore, **3** at 1 μM and Apt15 at 0.1 μM. Following, the addition of concentrations under extracellular conditions is as follows: 145 mM NaCl, 2.5 mM CaCl$_2$, and 1.5 mM MgCl$_2$. After adding different concentrations of K$^+$ at 0.04, 0.08, 0.2, 0.4, 0.8, 2, 4, 6 and 20 mM, the solution were adjusted a final volume to 1500 μL with Tris–HCl buffer and were incubated for 5 min at room temperature prior to the measurement.

2.5.5 Application for K$^+$ assays in real samples

Urine was used to confirm the feasibility of this aptasensor for the determination of K$^+$ ions for analysis of real-world samples. Urine samples were harvested from four members of our laboratory and centrifuged at 3500 Rev/min for 5 min then filtered twice through 0.45 μM membranes. KCl (10 mM) was added into the urine samples to test the recovery. Then the urine samples were 100-fold diluted with Tris-HCl buffer and analyzed in Tris-HCl buffer (10 mM, pH 7.4) which contained 0.1 μM Apt15 and 1 μM fluorophore.

2.5.6 Study of circular dichroism (CD) spectra

Circular dichroism (CD) spectroscopy was used to ascertain the changes in the interactions among **N^{3+}**, Apt15 and K$^+$. By fixing concentration of polycationic fluorophore, **3** at 10 μM and Apt15 0r nApt15 at the same concentration 10 μM, the final volume of the mixture was adjusted to 1500 μL using10 mM Tris–HCl buffer pH 7.4. Following, different K$^+$ concentration levels were added at the concentration (10 mM and 3200 mM).

CHAPTER III

RESULTS AND DISCUSSION

3.1 Synthesis and characterization of polycationic dendritic fluorophore N^{3+} ($3Cl^-$)

This thesis work began with the synthesis of the tricationic fluorophore **3**. Compound **3** was obtained by a Cl^--I^- ion exchange from compound **2** which was synthesized according to Scheme 3.1 following the literature procedure [59]. The Sonogashira coupling of triiodotriphenylamine with *N,N*-dimethyl-4-ethynylaniline using Pd-Cu catalysts in the presence of DBU base afforded the trisubstituted compound **1** in 51 % yield. Quaternization of all three dimethylamino groups of **1** by three equivalents of methyl iodide in methanol was completed within 30 minutes at room temperature yielding the desired compound **2** in 84% (See Appendix Figure **A.14 - A.16** for ^1H NMR, ^{13}C NMR and MS spectra of the synthesized compounds).
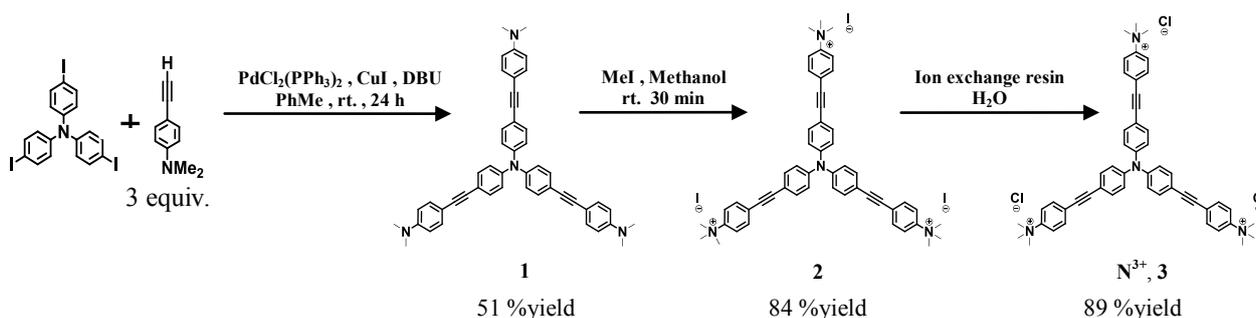
Scheme 3.1 Synthetic route to polycationic dendritic fluorophore **3**

In the form of iodide salt, compound **2**, however, tended to be demethylated upon storage in solid state. The mixture of demethylated compounds became poorly soluble in water and is no longer suitable for further study. Ion exchange from a strongly nucleophilic iodide ion to a less nucleophilic chloride ion was thus performed on an Amberlite IRA-410 anionic ion exchange resin column using DI-water as a mobile phase to afford the chloride salt **3**. A freshly prepared sample of **2** is readily soluble in both water and methanol and a clean ^1H NMR spectrum of fresh **2** in

CD$_3$OD was easily obtained (Figure 3.1A). After 7 days of storage in a solid form, **2** became partially soluble in CD$_3$OD (as well as water) and the ^{1}H NMR clearly showed significant signals of the demethylated moiety. On the other hand, the ^{1}H NMR spectrum of a stored sample of **3**, even after 25 days, did not show any change of signals from the fresh sample (Figure 3.1B). Insoluble material was also observed for the old iodide samples but not for the chloride sample as shown in the photographic insets of Figure 3.1. The fluorophore with chloride counter ion was indeed found to be stable indefinitely upon storage retaining its high water solubility. This chloride salt is thus more suitable for further study as an analytical fluorescent transducing reagent.
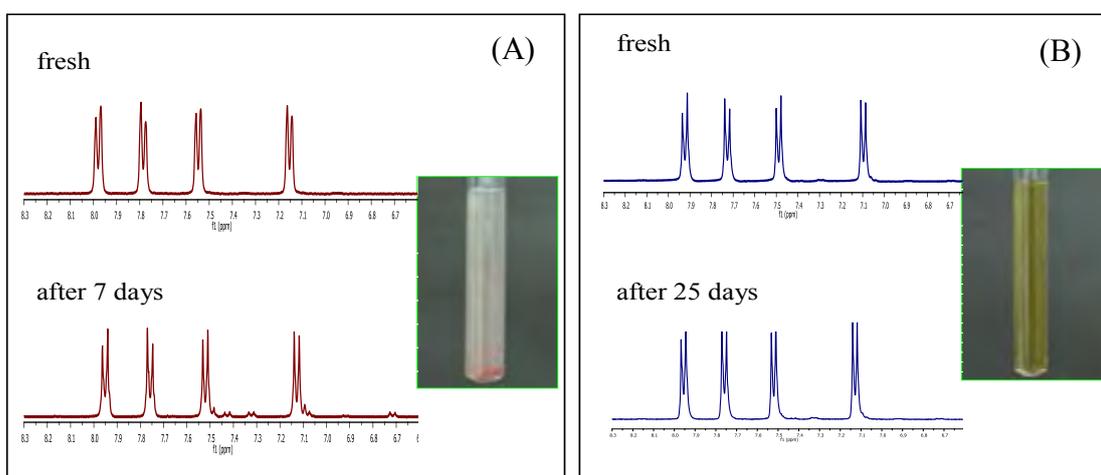
Figure 3.1 ^{1}H NMR spectra in CD$_3$OD of (A) **2** as a fresh sample and after *7* days of storage and (B) **3** as a fresh sample and after *25* days of storage. The photographic insets show the samples of compound **2** and **3** stored for 7 and 25 days, respectively.

The other technique used to confirm the new products is elemental analysis of which results are shown in **Table 3.1**. The observed elemental percentage and molecular ion mass were consistent with the values calculated from the formula associated with each molecular formula of compounds **1-3**.

Table 3.1 Elemental (C, H, N) analysis of compound**1-3**

Structure	Analytical found C:H:N	Calculated C:H:N	ESI-MS found	Calculate mass
1	-	-	674.845	674.341
2	54.49:4.95:4.97	55.65:4.67:5.09	239.177	239.99 (not include mass of I⁻)
3	70.82:6.34:6.40	74.13:6.22:6.78	239.213	239.99 (not include mass of Cl⁻)
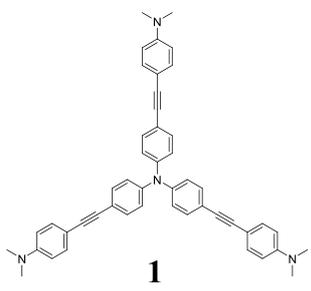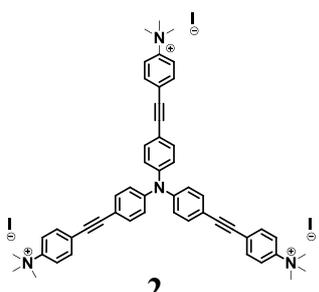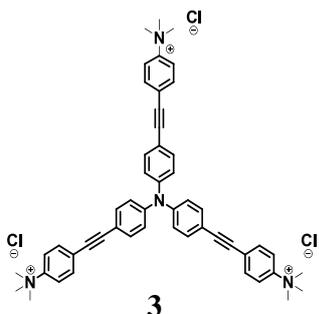
3.2 Photophysical property study

The effects of buffer on the photophysical properties of compounds **2-3** were studied in PBS buffer and Tris-HCl buffer solution pH 7.4 by absorption and emission spectroscopy. In Tris-HCl buffer, compounds **2** and **3** displayed absorption maxima at 374 and 372 nm with molar absorptivities of 37,000 and 34,000, respectively. The fluorophores in PBS buffer displayed absorption peaks at 358 and 362 nm with molar absorptivities of 23,000 and 27,000. The emission maxima of the fluorophores **2** and **3** appeared at 479 and 486 nm in Tris-HCl buffer with quantum efficiencies of 0.083

and 0.066 measured relative to quinine sulfate standard. These photophysical properties of the chloride salt, **3** is similar to those of the iodide salt, **2** but the fluorescence quantum yields (Φ_F) in Tris-HCl buffer more than in PBS. The normalized electronic absorption and fluorescence spectra of compound **3** was presented in **Figure 3.2** and their photophysical data are presented in **Table 3.2**.

The increase in fluorescence quantum yields (Φ_F) in Tris-HCl buffer suggested that the deaggregation of compounds **2-3** was caused by the structure of Tris buffer which can act like a surfactants. We also investigated the fluorogenic behaviors of **2-3** in Tris-HCl buffer because using the small volume of fluorophores gave high fluorescence emission signal. Its good sensitivity for made sensor detection of potassium ions in aqueous solution.

Table 3.2 Photophysical properties of compounds **2-3** in 10 mM sodium phosphate buffer saline (PBS) and Tris-HCl buffer (pH 7.4).

Compound	Solvent	Absorption		Fluorescence	
		λ_{max} (nm)	ε (M^{-1} cm^{-1})	λ_{max} (nm)	Φ_F
2	Tris-HCl	374	3.7 x 10^4	479	0.083
	PBS	362	2.7 x 10^4	476	0.014
3	Tris-HCl	372	3.4 x 10^4	486	0.066
	PBS	358	2.3 x 10^4	495	0.013

[α] Quinine sulfate in 0.1 M H$_2$SO$_4$ (Φ_F = 0.54) was the reference.
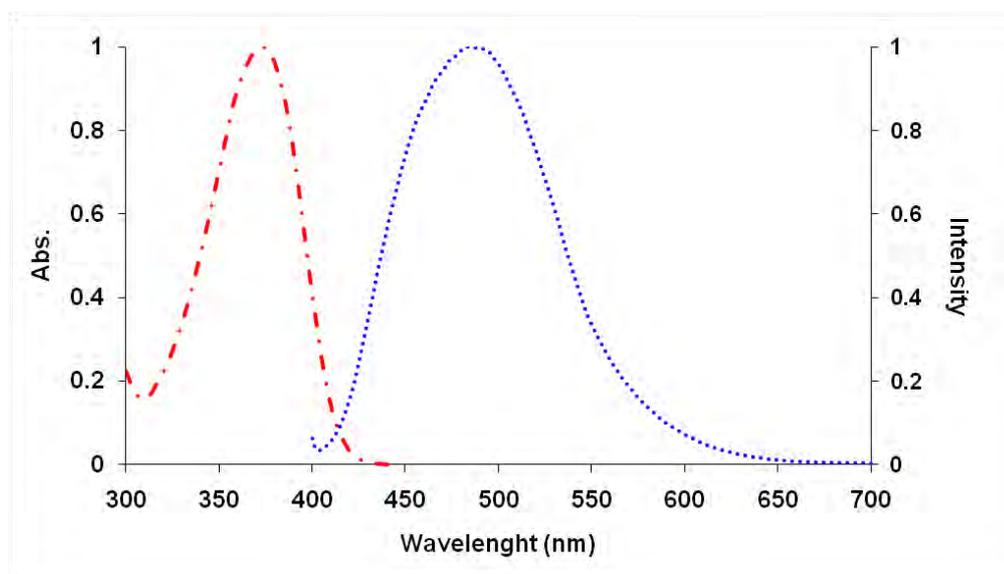
Figure 3.2 Normalized absorption (--·--) and emission (·····) spectra of N^{3+} (2 μM) in Tris-HCl buffer pH 7.4 (10 mM).

3.3 Fluorescent sensor study

3.3.1 Selectivity and sensitivity test

The solution of N^{3+} in Tris-HCl buffer solution pH 7.4 displayed absorption maximum at 372 nm (**Figure 3.2**) with molar absorptivity of 3.42×10^4. When being excited at 372 nm, the fluorophore showed emission maximum at 486 nm and quantum efficiency of 6.6%. The addition of Apt15, a K^+ aptamer consisting of 15 nucleotide bases, enhanced the fluorescent intensity over five folds and blue shifted it to 454 nm (**Figure 3.3A**). With one equivalent of Apt15, the system gave the quantum yield as high as 30%. These changes in the fluorescent signal reflect the expected interaction between the aptamer and N^{3+}. The interaction reduces the geometrical relaxation and self-associative quenching process resulting in the wavelength shift and intensity enhancement, respectively. The K^+ detection experiment gave results in good agreement with the principle proposed in **Scheme 1.1**. The fluorescence spectra shown in **Figure 3.3A** demonstrate that the enhanced fluorescent signal of N^{3+}/Apt15 system decreases by over 50% upon the addition of 1 mM K^+. The positively charged K^+ is expected to bind with the aptamer reducing its binding with N^{3+} and reinstalling

the self-associative quenching effect. To confirm that this behavior was result of the specific binding between K^+ and the aptamer, a non-aptameric oligonucleotide (nApt15) having a random sequence which cannot form a G-quadruplex structure was also tested. In this case, the addition of K^+ did not cause any changes in the fluorescence intensity of the N^{3+}/nApt15 mixture (**Figure 3.3B**).
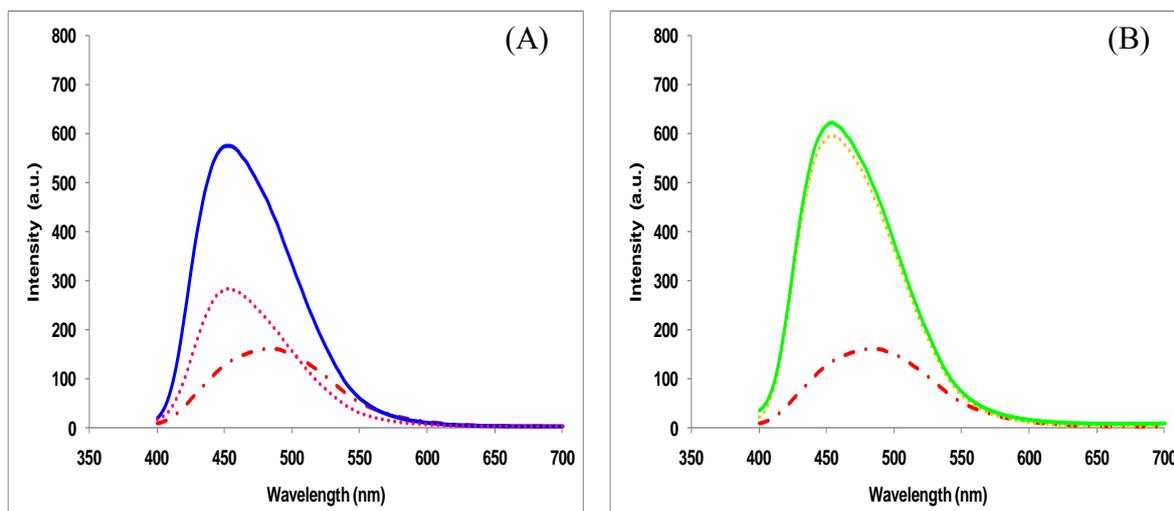
Figure 3.3 (A) Fluorescence spectra of compound **3** or N^{3+} (–·–·–), N^{3+}:Apt15, (——) and N^{3+}:Apt15:K^+, (·····). (B) Fluorescence spectra of N^{3+} (–·–·–), N^{3+}:nApt15, (——) and N^{3+}:nApt15:K^+, (·····). $[N^{3+}] = 0.20$ μM; [Apt15] = [nApt15] = 0.02 μM; $[K^+] = 1$ mM.

To gain insight into interactions between the fluorophore and aptamer, we investigated the mixtures of N^{3+} and four oligonucleotides (ODN) i.e. Apt12, Apt15 Apt21 and nApt15 (**Scheme 1.1**) three of which are K^+ aptamers. At the same molar concentration, the ODNs with different lengths gave different enhancement and shift of the fluorescent signal of N^{3+} suggesting different binding affinity with the fluorophore (**Figure 3.4**).
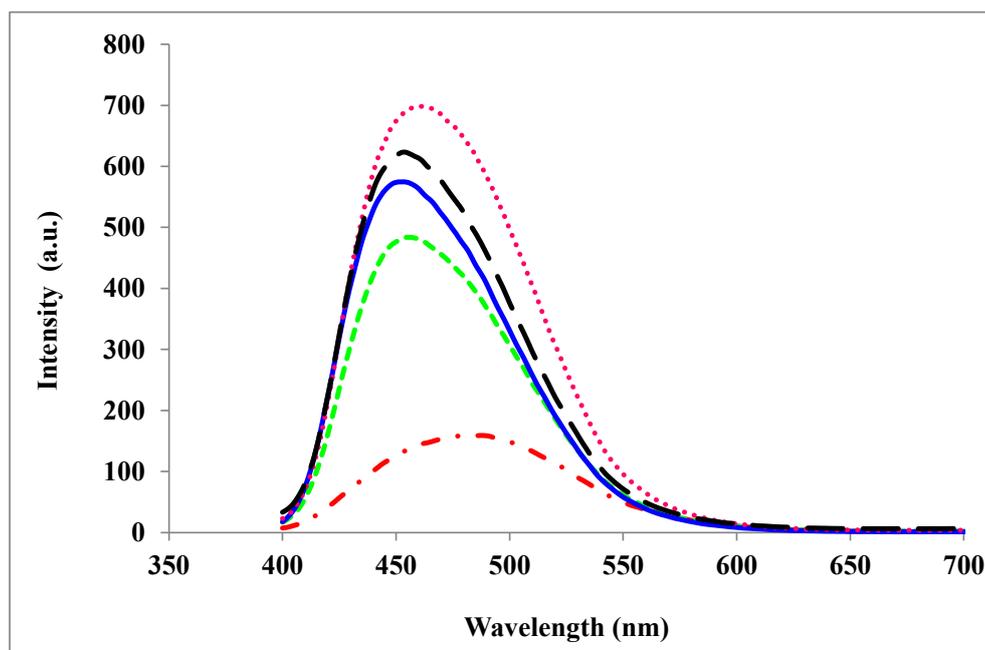
Figure 3.4 Fluorescence spectra of N^{3+} solution (0.20 μM) in Tris-HCl buffer pH 7.4 (10 mM) (–·–·–) in the presence of the aptamers (0.020 μM) with various lengths: Apt12 (----), Apt15 (——), Apt21 (·····) and nApt15 (— —), excited at 372 nm.

With the assumption of 1:1 complexation between N^{3+} and the aptamer, a linear relationship fit to Benesi-Hildelbrand equation [61, 62, 63] gave the affinity constant (K_a) of each fluorophore/ODN complex from intercept/slope. The K_a values for Apt12, Apt15, Apt21 and nApt15 were determined as 3.25×10^7, 9.14×10^7, 2.99×10^8 and 9.45×10^7 M^{-1}, respectively (**Figure 3.5**). The binding constants increase with the length of the ODNs in accordance to the increasing electrostatic interaction. The observation of similar values of the binding constants for the aptamer (Apt15) and non-aptamer (nApt15) confirmed that the electrostatic force is the main contribution for the binding.
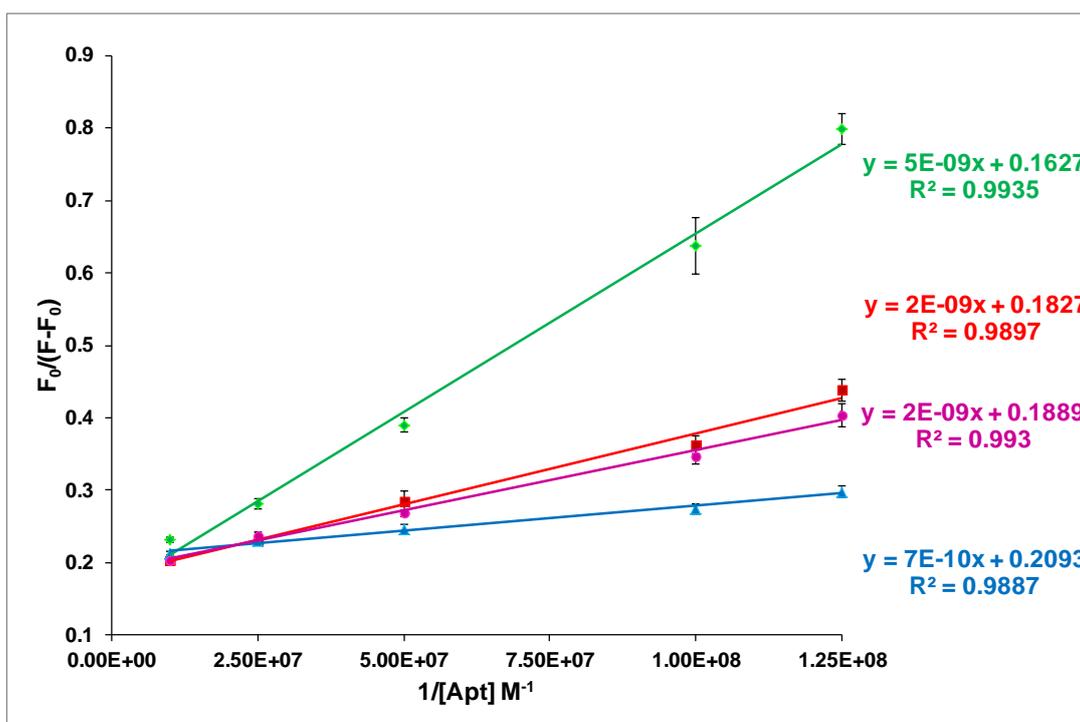
Figure 3.5 Linear least square fit for Benesi-Hildelbrand plots of fluorescence responses of N^{3+} (0.2 μM) to varying concentration of the ODNs (0.1 μM to 0.004 μM): Apt12 (——), Apt15 (——), nApt15 (——) and Apt21 (——) giving the affinity constant K_a from intercept/slope = 3.25×10^7, 9.14×10^7, 9.45×10^7 and 2.99×10^8 M^{-1}, respectively. The fluorescence data, F = fluorescence intensity of compound N^{3+} in the presence of the aptamers and F_0 = fluorescence intensity of compound N^{3+}, were collected at 454 nm using the excitation at 372 nm. Data are shown as the mean $\pm$ 1SD derived from three independent samples with three repeated measurements per sample.

Job's plot analysis of the fluorescence responses[34] revealed that the Apt12 formed 2:1 complex with N^{3+}, while all the other ODNs formed 1:1 complexes (**Figure 3.6**).
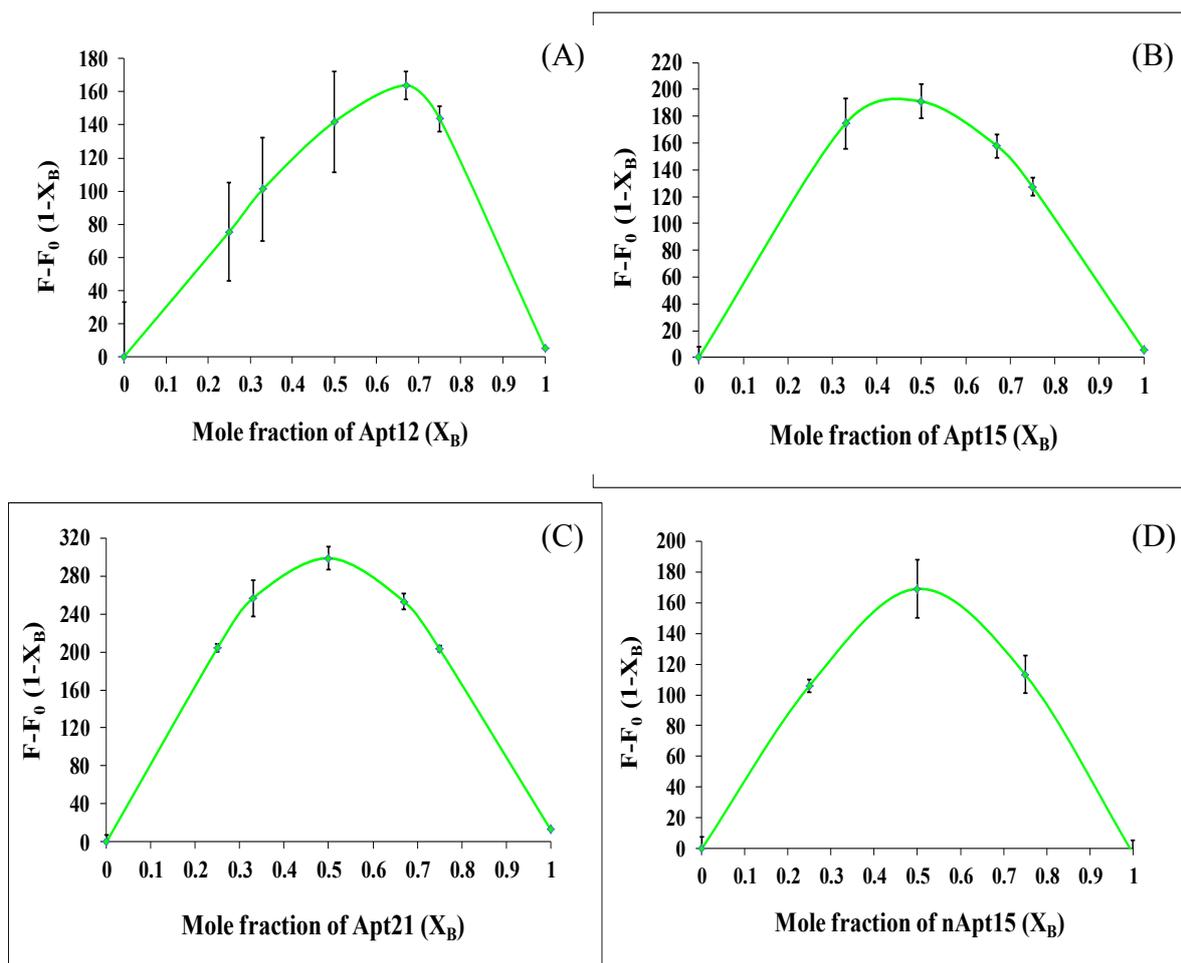
Figure 3.6 Job's plot of fluorescence responses of N^{3+} to various ODNs (A) Apt12 (B) Apt15 (C) Apt21 and (D) nApt15. The experiments were conducted in Tris-HCl buffer pH 7.4 (10 mM) with the total combined concentration of N^{3+} and ODNs of 0.1 μM. The fluorescence data, F = fluorescence intensity of compound **3** in the presence of the aptamers and F_0 = fluorescence intensity of compound **3**, were collected at 454 nm using the excitation at 372 nm. Data are shown as the mean $\pm$ 1SD derived from three independent samples with three repeated measurements per sample.

The K_a obtained from the plot for Apt12 is thus likely to be the product of two binding steps ($K_{a1} \times K_{a2}$) and each Apt12 chain should have even much lower binding affinity than that obtained from the Benesi-Hildelbrand plot. We attribute the difference in binding ratios to the molecular length of ODN. From AM1 geometrical optimization, the distance between two ammonium groups of N^{3+} was determined to

be 21.71 Å (**Figure 3.7**). Based on the length of a single nucleotide unit of 3.3 Å, the extended chain lengths of Apt12, Apt15 and Apt 21 are estimated to be 39.6, 49.5 and 69.3 Å, respectively. These values suggested that at least two Apt12 chains are required to fully interact with all three charge sites of N^{3+} while only one strand of Apt15 or Apt21 is long enough to interact with all three charge sites (**Figure 3.7**).

(A)   (B) Apt12   (C) Apt15   (D) Apt21
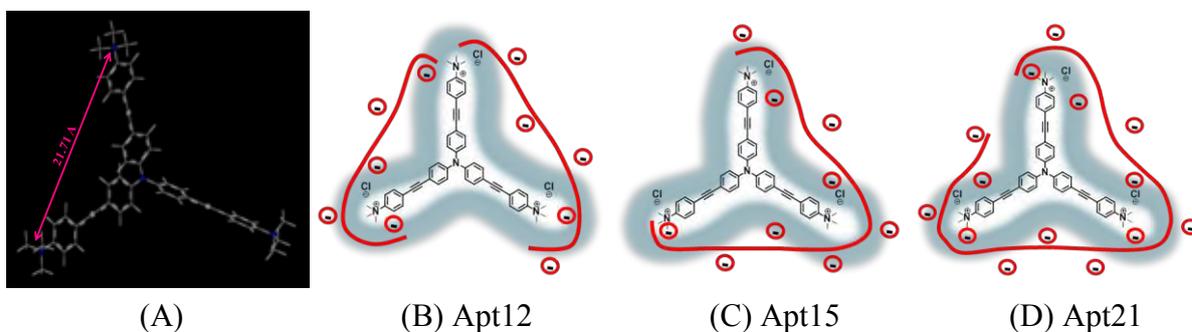
Figure 3.7 (A) AM1 geometrically optimized structure of N^{3+} and (B-D) proposed binding between N^{3+} and the aptamers.

According to the sensing mechanism presented in **Scheme 1.1**, the fluorescence quenching involves the competitive binding between K^+ and N^{3+} to the aptamer and greater sensitivity of K^+ may be obtained at the aptamer/fluorophore ratio lower than its stoichiometric ratio. We therefore investigated the effect of aptamer/fluorophore ratio on the sensitivity by varying the concentration of the aptamer from 0.1 to 0.01 μM at a fixed fluorophore concentration of 0.2 μM. The optimum aptamer/fluorophore ratio is determined as the ratio giving the highest quenching efficiency (1-F/F$_0$) upon the addition of K^+ at the physiological concentration (1 mM). **Figure 3.8** shows the highest quenching efficiency at the aptamer/fluorophore ratio of 1:10 for all aptameric ODN lengths. This optimum ratio is governed by the countered balance between two concentration effects *i.e.* the increases of initial fluorescence enhancement and the greater concentration of K^+ ion required for complexation. Apparently, Apt12 gave the highest quenching efficiency at all ratios as expected for its lower binding affinity to the fluorophore, for each individual chain. It is also important to point out that the lower aptamer/fluorophore ratio is translated into the lower amount of expensive aptameric ODN required for

sensitive detection. In this particular aptasensing system, the optimum condition for K^+ sensing required only 20 nM of the aptamer and 200 nM of the fluorophore. The plot also shows that K^+ gives very low quenching efficiency for nApt15, the non-aptameric ODN, at all ratios confirming that the detection is based on the specific aptamer-K^+ interaction. Since the sensitivity of a sensor is generally traded off with selectivity, our next investigation is to compare the selectivity of this aptasensing system against other cations.
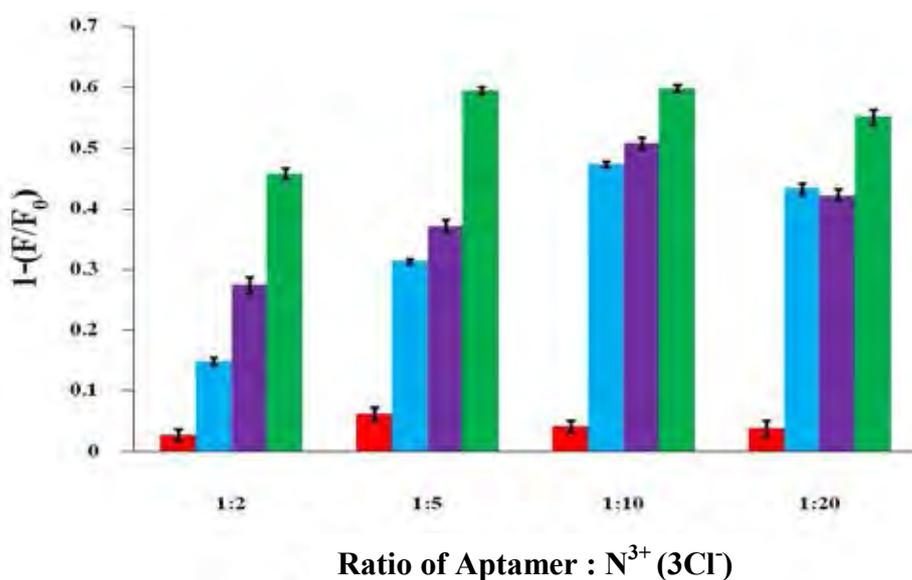
Figure 3.8 Quenching efficiencies (1-F/F$_0$) of K^+ in aptameric sensing systems with different ODNs: Apt12 (■), Apt15 (■), Apt21 (■) and nApt15 (■) and various ODN/fluorophore mole ratio.

We investigated the selectivity of each aptamer/N^{3+} pair at the optimum 1:10 mole ratio by comparing the quenching efficiency of K^+ with other cations such as Li^+, Na^+, NH_4^+, Mg^{2+}, Ca^{2+} and Sr^{2+}. **Figure 3.9** clearly reveals that the aptameric sensing systems have high sensing selectivity toward K^+ while the non-aptameric system gave no K^+ selectivity. Among three aptamers, Apt12 provided the lowest selectivity against other monovalent cations such as Li^+, Na^+ and NH_4^+. This should again be attributed to its low binding affinity to the fluorophore. For the divalent cationic species such as Mg^{2+}, Ca^{2+} and Sr^{2+}, we observed lower selectivity against these ions. Comparing with the monovalent cations, the divalent cations possess greater electrostatic attraction with the ODN chains [64, 65, 66] that led to greater

quenching effect to the sensing system. Interestingly, the selectivity against divalent cations is rarely reported for K^+ aptasensors, it is thus important to point out that this tricationic fluorophore N^{3+} provided greater selectivity than the monocationic dye for K^+ aptasensing system [56]. We thus attributed the factors for high selectivity not only to the specific binding between K^+ and the aptameric G-quadruplex structure but also to the binding affinity between the fluorophore and aptamer. Among the three aptamers, Apt15 presents the best choice for K^+ sensor as it gives high selectivity with only slightly lower sensitivity comparing to Apt12.
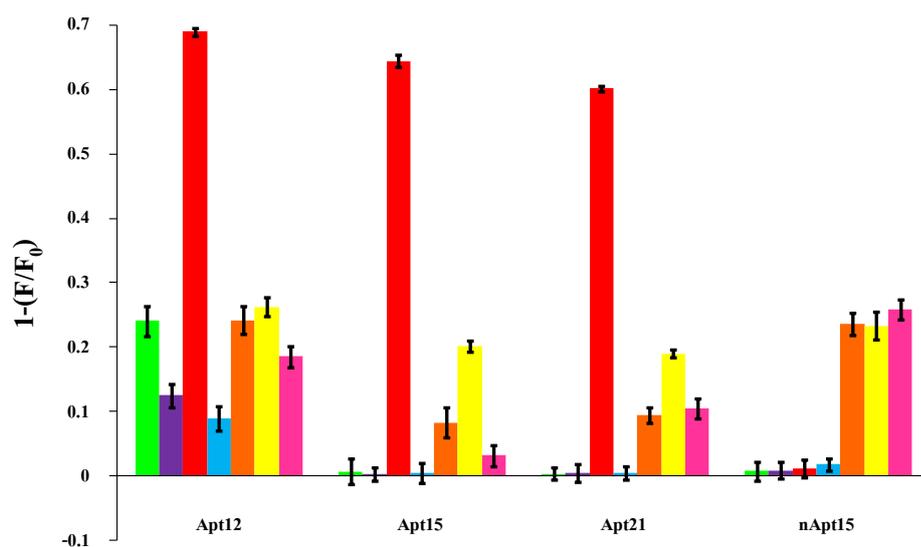
Figure 3.9 Quenching efficiencies $(1-F/F_0)$ of cations: Li^+ (■), Na^+ (■), K^+ (■), NH_4^+ (■), Mg^{2+} (■), Ca^{2+} (■)and Sr^{2+} (■) in the sensing systems constructing form various ODNs.

3.3.2 Fluorescence detection of potassium ion

For quantitative analysis of K^+, the fluorescent signal of Apt15/N^{3+} (1:10) solution in the presence of KCl (0.004-196 mM) was measured. The fluorescent signal decreased with the increasing K^+ concentration (**Figure 3.10A**). At low K^+ concentrations ($\leq$ 50 mM), the fluorescent signal was quenched without any peak shift. When the concentration of K^+ increased to 100 mM or more, the fluorescent signal was shifted to the original position of the free fluorophore. These results agree

well with the stepwise formation of 1:1 and 2:1 complexes between K^+ and Apt15 [48]. The 1:1 complex of K^+/Apt15 probably remains largely bound to N^{3+} while the 2:1 complex is likely to be dissociated from the fluorophore. This stepwise formation of 1:1 and 2:1 complexes is also evidenced from two linear dynamic ranges observed in the plot between quenching efficiency and $\log[K^+]$ before reaching the saturation (**Figure 3.10B**). At low K^+ concentration, most complex formed is likely to be the 1:1 complex whereas the 2:1 complex becomes predominant at higher K^+ concentration. The 2:1 complex has lower negative charge and thus its binding with N^{3+} is weaker resulting in greater quenching sensitivity and the greater slope of the second dynamic range. With K^+ concentration higher than 100 mM (5×10^5 equiv.), the quenching effect is clearly saturated and the fluorescent signal returned to the original position of N^{3+}. The plot in **Figure 3.10B** demonstrates a useful concentration range for quantitative analysis of K^+. The first linear dynamic range gave the limit of detection (LOD determined at the signal = 3 × noise) of K^+ as low as 9×10^{-7} M which is among the best for the label free systems reported to date [58].
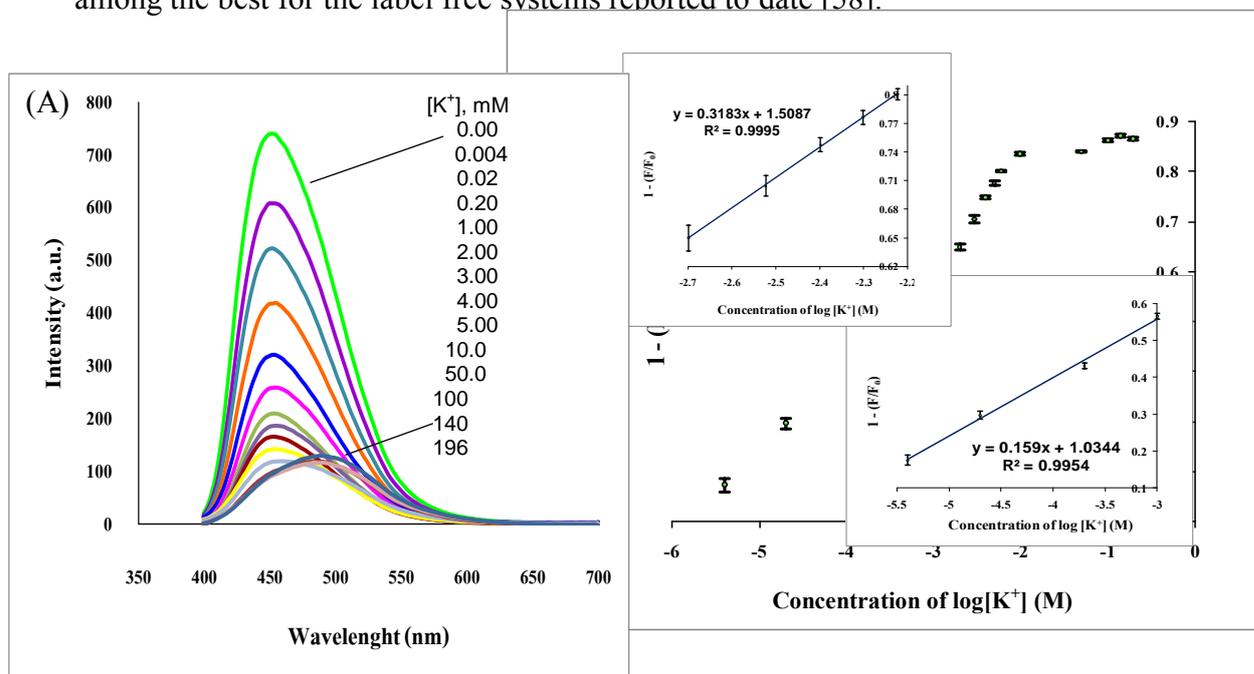

Figure 3.10 (A) Fluorescence responses of the Apt15/N^{3+} (20/200 nM) in Tris-HCl buffer pH 7.4 (10mM) upon addition of K^+ ion at various concentrations. λ_{ex}=372 nm. (B) Plot of the quenching efficiency of the fluorophore-aptamer complex at 354 nm as a function of $\log[K^+]$. The insets show two dynamic ranges of K^+, 4 μM-1 mM and 2-6 mM.

Circular dichroism (CD) spectroscopy was used to ascertain the changes in the interactions among N^{3+}, Apt15 and K^+ at different K^+ concentration levels. The negative CD signal near the absorption of N^{3+} around 385 nm signifies the interaction between Apt15 and N^{3+} (**Figure 3.11A**). In the presence of 10 mM K^+ (1.0×10^4 equiv.) clearly increased the positive CD signal at 290 nm corresponding to the increased formation of antiparallel G-qudruplex conformation. The CD signal near the absorption of N^{3+} however does not return to the original nil value indicating the interaction between the potassium-G-qudruplex complex and N^{3+}. The sign switching structure of the CD signal also implies the interactions with three branches of N^{3+} are uneven. Further addition of K^+ to 3.20 M (3.2×10^5 equiv.) return the CD signal near the absorption of N^{3+} back to zero confirming the full dissociation of the potassium-G-qudruplex complex from N^{3+}. With similar interpretation, **Figure 3.11B** confirms that nApt15 interacts with N^{3+} but not with K^+. No CD signal change is observed upon the addition of K^+.
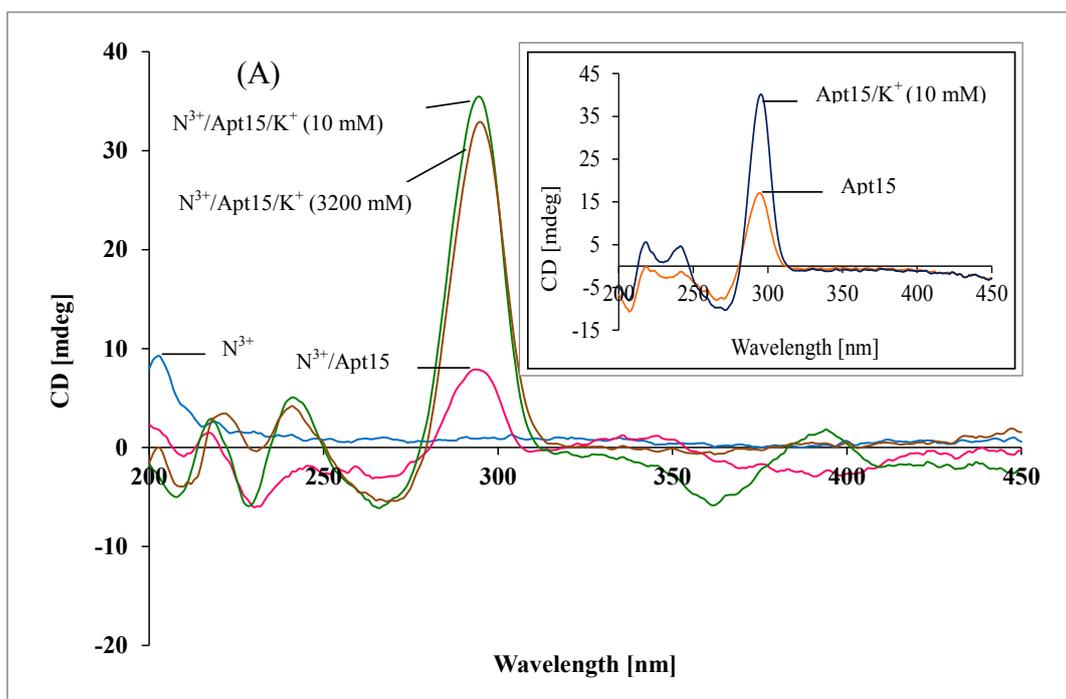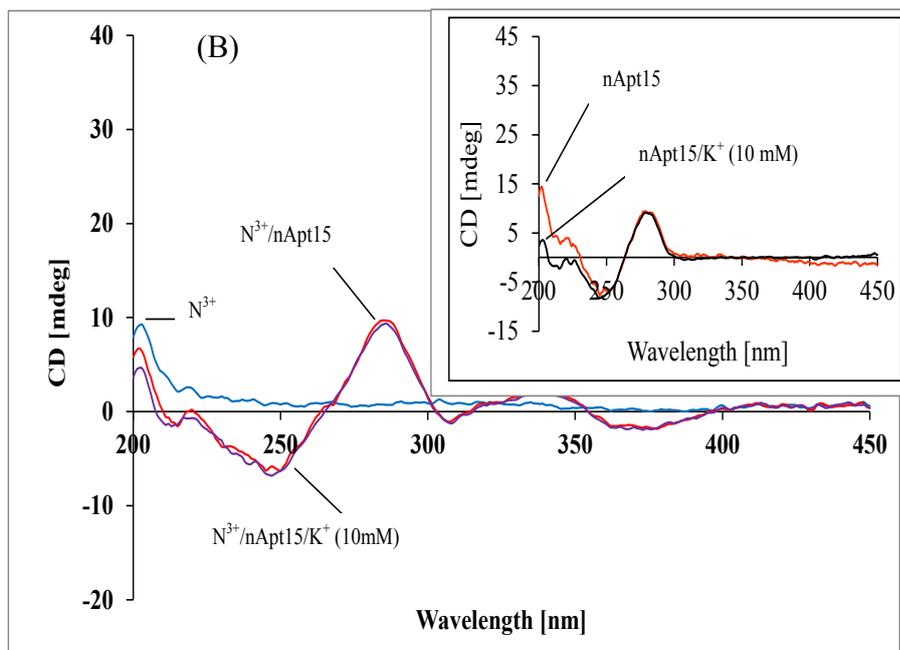
Figure 3.11 Circular dichroism (CD) spectra of (A) N^{3+} solution (10 μM); N^{3+}/Apt15 (10 μM/10μM) solution in the absence and presence of K^+ (10 mM); and K^+ (3200 mM). Insert: Apt15 solution (10 μM); Apt15/K^+ (10 μM/10 mM) solution. (B) N^{3+} solution (10 μM); N^{3+}/nApt15 (10 μM/10μM) solution in the absence and presence of K^+ (10 mM); in Tris–HCl buffer pH 7.4 (10 mM). Insert: nApt15 solution (10 μM); nApt15/K^+ (10 μM/10 mM) solution.

3.3.3 Interference test of potassium ion detection

Figure 3.12 shows interference condition no effect of potassium ion detection in the first dynamic range (4 μM-1 mM) used concentration of potassium 0.2 mM and the second dynamic range (2-6 mM) used concentration of potassium 6 mM. The result shows that aptasensor was good sensing for potassium ion detection.

Figure 3.12 Interference of K^+ detection of fluorophore-Apt15 complex at concentrations of K^+ ions, (■) 0.2 mM and 6 mM. Following the addition of another metal chloride that's LiCl (■), NaCl (■), NH_4Cl (■), $MgCl_2$ (■), $CaCl_2$ (■), and $SrCl_2$, (■)) had quantity more than concentrations of K^+ ions 10 times (2 mM and 60 mM).

3.3.4 Detection of potassium ion under biological conditions and application for K^+ assays in real samples
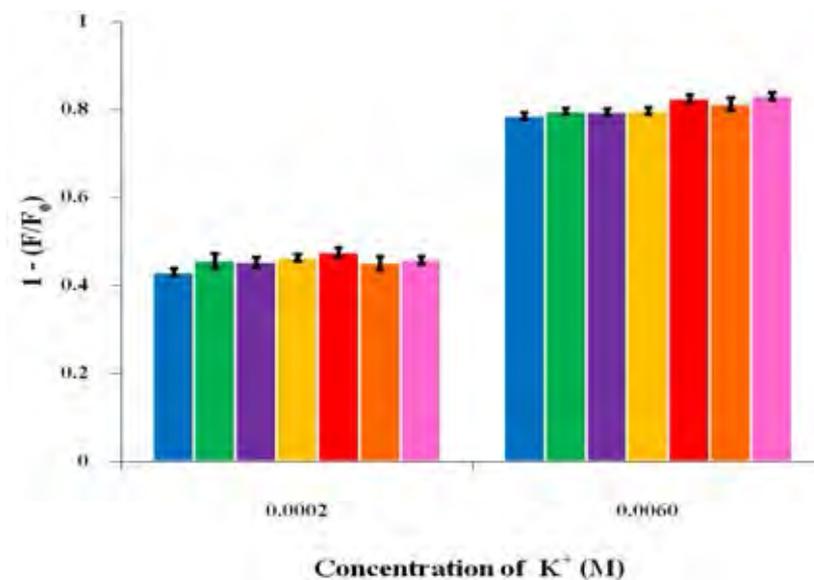
In the final stage of this work, the application of the Apt15-N^{3+} aptasensing system for determination of K^+ concentration in real human urine samples was evaluated. Using synthetic urine solutions containing 145 mM NaCl, 2.5 mM $CaCl_2$, 1.5 mM $MgCl_2$ and various concentrations of K^+ (0-20 mM). [67], a linear calibration line was obtained in the range of 0.04-2.0 mM (**Figure 3.13**). On the basis of an F-test at a 95% confidence level, the K^+ concentrations in four volunteers' urine samples determined by Apt15-N^{3+} sensor agree very well with the values obtained from inductively coupled plasma-optical emission spectrometry (ICP-OES) (**Table 3.3**). The recovery level of 97.4-99.5% of K^+, intentionally spiked at 10 mM concentration into the urine sample solutions, also confirmed the effectiveness of this sensing system for determination of K^+ content in urine. It is important to point out that this fluorescence aptasensing assay provides the advantages of simple sample preparation,

rapid detection and low cost instrumentation that are amenable to high throughput analysis.
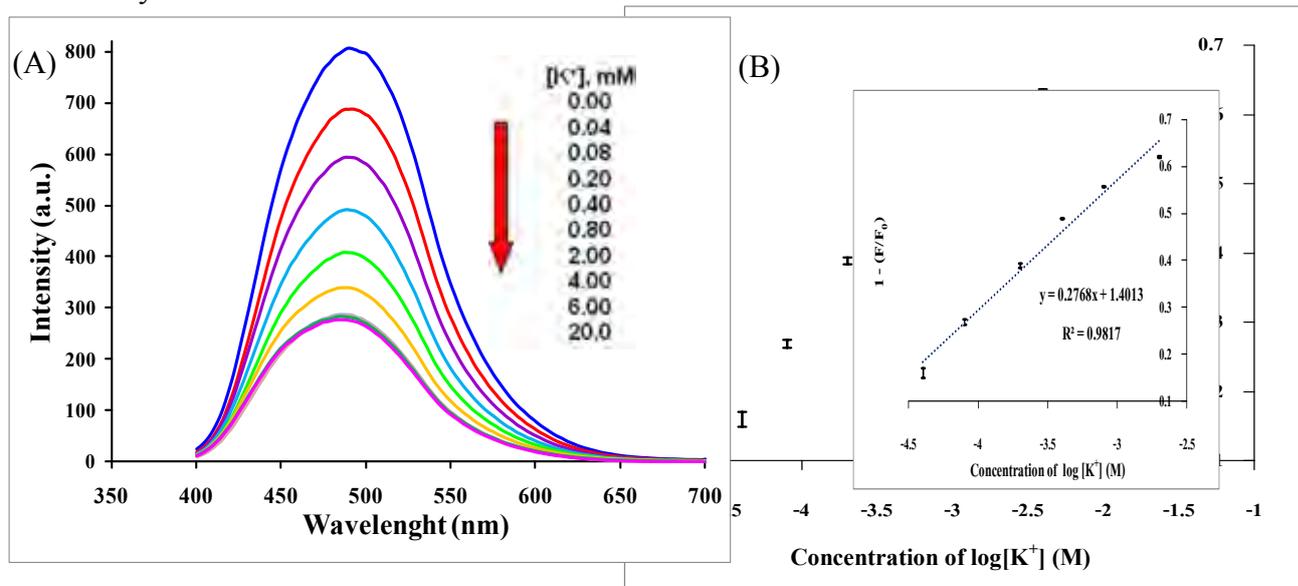

Figure 3.13 (A) Fluorescence responses of the Apt15-N^{3+} (0.1 μM/1 μM) complex at different concentrations of K^+ (0.04-2 mM) in synthetic urine solutions and (B) the quenching efficiency determined at 454 nm as a function of K^+ concentrations showing a linear response from 4×10^{-5} to 2×10^{-3} M (inset).

Table 3.3 Analytical results for K^+ content in urine samples from four healthy volunteers measured using the N^{3+}-Apt15 fluorescence sensor,[a] a [N^{3+}] = 1 μM, [Apt15] = 0.1 μM, ICP-OES and analytical results for K^+ in urine samples.

Sample	N^{3+}-Apt15 sensor Mean±SD/mM (n=5)	ICP-OES Mean±SD/mM (n=5)	F-test between two methods [b]	Add K^+ (mM)	Found K^+ (mM)	Recovery (%)
urine 1	4.20±0.006	4.15±0.033	2.43	10	9.875	98.8
urine 2	11.17±0.004	11.22±0.152	3.15	10	9.952	99.5
urine 3	14.58±0.003	14.59±0.063	2.30	10	9.753	97.5
urine 4	23.21±0.012	23.75±0.091	3.67	10	9.741	97.4

[a] 20/200 nM, [b] The F-test value is 6.39 at a 95% confidence level.
0.1/1 μM. [b] The F-test value is 6.39 at a 95% confidence level.

CHAPTER IV

CONCLUSION

4.1 Conclusion

The water soluble dendritic polycationic fluorophore was successfully synthesized. The tricationic phenylene-ethynylene (N^{3+}) is capable of transducing fluorescent signal in aptasensing system. The fluorescent signal of N^{3+} is enhanced upon electrostatic binding with the potassium aptamer. The addition of potassium ion selectively diminished this enhancement by inducing the formation G-quadruplex conformation of the aptamer chain which in turn weakens its electrostatic interaction with N^{3+}. Sensitivity and selectivity of the sensing system were optimized by the variation of the aptamer length in order to tune the electrostatic interactions between the fluorophore and aptamer. The 15-base aptamer gave higher selectivity than the 12-base aptamer and higher sensitivity than the 21-base aptamer. The N^{3+}-Apt15 aptasensor exhibited wide linear dynamic ranges from micro- to millimolar concentration of K^+ with the detection limit just below 1.0 μM. The sensing system is conveniently applicable for rapid K^+ assays in real urine samples.

4.2 Suggestion for future works

The future work should focus on

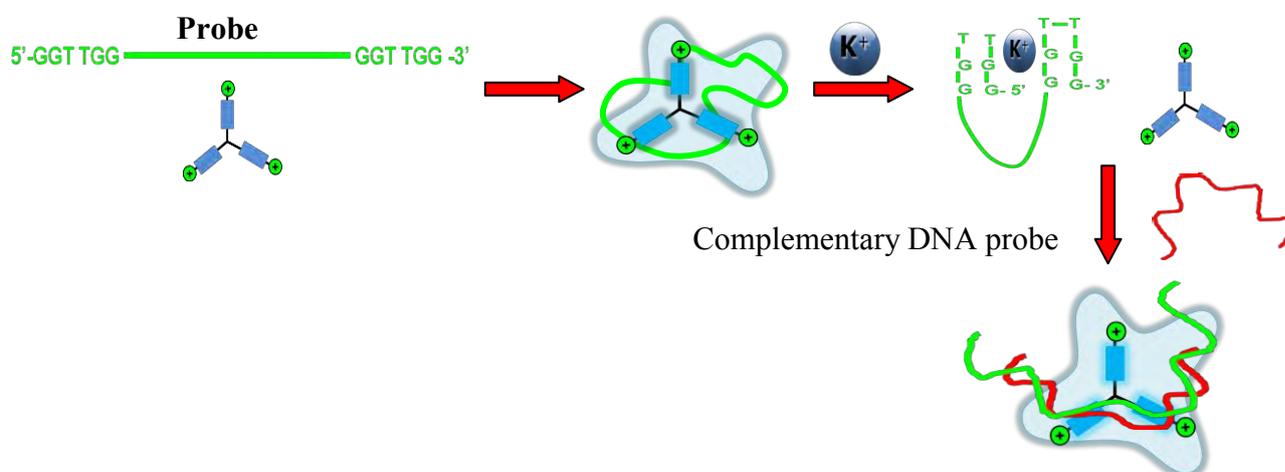1) To apply the fluorophore and aptamer for DNA sequence detection.

Figure 4.1 Suggested future work on application of fluorophore (N^{3+}) and aptamer for DNA sequence detection.

REFERENCES

[1]   Lehn, J. M. Supramolecular chemistry. *Science.* 260 (1993): 1762-1763.

[2]   Rotello, V. M.; and Thayumanavan, S. *Molecular recognition and polymers: Control of polymer structure and self-assembly*; John Wiley & Sons, Inc., Hoboken: New Jersey. 2008.

[3]   Oshovsky, G. V.; Reinhoudt, D. N.; and Verboom, W. Supramolecular chemistry in water. *Angew. Chem. Int. Ed.* 46 (2007): 2366-2393.

[4]   Uhlenheuer, D. A.; Petkau, K.; and Brunsveld, Luc. Combining supramolecular chemistry with biology. *Chem. Soc. Rev.* 39 (2010): 2817-2826.

[5]   Schemberg, J.; Schneider, K.; Demmer, U.; Warkentin, E.; Müller, A.; and Ermler, U. Towards biological supramolecular chemistry: A variety of pocket-templated, individual metal oxide cluster nucleations in the cavity of a Mo/W-storage protein. *Angew. Chem. Int. Ed.* 46 (2007): 2408-2413.

[6]   Caballero, A. Highly selective chromogenic and redox or fluorescent sensors of Hg^{2+} in aqueous environment based on 1, 4-disubstituted azines. *J. Am. Chem. Soc.* 127 (2005): 15666–15667.

[7]   Tang, Y. L. Direct visualization of glucose phosphorylation with a cationic polythiophene. *Adv. Mater.* 20 (2008): 703-705.

[8]   McQuade, D. T.; Pullen, A. E.; and Swager, T. M. Conjugated polymer-based chemical sensors. *Chem. Rev.* 100 (2000): 2537-2574.

[9]   Thomas, S. W.; Joly, G. D.; and Swager, T. M. Chemical sensors based on amplifying fluorescent conjugated polymers. *Chem. Rev.* 107 (2007): 1339-1386.

[10]   Service, R. F. Getting a charge out of plastics. *Science.* 290 (2000): 425-427.

[11]   Perepichka, I. F.; Perepichka, D. F.; Meng, H.; and Wudl, F. Light-emitting polythiophenes. *Adv. Mater.* 17 (2005): 2281-2305.

[12]   Patil, A. O.; Heeger, A. J.; and Wudl, F. Optical properties of conducting polymers. *Chem. Rev.* 88 (1988): 183-200.

[13] Scherf, U.; and List, E. J. W. Semiconducting polyfluorenes towards reliable structure property relationships. *Adv. Mater*. 14 (2002): 477-487.

[14] Kraft, A.; Grimsdale, A. C.; and Holmes, A. B. Electroluminescent Conjugated polymers seeing polymers in a new light. *Angew. Chem. Int. Ed*. 37 (1998): 402-428.

[15] Bunz, U. H. F. Poly(aryleneethynylene)s: syntheses, properties, structures, and applications. *Chem. Rev.* 100 (2000): 1605-1644.

[16] Pinto, M. R.; and Schanze, K. S. Conjugated polyelectrolytes: synthesis and applications. *Synthesis-Stuttgart*. 2002: 1293-1309.

[17] Swager, T. M. The molecular wire approach to sensory signal ampli-fication. *Acc. Chem. Res*. 31 (1998): 201-207.

[18] Sirringhaus, H. Device physics of solution-processed organic field- effect transistors. *Adv. Mater*. 17 (2005): 2411-2425.

[19] Bunz. U. H. F. Poly(aryleneethynylene)s. *Macromol. Rapid Commun*. 30 (2009): 772–805.

[20] Chen, L. H., et al. Highly sensitive biological and chemical sensors based on reversible fluorescence quenching in a conjugated polymer. *Proc. Natl. Acad. Sci. U. S. A*. 96 (1999): 12287-12292.

[21] Weder, C.; Sarwa, C.; Montali, A.; Bastiaansen, G.; and Smith, P. Incorporation of photoluminescent polarizers into liquid crystal displays. *Science*. 279 (1998): 835-837.

[22] Tan, C. Y.; Pinto, M. R.; and Schanze, K. S. Photophysics, aggregation and amplified quenching of a water-soluble poly(phenylene ethynylene). *Chem. Commun.* 2002: 446-447.

[23] Zheng, J., and Swager, T. M. Poly(arylene ethynylene)s in chemosensing and biosensing. *Adv. Polym. Sci*. 177 (2005): 151-179.

[24] Zhou, Q.; and Swager, T. M. Fluorescent chemosensors based on energy migration in conjugated polymers: The molecular wire approach to increased sensitivity. *J. Am. Chem. Soc*. 117 (1995): 12593-12602.

[25] Long, Y. Electrospun nanofibrous film doped with a conjugated polymer for DNT fluorescence sensor. *Macromolecules*. 42 (2009): 6501–6509.

[26] Wang, B.; and Wasielewski, M. R. Design and synthesis of metal ion recognition induced conjugated polymers: an approach to metal ion sensory Materials. *J. Am. Chem. Soc.* 119 (1997): 12-21.

[27] Zheng, J.; and Swager, T. M. In poly(arylene etynylene)s: from synthesis to application, Springer-Verlag Berlin, Berlin. 2005: 151-179.

[28] Niamnont, N.; Mungkarndee, R.; Techakriengkrai, I.; Rashatasakhon, P.; and Sukwattanasinitt, M. Protein discrimination by fluorescent sensor array constituted of variously charged dendritic phenylene–ethynylene fluorophores. *Biosens. Bioelectron.* 26 (2010): 863-867.

[29] Lakowicz, J. R. Principles of fluorescence spectroscopy; 3rd ed.; John Wiley & Sons, Inc, Kluwer. 2006.

[30] Yu, S. P.; Canzoniero, M. T.; and Choi, D. W. Ion homeostasis and apoptosis. *Curr. Opin. Cell Biol.* 13 (2001): 405–411.

[31] Walz, W. Role of astrocytes in the clearance of excess extracellular potassium. *Neurochem. Int.* 36 (2000): 291–300.

[32] Kofuji, P.; and Newman, E. A. Potassium buffering in the central nervous system. *Neuroscience.* 129 (2004): 1045–1056.

[33] Suter, P. M. Potassium and hypertension. *Nutr. Rev.* 56 (1998): 151–153.

[34] Pedersen, S. F.; O'Donnell, M. E.; Anderson, S. E.; and Cala, P. M. Physiology and pathophysiology of Na^+/H^+ exchange and Na^+-K^+-$2Cl^-$ cotransport in the heart, brain and blood. *Am. J. Physiol.: Regul., Integr. Comp. Physiol.* 291 (2006): R1–R25.

[35] Modesto, K. M.; Møller, J. E.; Freeman, W. K.; Shub, C.; Bailey, K. R.; and Pellikka, P. A. Safety of exercise stress testing in patients with abnormal concentrations of serum potassium. *Am. J. Cardiol.* 97 (2006): 1247-1249.

[36] Michaud, G. F.; and Strickberger, S. A. Should an abnormal serum potassium concentration be considered a correctable cause of cardiac arrest?. *J. Am. Coll. Cardiol.* 38 (2001): 1224-1225.

[37] http://content.karger.com/ProdukteDB/produkte.asp?Aktion=ShowPDF&Produkt Nr=223977&Ausgabe=230671&ArtikelNr=83312&filename=83312. pdf**.

[38] Karger, S. Energy and nutrient intake in the European Union. *Ann Nutr Metab.* 48 (2004): 1–16.

[39] D'Elia, L.; Barba, G.; Cappuccio, F.; and Strazzullo, P. Potassium intake, stroke, and cardiovascular disease: A meta-analysis of prospective studies. *J. Am. Coll. Cardiol..* 57 (2011): 1210–1219.

[40] Szmacinski, H.; and Lakowicz, J.R. Potassium and sodium measurements at clinical concentrations using phase-modulation fluorometry. *Sens. Act. B.* 60 (1999): 8–18.

[41] Wongyingsinn, M.; and Suksuriyayothin, S. Use of rapid ABG analyzer in measurement of potassium concentration: Does it agree with venous potassium concentration?. *J. Med. Assoc. Thai.* 2009: 925-928.

[42] Yamauchi, A.; Hayashita, T.; Nishizawa, S.; Watanabe, M.; and Teramae, N. Benzo-15-crown-5 fluorophore/γ-cyclodextrin complex with remarkably high potassium ion sensitivity and selectivity in water. *J. Am. Chem. Soc.* 121 (1999): 2319–2320.

[43] Upadhyay, S. P.; Pissurlenkar, R. R. S.; and Coutinho, E. C., Karnik, A. V. A Furo-fused BINOL based crown as fluorescent chiral sensor for enantioselective recognition of phenyl ethylamine and ethyl ester of valine. *J. Org. Chem.* 72 (2007): 5709-5714.

[44] Zhang, J.; Wang, L.; Pan, D.; Song, S.; Boey, F. Y. C.; Zhang, H.; and Fan, C. Visual cocaine detection with gold nanoparticles and rationally engineered aptamer structures. *small-journal.* 4 (2008): 1196–1200.

[45] Arthanari, H.; Basu, S.; Kawano, T. L.; and Bolton, P. H. Fluorescent dyes specific for quadruplex DNA. *Nucl. Acids Res.* 26 (1998): 3724–3728.

[46] Ho, H. A.; and Leclerc, M. Optical sensors based on hybrid aptamer/ conjugated polymer complexes. *J. Am. Chem. Soc.* 126 (2004): 1384-1387.

[47] Phan, A. T.; Kuryavyi, V. D.; and Patel, J. DNA architecture: from G to Z. *Curr. Opin. Struct. Biol.* 16 (2006): 288–298.

[48] Marathias, V. M.; and Bolton, P. H. Structures of the potassium-saturated, 2:1, and intermediate, 1:1, forms of a quadruplex DNA. *Nucl. Acids Res.* 28 (2000): 1969–1977.

[49] Rujan, L. N.; Meleney, J. C.; and Bolton, P. H. Vertebrate telomere repeat DNAs favor external loop propeller quadruplex structures in the presence of high concentrations of potassium. *Nucl. Acids Res*. 33 (2005): 2022–2031.

[50] Radi, A. E.; and O'Sullivan, C. K. Aptamer conformational switch as sensitive electrochemical biosensor for potassium ion recognition. *Chem. Commun*. (2006): 3432–3434.

[51] Ueyama, H.; Takagi, M.; and Takenaka, S. A novel potassium sensing in aqueous media with a synthetic oligonucleotide derivative. Fluorescence resonance energy transfer associated with guanine quartet-potassium ion complex formation. *J. Am. Chem. Soc*. 124 (2002)*:* 14286–14287.

[52] He, F.; Tang, Y.; Wang, S.; Li, Y.; and Zhu, D. Fluorescent amplifying recognition for DNA G-Quadruplex folding with a cationic conjugated polymer: A platform for homogeneous potassium detection. *J. Am. Chem. Soc*. 127 (2005): 12343-12346.

[53] Nagatoishi, S.; Nojima, T.; Galezowska, E.; Gluszynska, A.; Juskowiak, B.; and Takenaka, S. Fluorescence energy transfer probes based on the guanine quadruplex formation for the fluorometric detection of potassium ion. *Anal. Chim.Acta*. 581 (2007): 125–131.

[54] Chen, B.; Liang, J.; Tian, X.; and Liu, X. G-quadruplex structure: a target for anticancer therapy and a probe for detection of potassium. *Biochemistry—Moscow*. 73 (2008): 853–861.

[55] Chao, S .; Hongxi, G .; and Cuiping, M. An aptamer-based fluorescent biosensor for potassium ion detection using a pyrene-labeled molecular beacon. *Anal. Biochem* . 400 (2010): 99–102.

[56] Huang, C. C.; and Chang, H. T. Aptamer-based fluorescence sensor for rapid detection of potassium ions in urine. *Chem. Commun*. (2008): 1461–1463.

[57] Kong, D. M.; Guo, J. H.; Yang, W.; Ma, Y. E.; and Shen, H. K. Crystal violet–G-quadruplex complexes as fluorescent sensors for homogeneous detection of potassium ion. *Biosens. Bioelectron*. 25 (2009): 88–93.

[58] Qin, H.; Ren, J.; Wang, J.; Luedtke, N. W.; and Wang, E. G-Quadruplex-modulated fluorescence detection of potassium in the presence of a 3500-fold excess of sodium ions. *Anal. Chem.* 82 (2010): 8356–8360.

[59] Niamnont, N.; Siripornnoppakhun, W.; Rashatasakhon, P.; and Sukwattanasinitt, M. A Polyanionic dendritic fluorophore for selective detection of Hg^{2+} in Triton X-100 aqueous media. *Org. Lett.* 11 (2009): 2768-2771.

[60] Du, H.; Fuh, R. A.; Li, J.; Corkan, A.; and Lindsey, J. S. Photochem CAD: A computer-aided design and research tool in photochemistry. *Photochem Photobiol.* 68 (1998): 141-142.

[61] Fery-Forgues, S.; and Lavabe, D. Are fluorescence quantum yields so tricky to measure? a demonstration using familiar stationery products. *J. Chem. Educ.* 76 (1999): 1260-1264.

[62] Mukhopadhyay, M.; Banerjee, D.; Koll, A.; Mandal, A.; Filarowski, A.; Fitzmaurice, D.; Das, R.; and Mukherjee, S. *J. Photochem. Photobiol. A: Chem.* 175 (2005): 94-99.

[63] Chakraborty, A.; and Guchhait, N. *J. Incl. Phenom. Macrocycl. Chem.* 62 (2008): 91-97.

[64] Upadhyay, S. P.; Pissurlenkar, R. R. S.; Coutinho, E. C.; and Karnik. A. V. *J. Org. Chem.* 72 (2007): 5709-5714.

[65] Yoshikawa, K. Controlling the higher-order structure of giant DNA molecules. *Adv. Drug Del. Rev.* 52 (2001): 235–244.

[66] Declan, A. D; and Wallace, B. A. Shifting the Equilibrium Mixture of Gramicidin Double Helices Toward a Single Conformation with Multivalent Cationic Salts. *Biophys. J..* 75 (1998): 635-640.

[67] Baigl, D; and Yoshikawa, K. Dielectric control of counterion-induced single-chain folding transition of DNA. *Biophys. J.* 88 (2005): 3486–3493.

[68] Nagatoishi, S.; Nojima, T.; Juskowiak, B.; and Takenaka, S. A pyrene-labeled G-quadruplex oligonucleotide as a fluorescent probe for potassium ion detection in biological applications. *Angew. Chem. Int. Ed. Engl*. 44 (2005): 5067–5070.
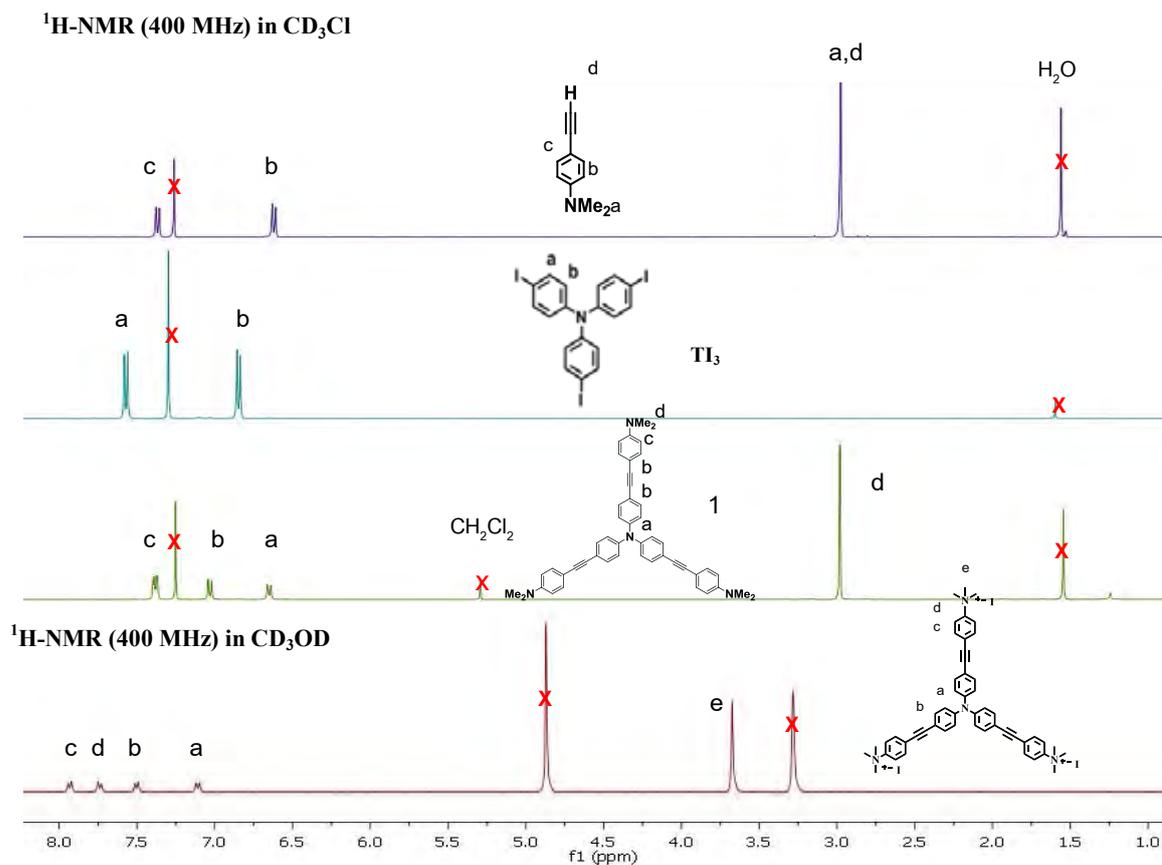
APPENDIX

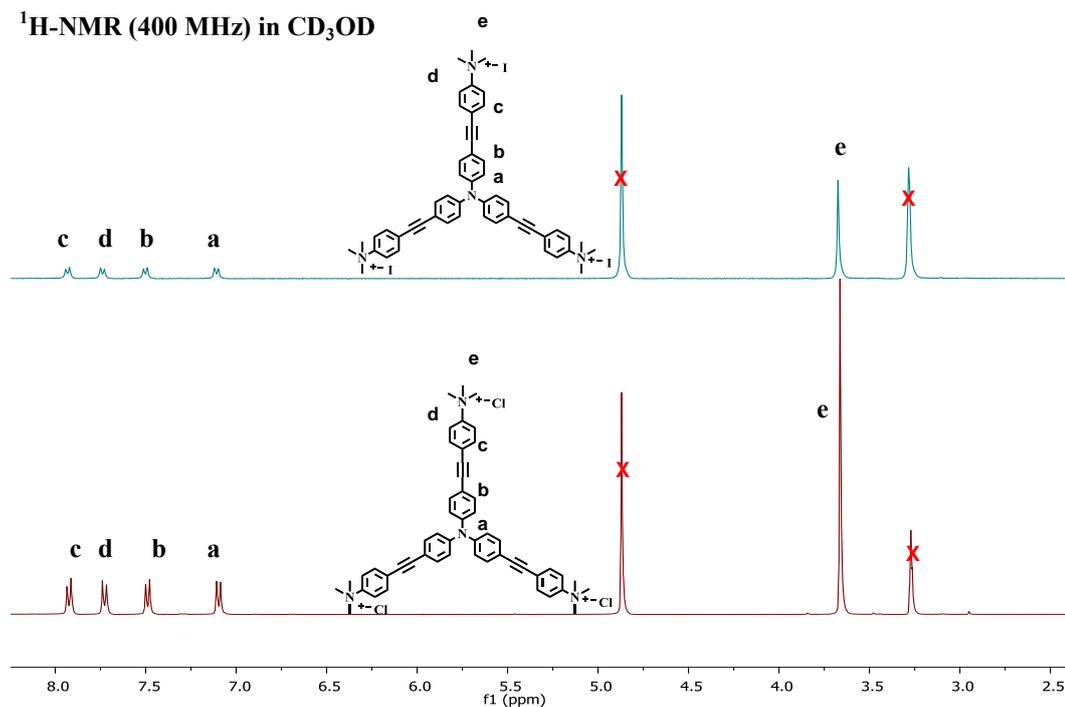**Figure A.1** ^{1}H NMR spectra of starting material compound **1-2**.

Figure A.2 ^{1}H NMR spectra of compound **2-3**.
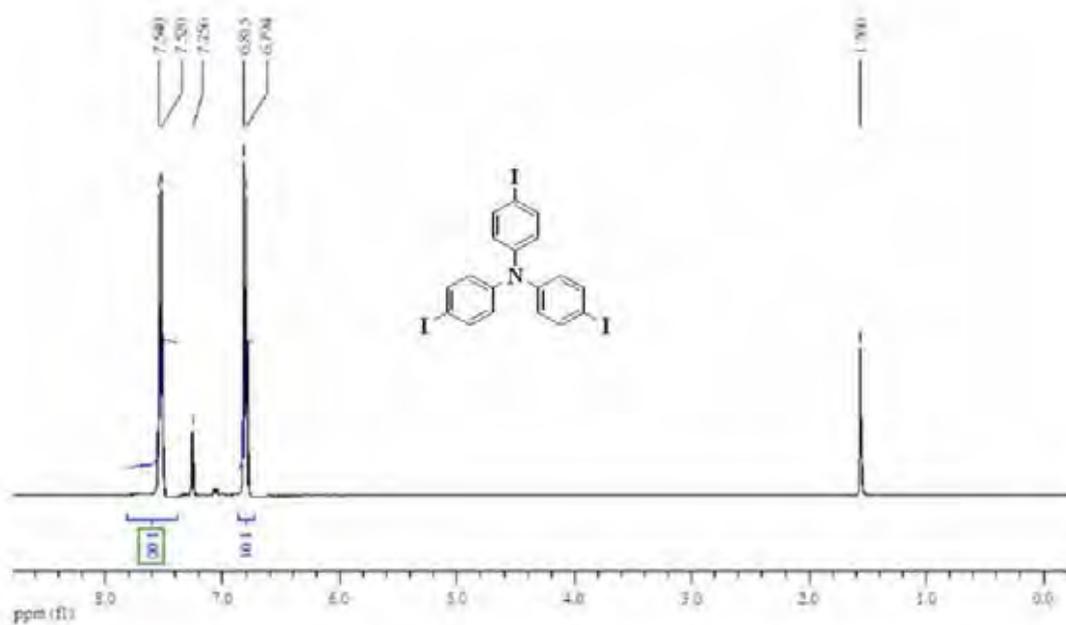
Figure A.3 ^{1}H NMR of **TI$_3$** in CDCl$_3$.
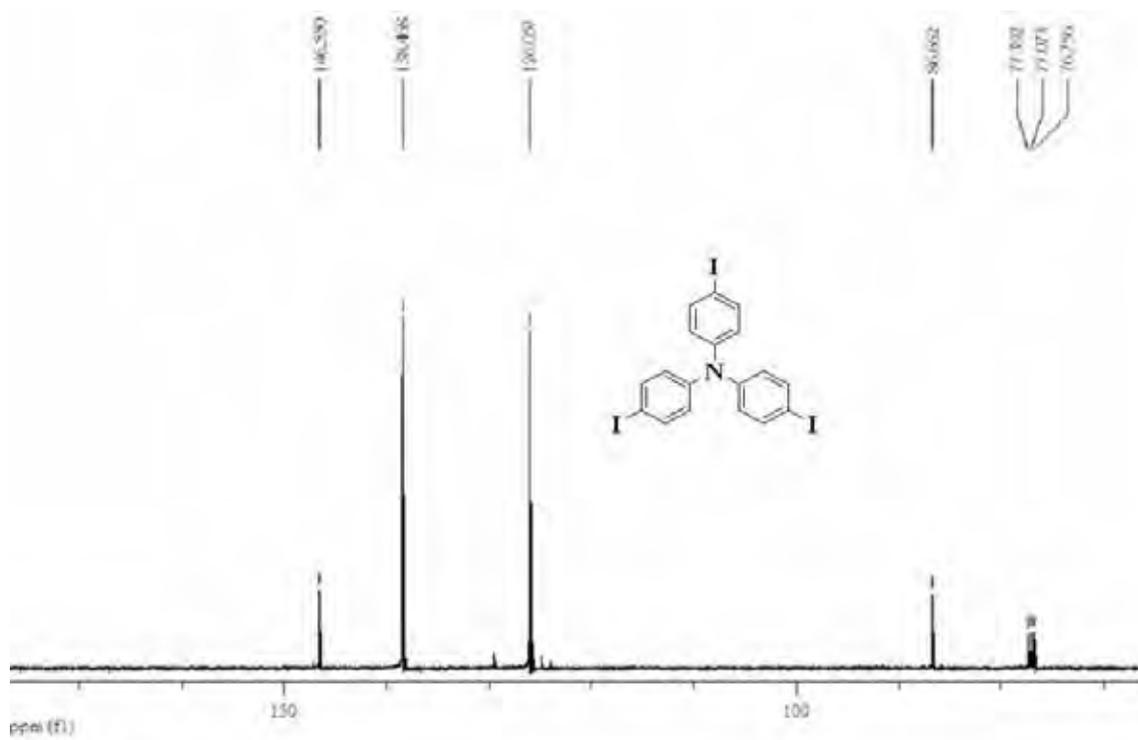
Figure A.4 ^{13}C NMR of **TI$_3$** in CDCl$_3$.
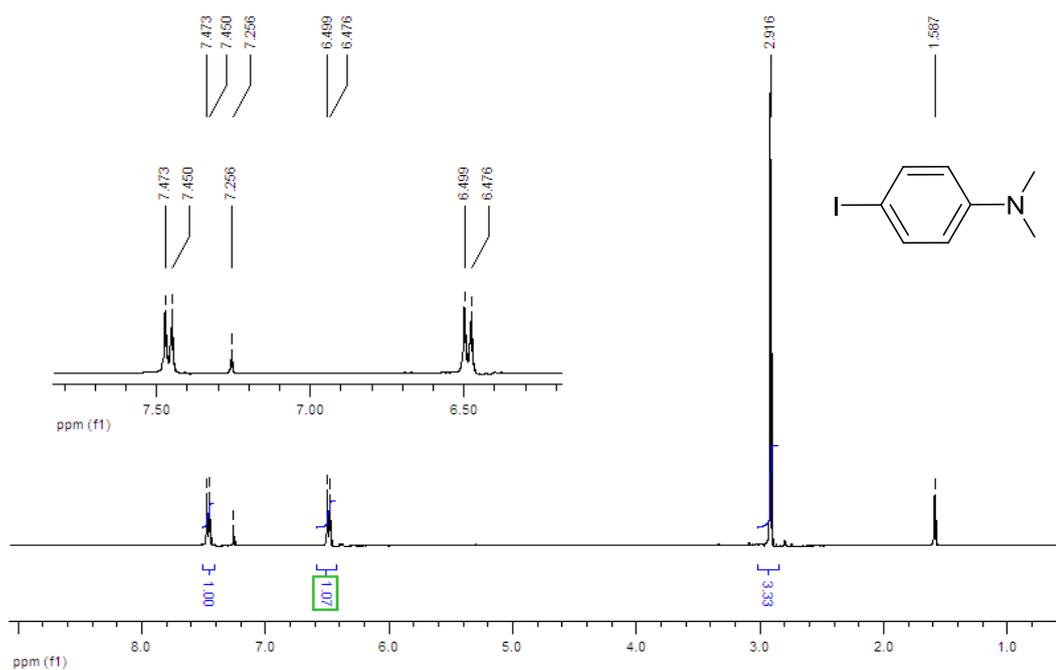
Figure A.5 ^{1}H NMR of 4-iodo-*N*,*N*-dimethylaniline in CDCl$_3$.
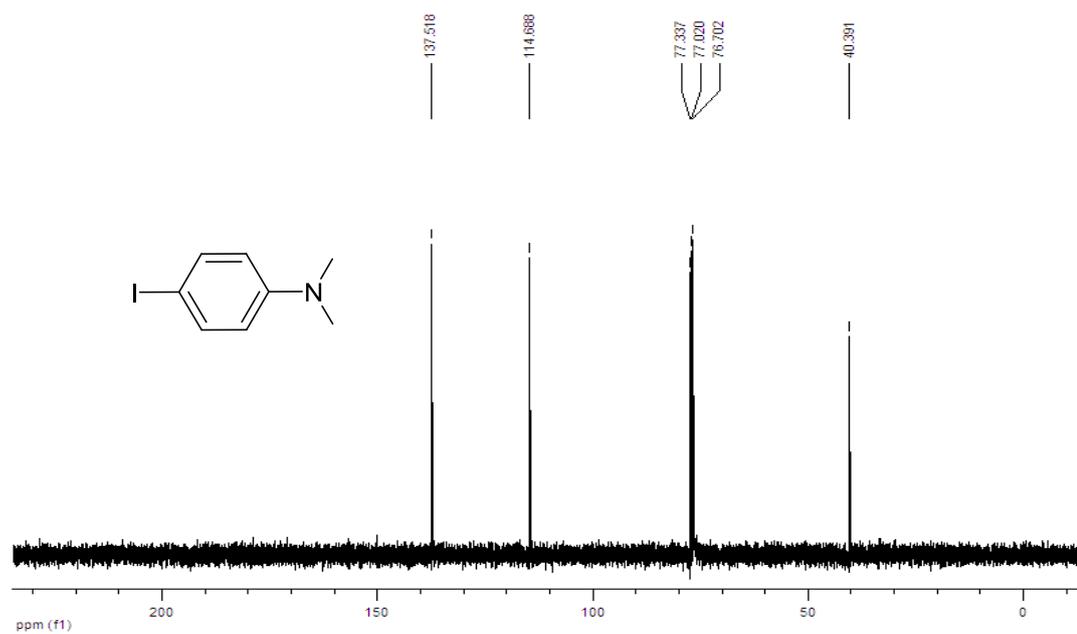
Figure A.6 ^{13}C NMR of 4-iodo-*N*,*N*-dimethylaniline in CDCl$_3$.
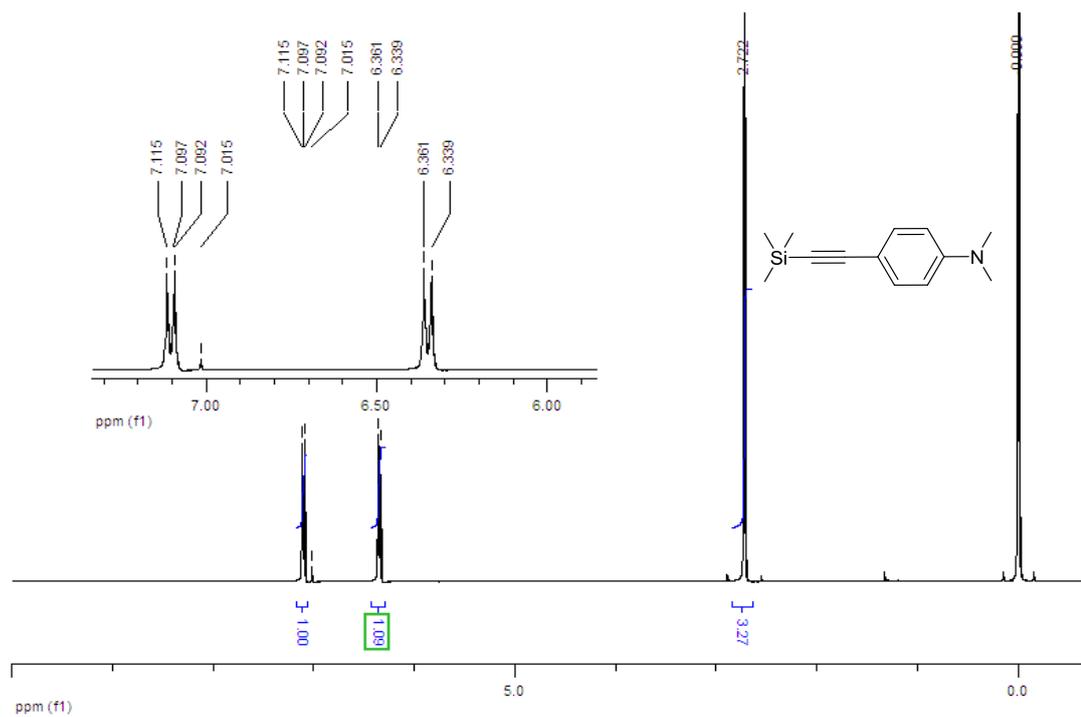
Figure A.7 ¹H NMR of *N,N*-dimethyl-4-((trimethylsilyl)ethynyl)aniline in CDCl₃.
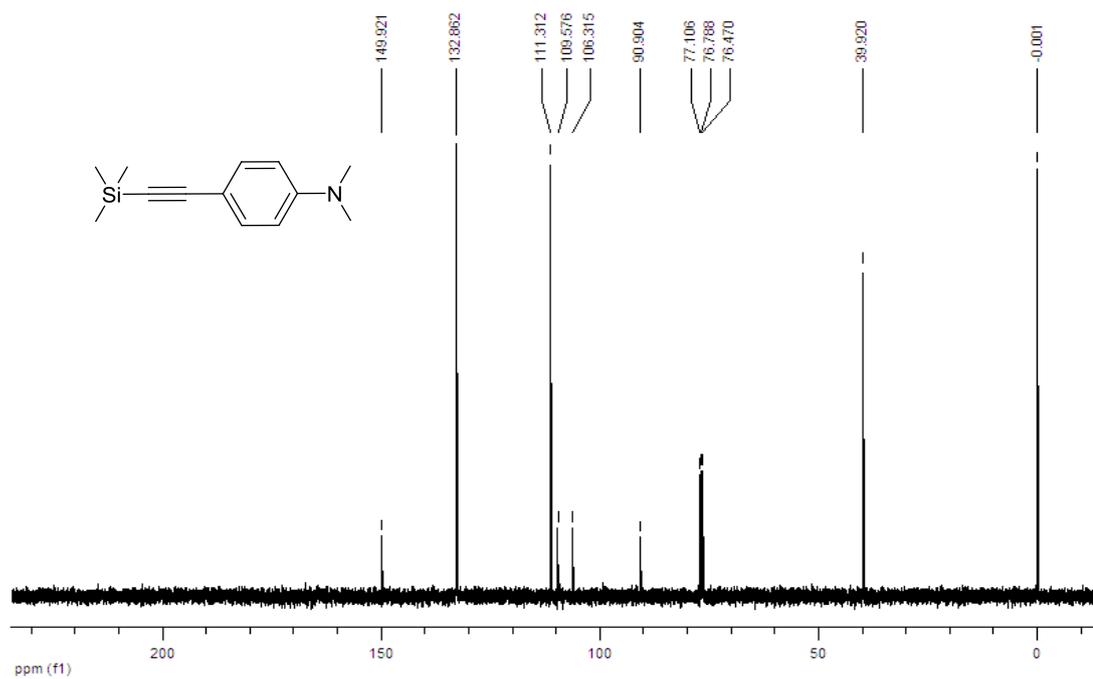
Figure A.8 ¹³C NMR of *N,N*-dimethyl-4-((trimethylsilyl)ethynyl)aniline in CDCl₃.
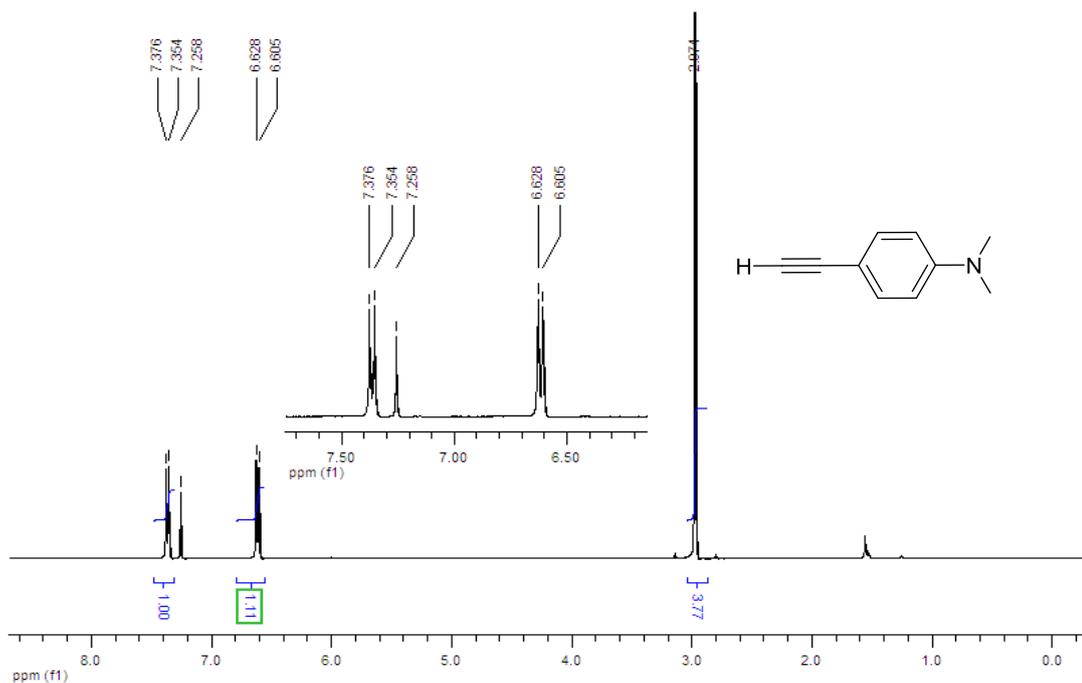
Figure A.9 ^{1}H NMR of 4-ethynyl-*N*,*N*-dimethylaniline in CDCl$_3$.
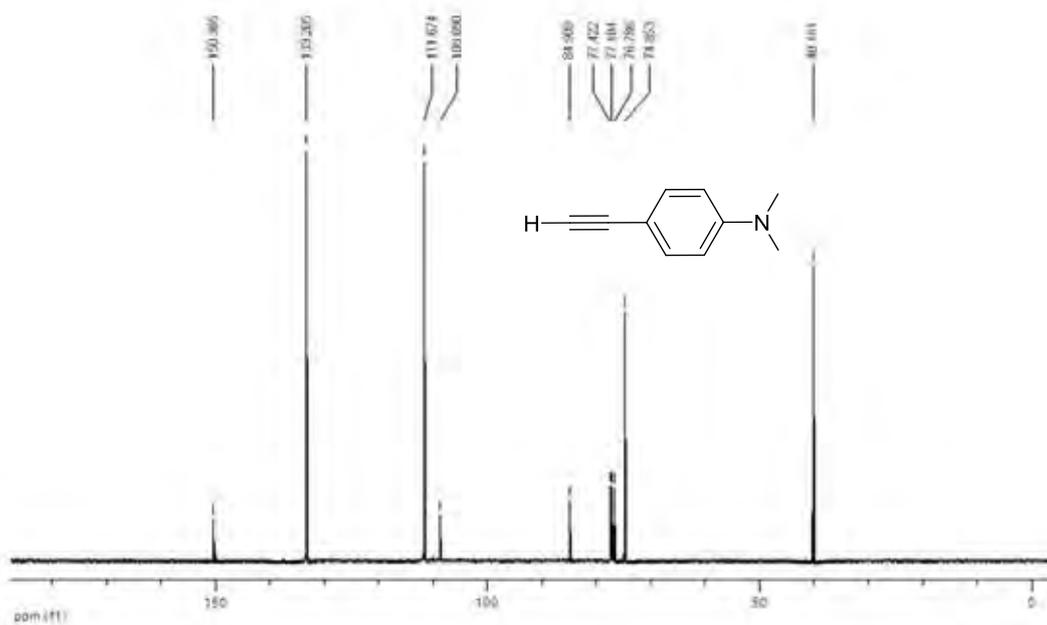
Figure A.10 ^{13}C NMR of 4-ethynyl-*N*,*N*-dimethylaniline in CDCl$_3$.
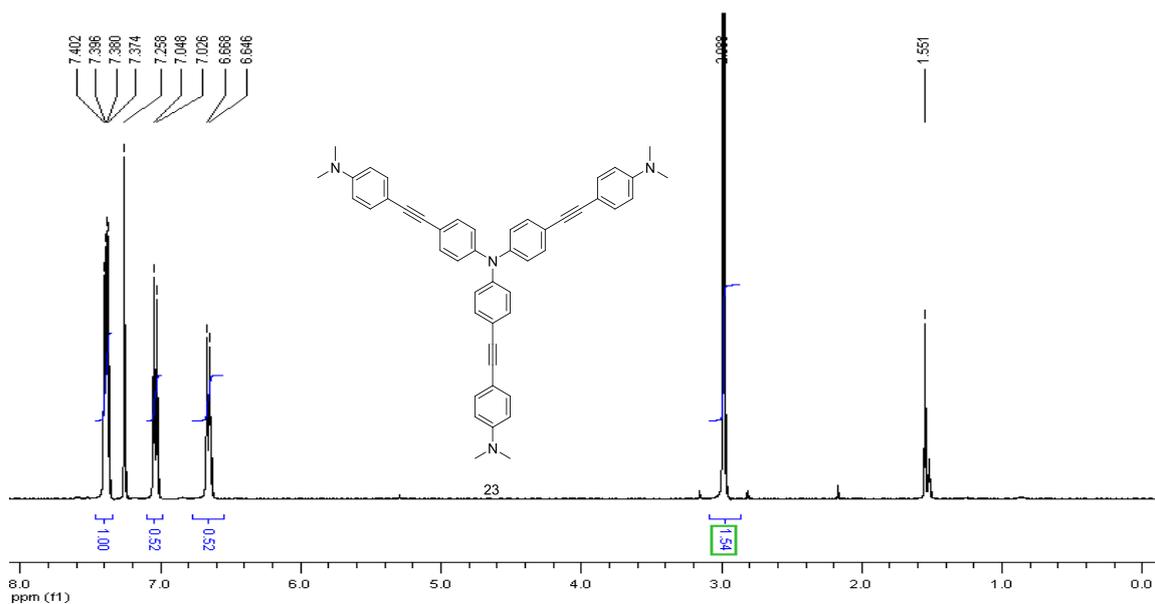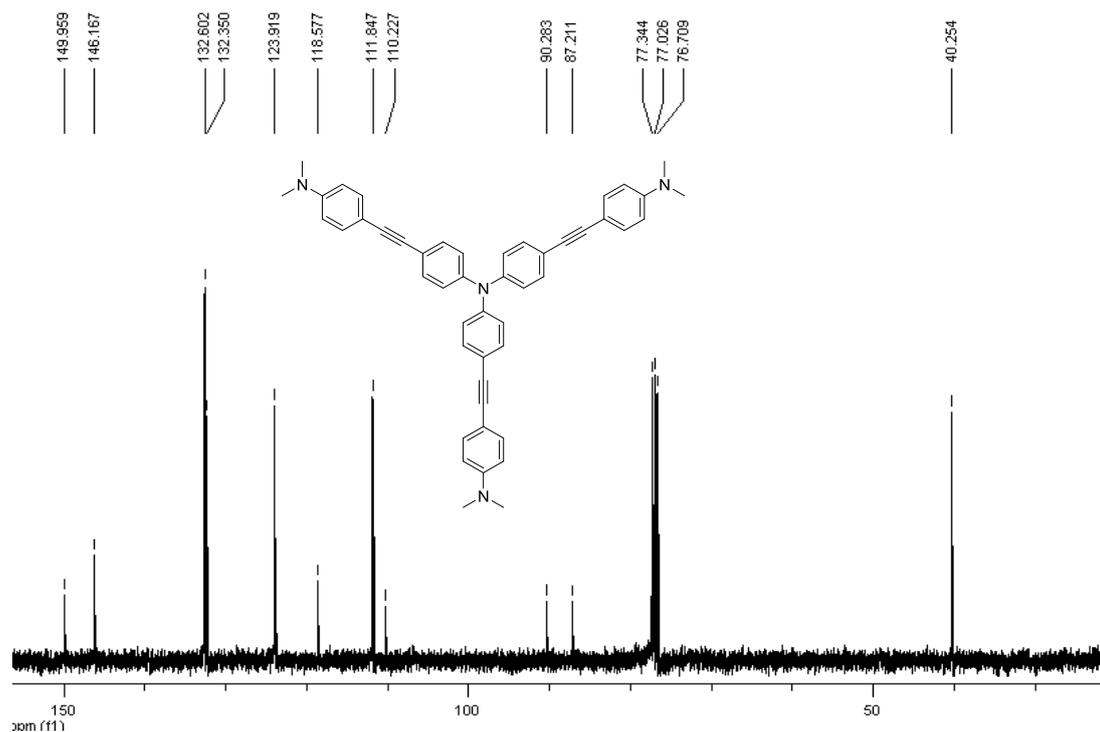
Figure A.11 ^{1}H NMR of **3N^0 (1)** in CDCl$_3$.

Figure A.12 ^{13}C NMR of **3N^0 (1)** in CDCl$_3$.
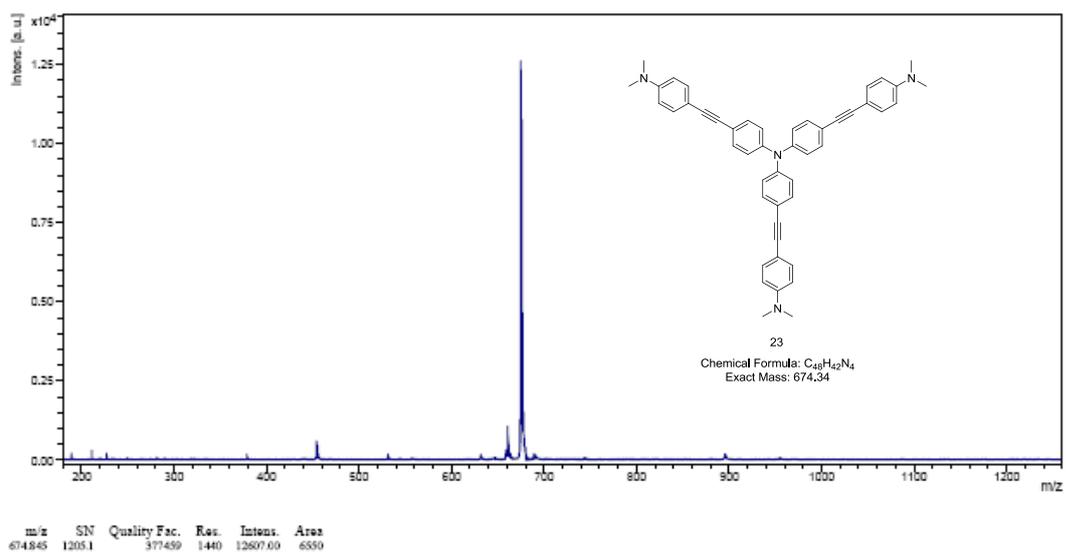
Figure A.13 MALDI-TOF-MS of **3N⁰** (**1**).
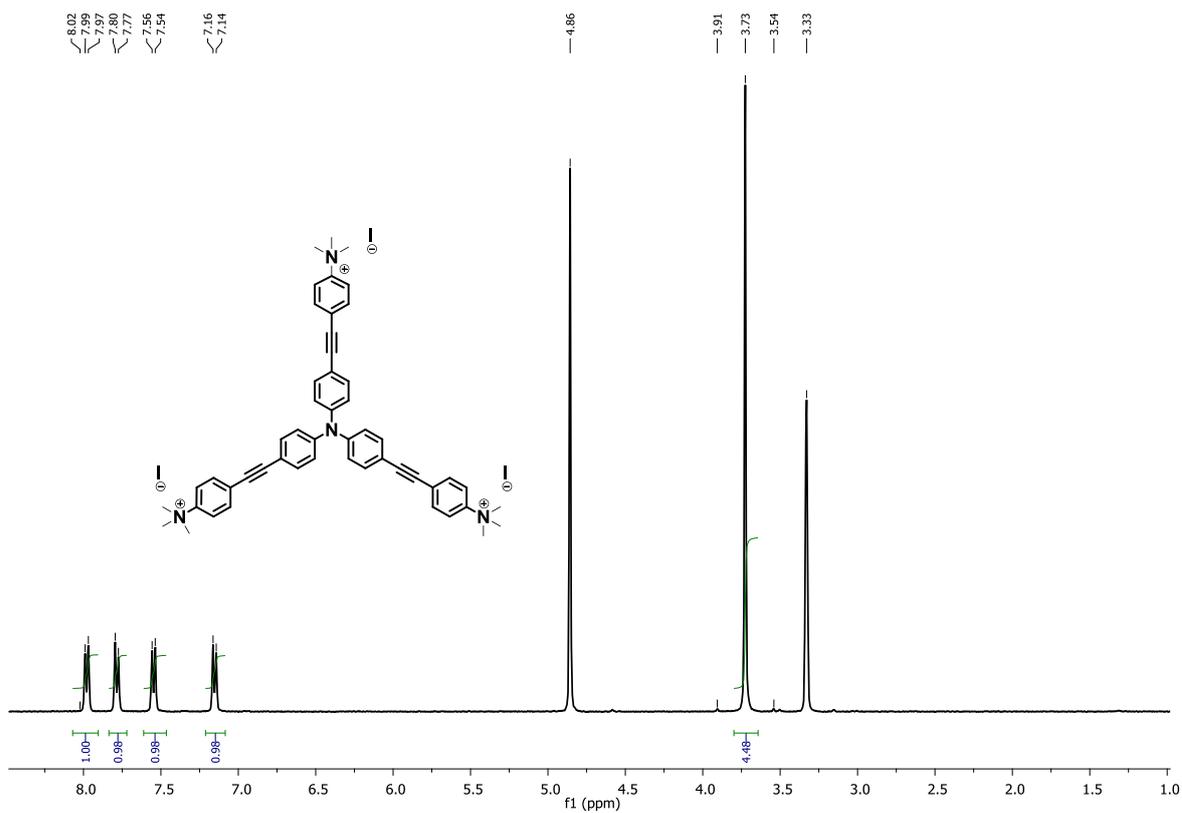
Figure A.14 ¹H NMR of **N³⁺ (3I⁻)**, (**2**) in CD₃OD.
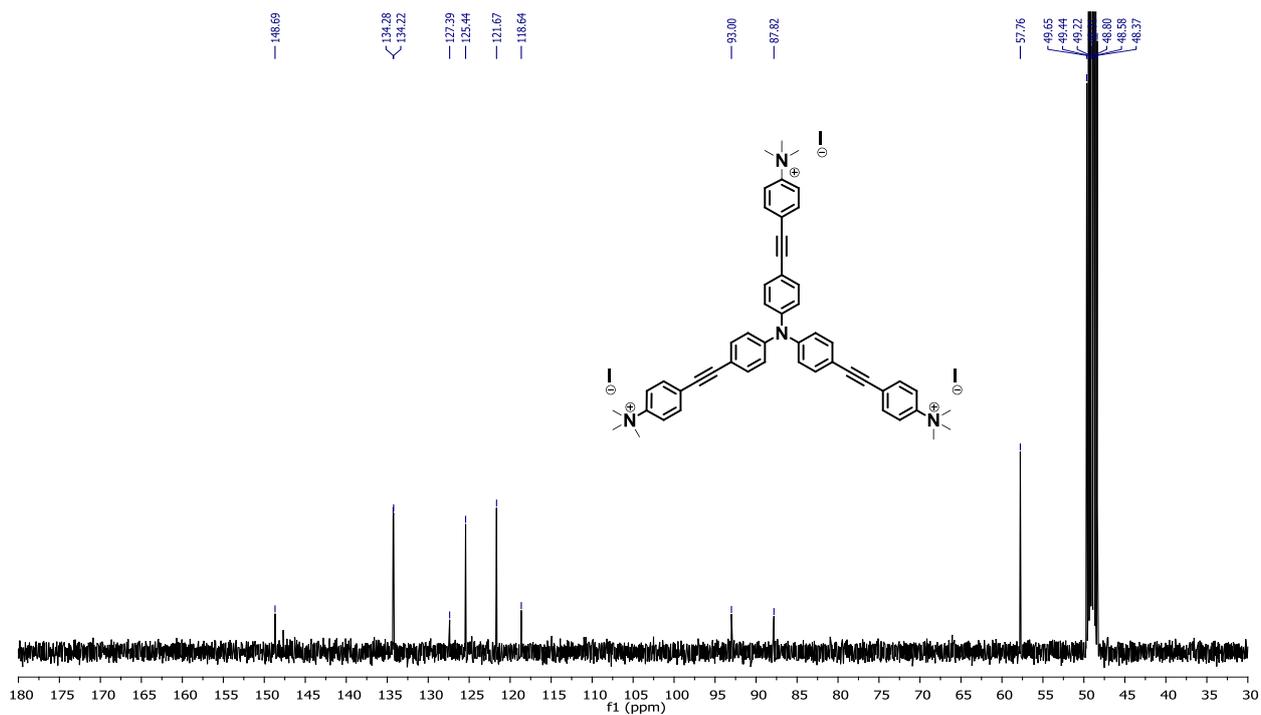
Figure A.15 ^{13}C NMR of **N^{3+} (3I$^-$)**, **(2)** in CD$_3$OD.

Chemical Formula: C$_{51}$H$_{51}$N$_4$$^{3+}$
Exact Mass: 719.41
Molecular Weight: 719.98

719.98/3 = 239.99
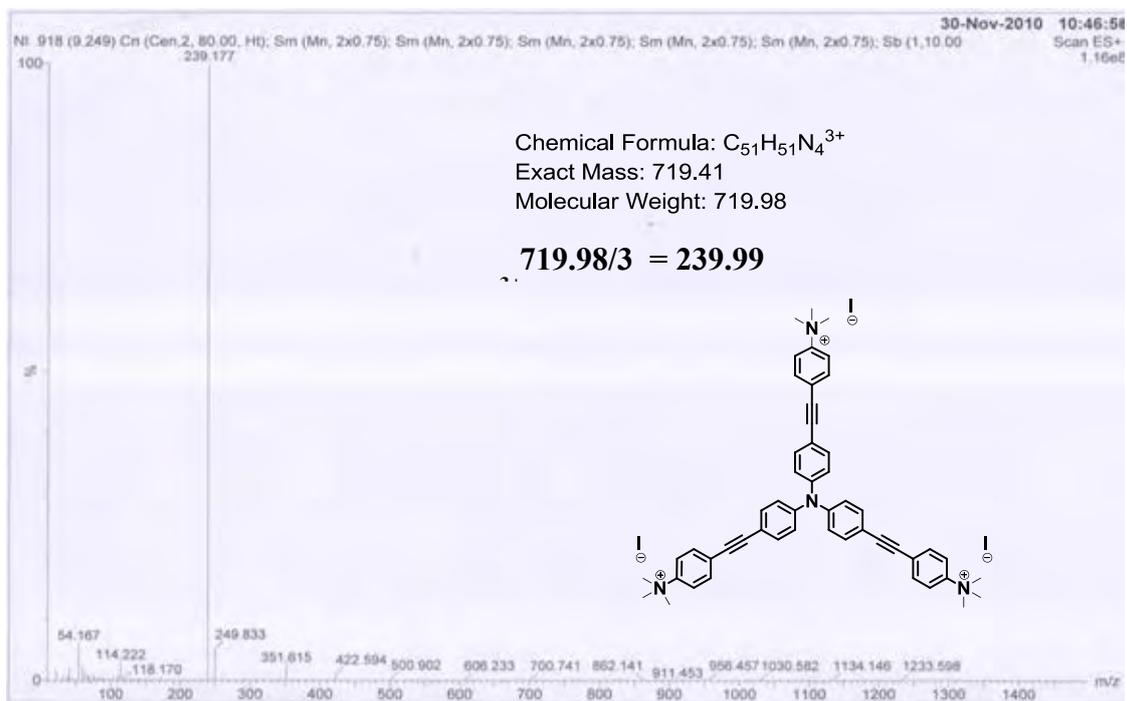
Figure A.16 ESI-MS of **N^{3+} (3I$^-$)**, **(2)** in CH$_3$OH.
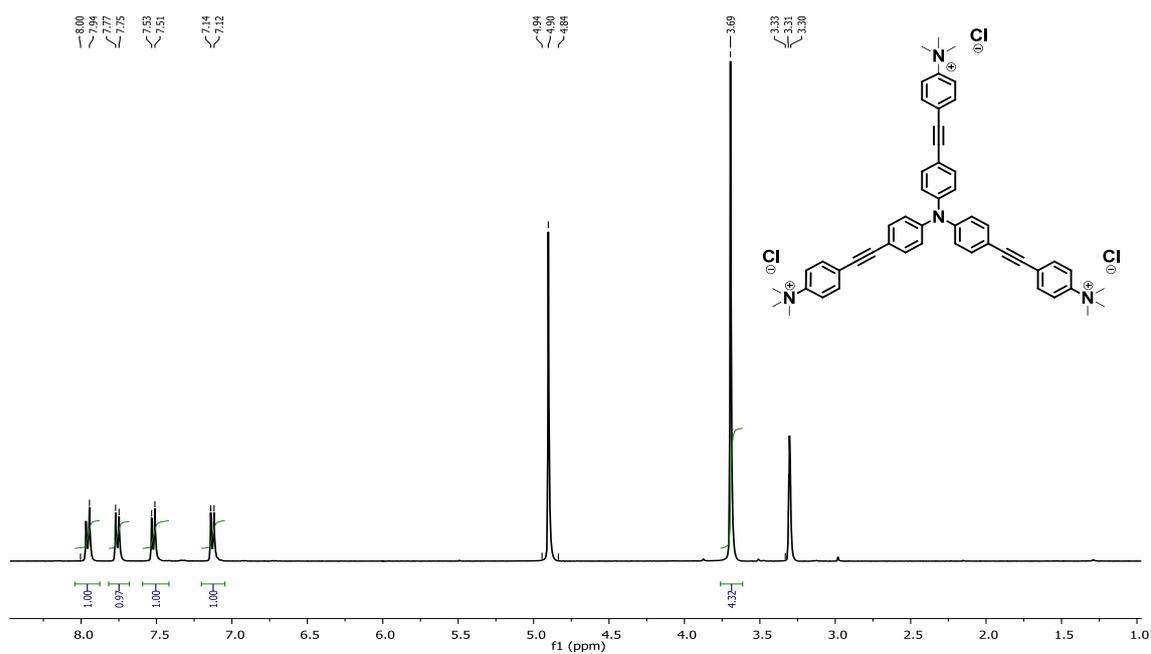
Figure A.17 ^{1}H NMR of $\mathbf{N^{3+}}$ **(Cl$^-$)**, **(3)** in CD$_3$OD.
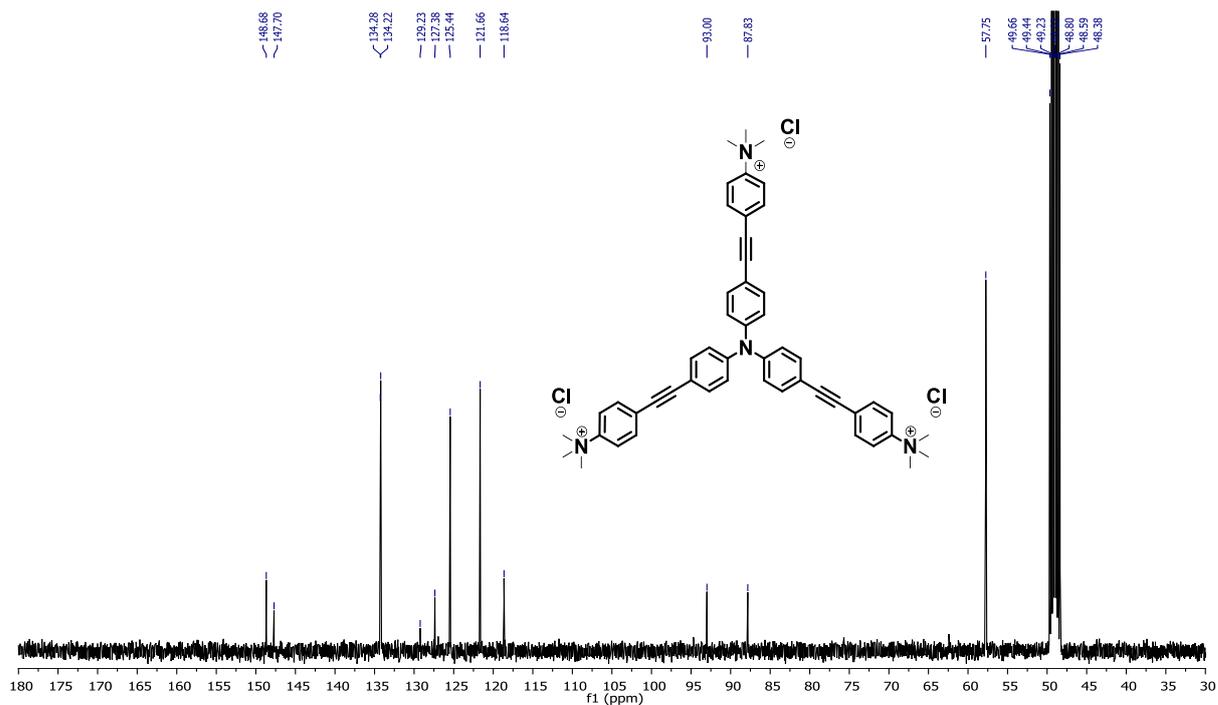
Figure A.18 ^{13}C NMR of $\mathbf{N^{3+}}$ **(Cl$^-$)**, **(3)** in CD$_3$OD.
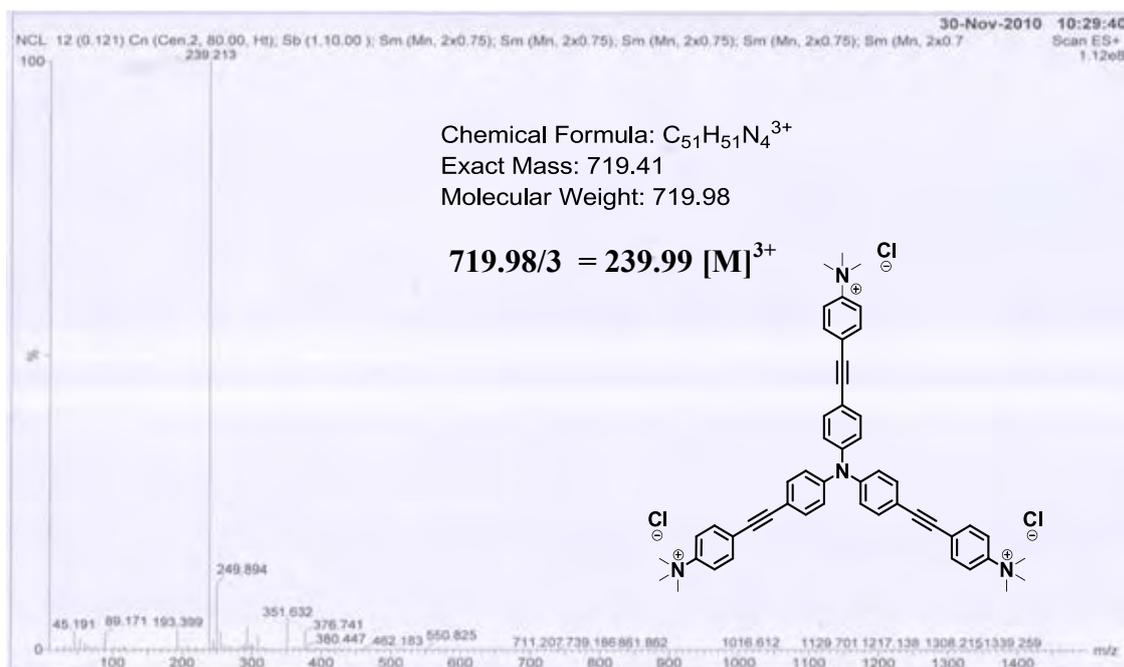
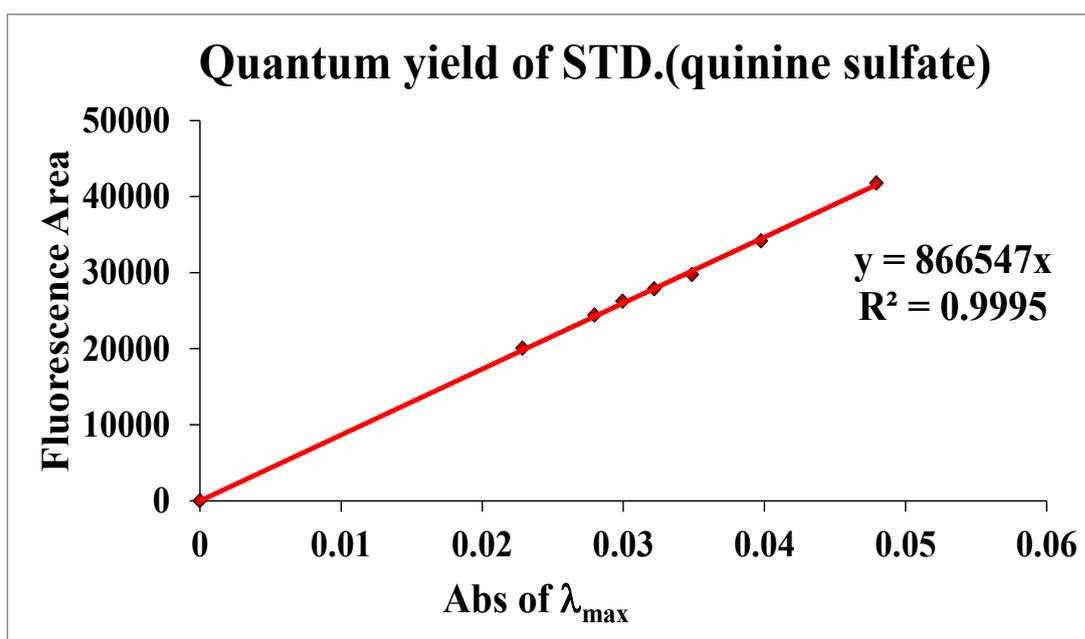**Figure A.19** ESI-MS of N^{3+} **(3Cl⁻), (3)** in CH_3OH.

Figure A.20 Quantum yield of quinine sulfate standard.
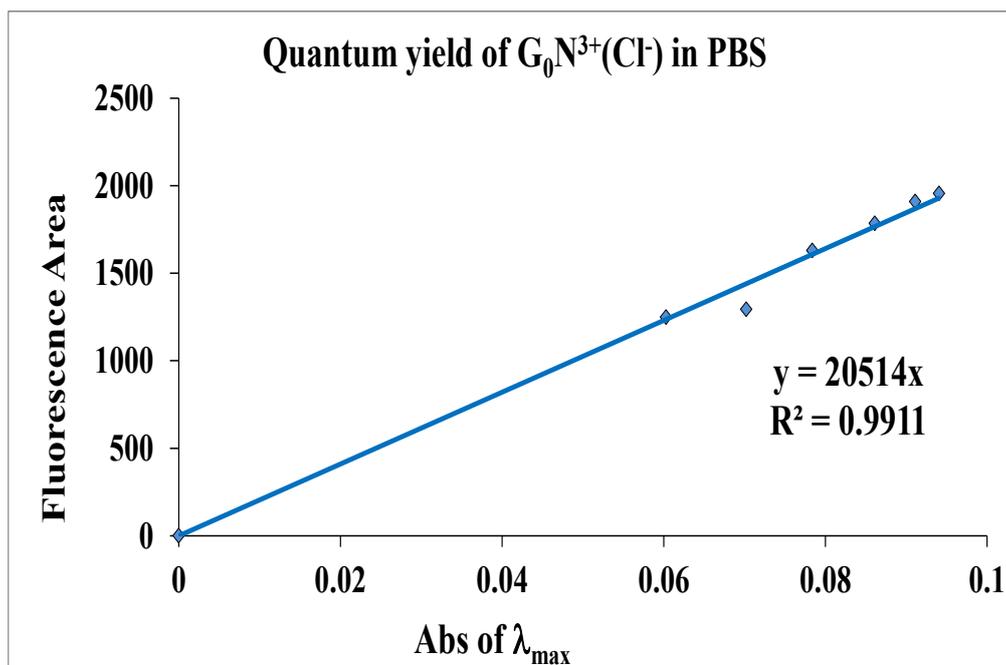
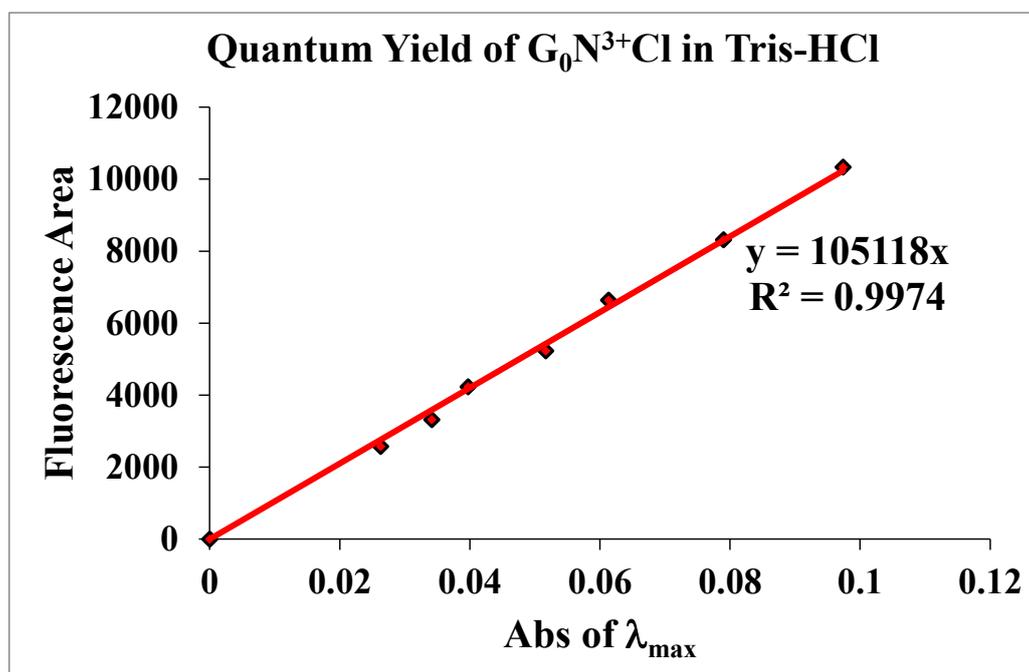**Figure A.21** Quantum yield of N^{3+} **(3Cl$^-$)** in PBS buffer.

Figure A.22 Quantum yield of N^{3+} **(3Cl$^-$)** in Tris-HCl buffer.
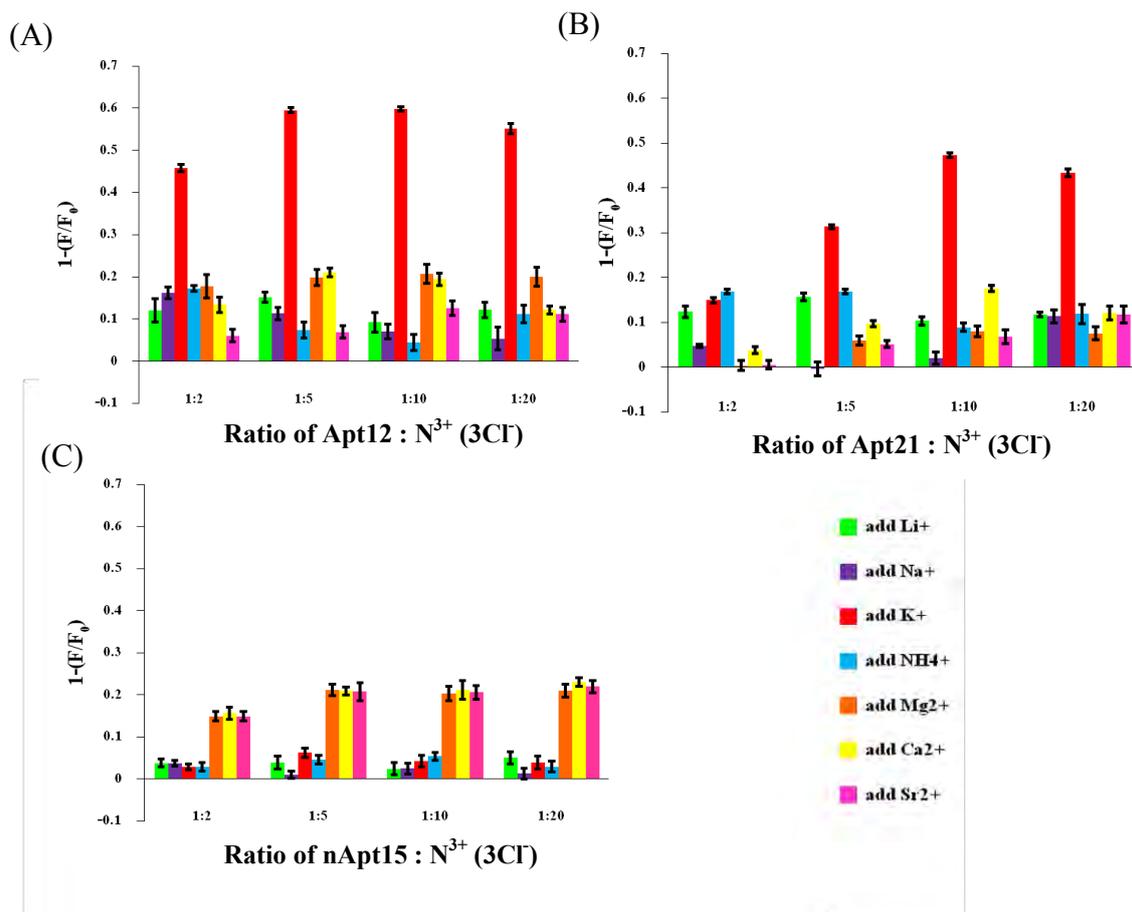
Figure A.23 The sensing system was also tested against other cations such as Li$^+$, Na$^+$, NH$_4^+$, Mg^{2+}, Ca^{2+} and Sr^{2+}. The results shown clearly display high selectivity of this sensor over other cation. The plot between quenching efficiency values (1-I/I$_0$) and aptamer to fluorphore mole ratio (1:2, 1:5, 1:10 and 1:20). (A) Shown the maximum ratio at the one to five ratio and the one to ten ratio. (B) Shown the maximum ratio at the one to ten ratio. And (C) Shown the complex cannot form G-quadruplex with K$^+$.

Figure A.24 Fixing concentration of the fluorophore at 0.2 μM and Apt 15 mer at 0.02 μM in 10mM Tris–HCl buffer pH 7.4. Following the addition of different concentrations of K^+ ions (0.2 mM, 0.2 mM, 2 mM, 4 mM and 6 mM) and adding another metal chloride (LiCl, NaCl, KCl, NH_4Cl, $MgCl_2$ $CaCl_2$, and $SrCl_2$) had quantity more than concentrations of K^+ ions 10 times (2 mM and 60 mM).
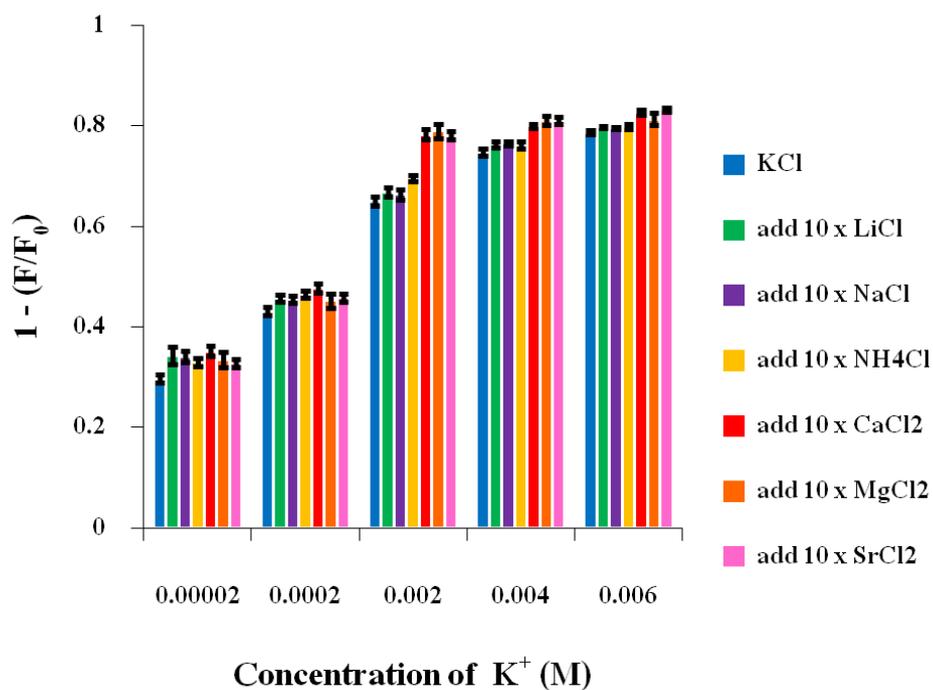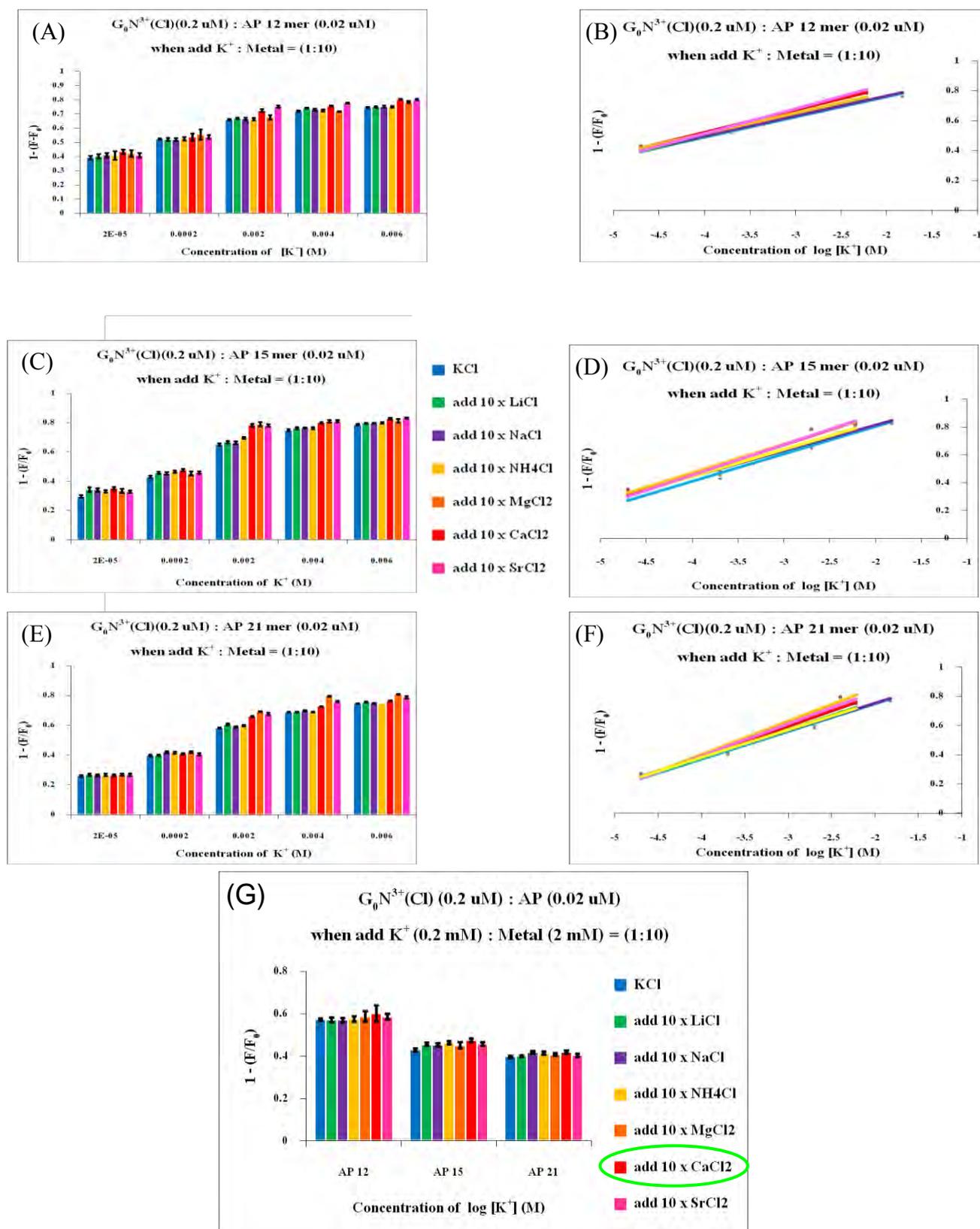
Figure A.25 Fixing concentration of the fluorophore at 0.2 μM and aptamers at 0.02

μM in 10 mM Tris–HCl buffer pH 7.4. Following the addition of different

concentrations of K^+ ions (0.02, 0.2, 2, 4 and 6 mM) and adding another metal chloride (LiCl, NaCl, KCl, NH_4Cl, $MgCl_2$ $CaCl_2$, and $SrCl_2$) had quantity more than concentrations of K^+ ions 10 times (0.2, 2, 20, 40 and 60 mM), except Na^+ used until 150 mM. (A) and (B) Chart and plot shown interference of potassium ion detection of fluorophore-Apt12 complex. (C) and (D) Chart and plot shown interference of potassium ion detection of fluorophore-Apt15 complex. (E) and (F) Chart and plot shown interference of potassium ion detection of fluorophore-Apt21 complex. (G) Chart shown interference condition no effect of potassium ion detection because in plasma had concentration of calcium (0.8 ± 0.28 mmol/L). So, this condition gave good sensing for potassium ion detection.
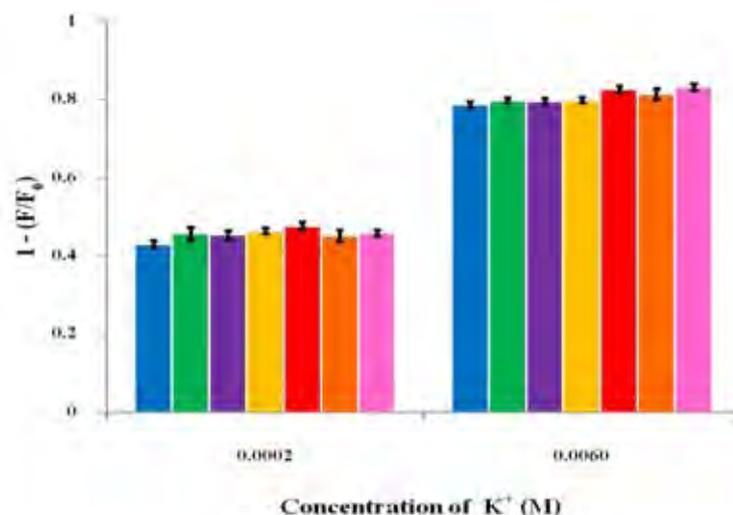

Figure A.26 Interference of K^+ detection of fluorophore-Apt15 complex at concentrations of K^+ ions, (■) 0.2 mM and 6 mM. Following the addition of another metal chloride that's LiCl (■), NaCl (■), NH_4Cl (■), $MgCl_2$ (■), $CaCl_2$ (■), and $SrCl_2$, (■)) had quantity more than concentrations of K^+ ions 10 times (2 mM and 60 mM).
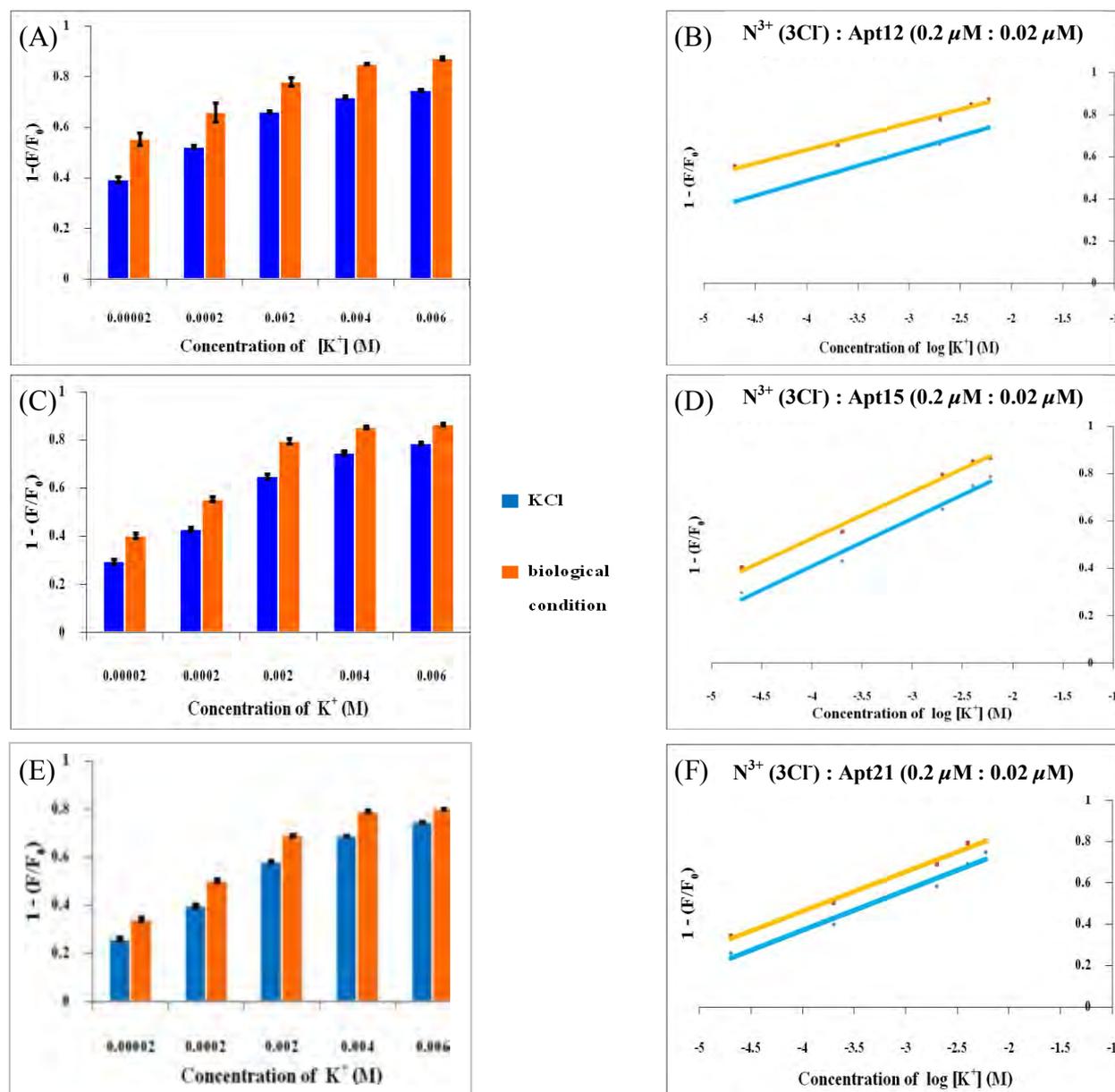
Figure A.27 Fluorescence detection of potassium ion under biological conditions (145 mM NaCl, 5 mM KCl, 2.5 mM CaCl$_2$, and 1.5 mM MgCl$_2$). Fixing concentration of the fluorophore at 0.2 μM and aptamers at 0.02 μM in 10 mM Tris–HCl buffer pH 7.4. Following the addition of different concentrations of K$^+$ ions (0.02, 0.2, 2, 4 and 6 mM) and adding free cations concentrations under extracellular conditions. (A) and (B) Chart and plot shown the different quenching efficiency between potassium ion and potassium ion in biological conditions of fluorophore-Apt12 complex. (C) and (D) Chart and plot shown the different quenching efficiency between potassium ion and potassium ion in biological conditions of fluorophore-

Apt15 complex. (E) and (F) Chart and plot shown the different quenching efficiency between potassium ion and potassium ion in biological conditions of fluorophore-Apt21 complex.
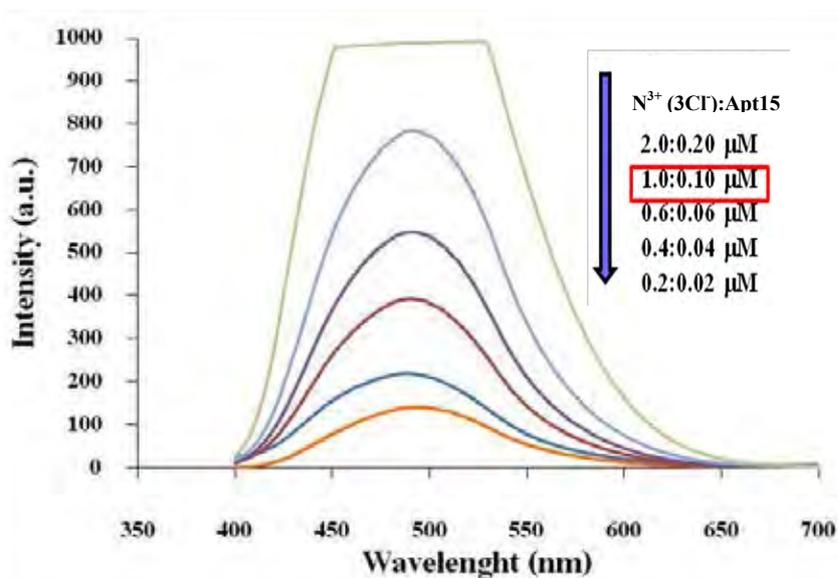

Apt12: s(5'- GGC GGG TTG GGG -3')

Apt15: s(5'- GGT AGG GTT AGG GTT AGG GTT AGG G-3')

Apt21: s(3'- GGG TTA GGG TTA GGG TTA GGG-3')

nApt15: s(5'- CAT TCA TGT CAT TCA-3')

Figure A.28 Schematic representation of a K^+ sensor that operates based on modulation of the fluorescence of the complex formed between the compound, N^{3+} and Apt15.

$y = 2.528x + 4611.2$
$R^2 = 0.9966$

$y = 2.3012x + 2495.2$
$R^2 = 0.9968$

$y = 2.4053x + 1990.2$
$R^2 = 0.9984$

$y = 2.6214x + 440.95$
$R^2 = 0.9824$

— Linear (sample 1)
— Linear (sample 2)
— Linear (sample 3)
— Linear (sample 4)

Figure A.29 Data from ICP-OES for K^+ ions detection

Figure A.30 Fluorescence intensity of compound **3** or **N^{3+}** and Apt15 when vary ratio of concentration. The spectrum shown the optimization ratio at 1 : 0.1 μM.
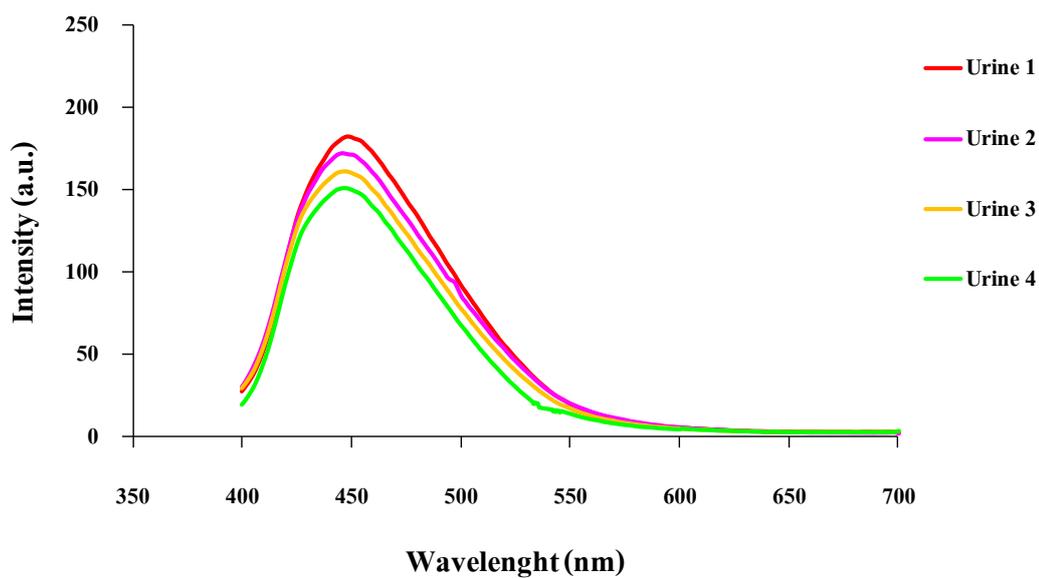

Figure A.31 Fluorescence intensity of four urine samples for recovery test.
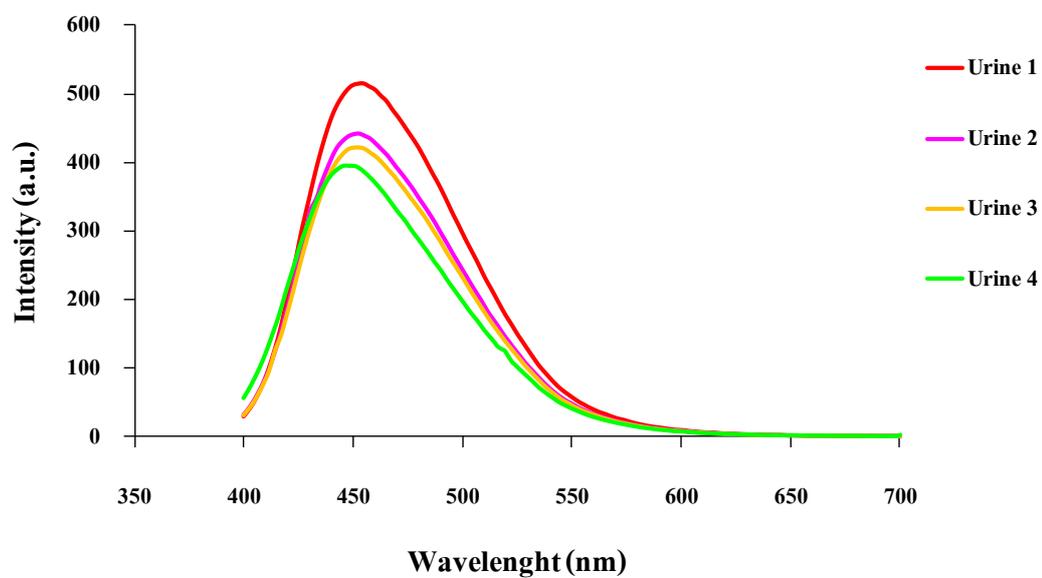
Emission of D^{3+} (Cl$^-$) + Apt 15 mer (10:1) in Real Sample

Figure A.32 Fluorescence intensity of four urine samples for potassium detection test.

VITAE

Ms. WannapaYuanboonlim was born on April 2nd, 1985 in Khon Kaen, Thailand. She graduated with high school degree from Witsetchaichan Tantiwittayapoom School, Ang-Thong. She graduated with Bachelor Degree of Science, majoring in Chemistry from Srinakarinwitrot University in 2007. In 2009, she has been a graduate student in organic chemistry and become a member of Organic Synthesis Research Unit under supervision of Assoc. Prof. Dr. Mongkol Sukwattanasinitt and she further received a Master Degree in Department of Chemistry from Chulalongkorn University. During the course of study, she received the scholarship from the ADB under the Petroleum & Petrochemical Technology Consortium and 100th anniversary of Chulalongkorn University Fund.

Her present address is 31 Moo. 3 Klong Kanak, Witsetchaichan, Ang-Thong, Thailand 14110.